AD-A093 882 APPLIED RESEARCH ASSOCIATES INC ALBUQUERQUE NM F/G 18/3
BASIC MECHANISMS OF SPALL FROM NEAR-SURFACE EXPLOSIONS.(U)
NOV 80 D H MERKLE F49620-80-C-0059
UNCLASSIFIED AFOSR-TR-80-1379 NL

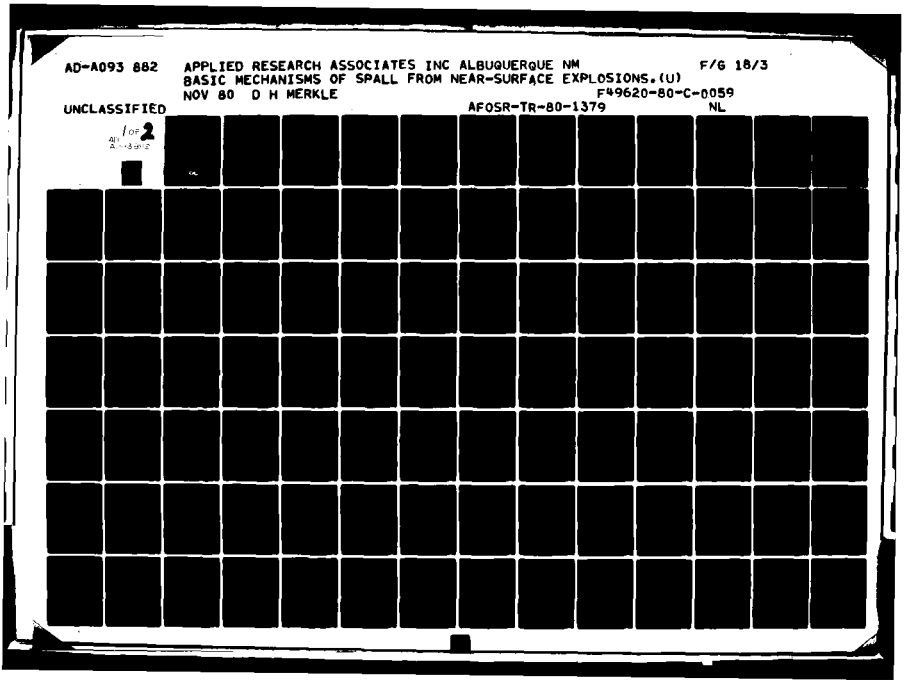

LEVEL II

6



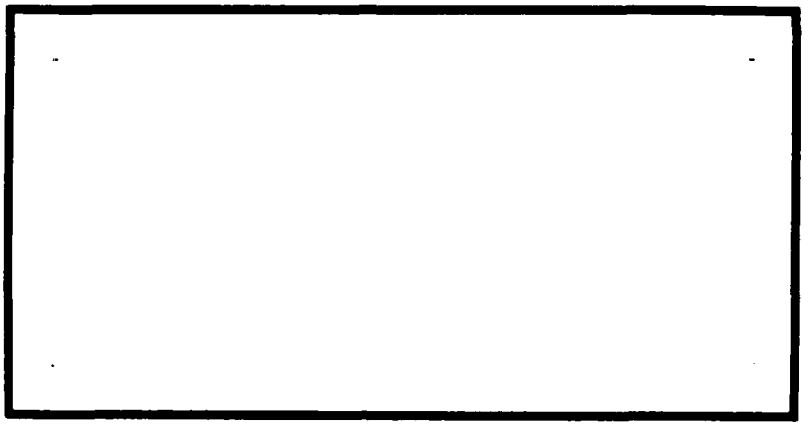


APPLIED RESEARCH ASSOCIATES, INC.
Engineering and Applied Science

UNCLASSIFIED

# BASIC MECHANISMS OF SPALL FROM NEAR-SURFACE EXPLOSIONS(U)

Douglas H. Merkle

Applied Research Associates, Inc.
2601 Wyoming Blvd., NE
Albuquerque, NM 87112

30 November 1980

Final Report, Period 1 April 1980 — 31 October 1980

Contract No. F49620-80-C-0059

This work sponsored by the Air Force Office of Scientific Research under

Program Element 61102F
Project 2309
Task A1

Prepared for

Director of Physics
Air Force Office of Scientific Research
Bolling AFB, D.C. 20332

412136

UNCLASSIFIED

UNCLASSIFIED

SECURITY CLASSIFICATION OF THIS PAGE *(When Data Entered)*

| REPORT DOCUMENTATION PAGE | READ INSTRUCTIONS BEFORE COMPLETING FORM |
|---|---|
| 1. REPORT NUMBER **AFOSR-TR- 80 - 1379** 2. GOVT ACCESSION NO. AD-A093 882 | 3. RECIPIENT'S CATALOG NUMBER |
| 4. TITLE *(and Subtitle)*<br>Basic Mechanisms of Spall From Near-Surface Explosions (U) | 5. TYPE OF REPORT & PERIOD COVERED<br>Final<br>1 April 80 - 31 October 80<br>6. PERFORMING ORG. REPORT NUMBER |
| 7. AUTHOR(s)<br>Douglas H. Merkle | 8. CONTRACT OR GRANT NUMBER(s)<br>F49620-80-C-0059 |
| 9. PERFORMING ORGANIZATION NAME AND ADDRESS<br>Applied Research Associates, Inc.<br>2601 Wyoming Blvd., N.E.<br>Albuquerque, NM 87112 | 10. PROGRAM ELEMENT, PROJECT, TASK AREA & WORK UNIT NUMBERS<br>61102F<br>2309 /A1 |
| 11. CONTROLLING OFFICE NAME AND ADDRESS<br>Director of Physics<br>Air Force Office of Scientific Research<br>Attn: NP, Bldg. 410, Bolling AFB, D.C. 20332 /NP | 12. REPORT DATE<br>30 November 80<br>13. NUMBER OF PAGES<br>94 |
| 14. MONITORING AGENCY NAME & ADDRESS *(if different from Controlling Office)* | 15. SECURITY CLASS. *(of this report)*<br>Unclassified<br>15a. DECLASSIFICATION/DOWNGRADING SCHEDULE |

16. DISTRIBUTION STATEMENT *(of this Report)*

Approved for public release;
distribution unlimited.

17. DISTRIBUTION STATEMENT *(of the abstract entered in Block 20, if different from Report)*

18. SUPPLEMENTARY NOTES

19. KEY WORDS *(Continue on reverse side if necessary and identify by block number)*

Spall
Ground Motion
Nuclear Weapons Effects

20. ABSTRACT *(Continue on reverse side if necessary and identify by block number)*

(U) The current state of the art on explosion-induced spall in geologic materials is examined, with emphasis on spall in soil due to near surface explosions. At present there is neither a generally accepted, precise, technical definition of, nor a generally accepted technique for predicting explosion-induced spall in soil. Several mechanisms can cause spall in soil, and the key to a better understanding of soil spall is a better understanding of soil tensile stress-strain behavior.

DD FORM 1 JAN 73 1473 EDITION OF 1 NOV 65 IS OBSOLETE

UNCLASSIFIED

SECURITY CLASSIFICATION OF THIS PAGE *(When Data Entered)*

## PREFACE

The research reported herein was funded by the Air Force Office of Scientific Research (AFOSR), to address problems relating to explosion-induced spall in geologic materials of common concern to both AFOSR and the Air Force Weapons Laboratory (AFWL).

The author is indebted to Lt. Brian Stump and Drs. Robert Reinke and Eric Rinehart of AFWL, and to Dr. Harry Auld for numerous discussions during the course of the research, which helped to better define the problem of spall in soil, and to illustrate its various modes of occurrence in field test records.



AIR FORCE OFFICE OF SCIENTIFIC RESEARCH (AFSC)
NOTICE OF TRANSMITTAL TO DDC
This technical report has been reviewed and is approved for public release IAW AFR 190-12 (7b).
Distribution is unlimited.
A. D. BLOSE
Technical Information Officer

TABLE OF CONTENTS

LIST OF FIGURES

Figures (Continued)

Figures (Continued)

## I. PURPOSE AND SCOPE

The purpose of the spall research described herein is defined in the Statement of Work for Air Force Office of Scientific Research Contract Number F49620-80-C-0059, dated 7 April 1980, viz.:

> Evaluate the present state of the art on spalling, to include initial conditions, ground motion characteristics, spall mechanisms, and the relationship between spall parameters and weapon yields, depth of burial and material properties.

As the above Statement of Work clearly indicates, emphasis in this initial research effort was on evaluating the current state of knowledge concerning spall. Although not stated explicitly above, the principal concern was with spall in soil due to near-surface nuclear (NE) and high explosive (HE) detonations. The main areas of interest were:

1. initial conditions (spall initiation criteria),
2. ground motion characteristics (spall definition and identification),
3. spall mechanisms, and
4. relation between spall parameters and weapon yields, depth of burial and material properties (spall prediction).

## II. INTRODUCTION

### A. Background

Spall is a familiar phenomenon for many, and an everyday occurrence for some. Automobile drivers and building owners are acquainted with the conical fracture caused by impact of a small, fast moving projectile against a glass pane. Insurance companies must budget annually to pay claims for such incidents. Construction workers and miners depend on spall as the basic mechanism of excavation for tunnels, highways, trenches, foundations and mine shafts in competent rock. The study of ballistic penetration and armor plating, protection of spacecraft against meteoroid impact or high energy radiation deposition, and protection of nuclear power plants against penetration by tornado-driven missiles may also involve the physics of spall. For discussions of these classic, though not necessarily simple cases of spall see [Kolsky (1953: Ch. VIII); Rinehart and Pearson (1954); O'Brien and Davis (1961); Coates (1967: Ch. 8); Stagg and Zienkiewicz (1968: Ch. 7); Jaeger and Cook (1969: Ch. 18); Kinslow (1970); Duvall (1972); Swift (1972); Rohde et. al. (1973: Session E); DuPont (1976); DuPont (1977: Section IV); Hemphill (1980: Ch. 4); and Curran (1980)].

### B. Spall From Nuclear and High Explosive Detonations

The use of nuclear explosives to produce spall has been contemplated for over twenty years [Rinehart (1959)]. The classic case of surface spall in rock directly above a contained nuclear explosion occurred during the RANIER Event of Operation Plumbob, a 1.7 KT nuclear detonation 900 FT below the top of Ranier Mesa in Area 12 of the Nevada Test Site, on September 19, 1957 [Perret (1961:35); Perret (1971: Ch. 5)]. It was RANIER groundshock data which prompted the still ongoing detailed study of explosion-induced groundshock spall [Perret (1978:33)]. Figure 2.1 shows the surface vertical motion (recorded acceleration, and velocity obtained by integrating the recorded acceleration) which occurred directly above the RANIER detonation. Three distinct phases are evident in both the acceleration and velocity curves:

1. an initial upward motion,
2. a prolonged -1g free-fall, or "dwell", in this case of about 380 milliseconds duration, and
3. a sharp upward impact, or "rejoin".

Perret postulated that the above curves describe the motion of a rock mass given initial upward momentum by the upward-propagating compressive stress wave generated by the weapon detonation, then separated from the rock mass below by a distinct horizontal fracture, caused by the reflected tensile wave propagating downward from the free surface. The separated mass then undergoes "free" (ballistic) motion under the influence of gravity, until impacting the rock mass below. [Glasstone and Dolan (1977: para 2.91)] describe spalling from a shallow underground burst as follows:

> When a nuclear weapon is exploded under the ground, a sphere of extremely hot, high-pressure gases, including vaporized weapon residues and rock, is formed. This is the equivalent of the fireball in an air or surface burst. The rapid expansion of the gas bubble initiates a ground shock wave which travels in all directions away from the burst point. When the upwardly directed shock (compression) wave reaches the earth's surface, it is reflected back as a rarefaction (or tension) wave. If the tension exceeds the tensile strength of the surface material, the upper layers of the ground will spall, i.e., split off into more-or-less horizontal layers. Then, as a result of the momentum imparted by the incident shock wave, these layers move upward at a speed which may be about 150 (or more) feet per second.

Figure 2.2 shows the effects of spalling from the Plowshare SULKY Event, a 0.087 KT nuclear detonation at a depth of 90 FT in basalt, in the Buckboard Mesa area of the Nevada Test Site, on December 18, 1964 [Glasstone and Dolan (1977: para 6.05); Bolt (1976:261)].

## C. Spall in Soil

Spall-type ground motion has by no means been restricted to contained detonations in competent rock. Numerous groundshock records have been obtained in soil, for both contained and near-surface detonations, in which the vertical ground motion has exhibited all three of the characteristic spall features shown in Figure 2.1. Nor are such motions seen only near

the ground surface. There are, however, significant differences in waveform detail between spall in soil and spall in rock.

Following RANIER, a further study of spall was undertaken in 1961, using a vertical string of gages in a boring offset 30 FT from the MINK emplacement hole, and later using similar vertical gage arrays on other events in various environments [Perret (1978:33)].

The MINK Event was a low yield (less than 20 KT) nuclear detonation at a depth of 630 FT in alluvium, in Area 3 of the Nevada Test Site, on October 29, 1961. Figure 2.3 shows how MINK vertical acceleration waveforms varied with depth, and also the results of Perret's "ray tracing" analysis, by which he described the propagation, or at least the sequence, of particular spall waveform features. In Figure 2.3 the time axis for each vertical acceleration waveform is drawn at gage depth. Therefore a ray connecting the time abscissae of adjacent corresponding waveform features has a slope proportional to the "propagation" velocity of that feature. Significant similarities as well as differences between the MINK spall records in alluvium and previous spall records in rock were noted [Perret (1978:37)]:

> Specifically, all of these MINK acceleration records include an initial positive acceleration pulse followed by one or two periods of negative acceleration of roughly one-g amplitude which terminate in large amplitude positive acceleration pulses. However, significant departures in these alluvium records from those obtained in a tuff or hard rock environment include: (1) free fall signature arrivals which occur earlier in each succeedingly deeper record, and in the deepest record occurs only 10 msec after arrival of the first signal, and 11 msec before arrival of the initial peak acceleration in the shallowest record; (2) an initial positive acceleration pulse of relatively low amplitude broadened by a following plateau which is of roughly equal duration, and about half peak amplitude; and (3) gradual initiation of free fall signals (about 20 msec between zero and -1 g) and free fall terminations that are gradual in the deeper records although abrupt in the shallower ones. Mink vertical acceleration records from depths of 50 and 100 feet include a series of oscillations immediately following the impact spike signals which have periods of approximately 11 msec and amplitudes ranging from 2 to 0.5 g. These oscillations are probably not related directly to the mechanics of spallation but appear to be unique to the Mink records.

The MERLIN Event was a 10 KT nuclear detonation at a depth of 972 FT in alluvium, also in Area 3 of the Nevada Test Site, on February 16, 1965. The MERLIN data was intended to supplement previously obtained free-field alluvium motion data from the nuclear events MINK (10/29/61), FISHER (12/3/61), HOGNOSE (3/15/62) and HAYMAKER (6/27/62) [Perret (1971: 17)]. Figures 2.4, 2.5 and 2.6 show vertical acceleration waveforms for two MERLIN borings, and the RANIER event for comparison. Perret noted that although the "spall signatures" are basically similar in all the vertical acceleration records for RANIER (9/19/57), MINK (10/29/61), MERLIN (2/16/65) and MILROW (10/2/69), application of the same spall analysis procedures resulted in very different interpretations between records from contained nuclear detonations in competent rock (RANIER and MILROW) and in a dry desert alluvium (MINK and MERLIN). The two fundamental differences which he identified were:

> (1) In desert alluvium the onset of free fall occurs at the deepest stations first, and progressively later at shallower stations, and phase changes, free fall and impact occur gradually.
> (2) In rock, free fall appears first at the surface, and phase changes are abrupt.

The above general comparison was subject, as Perret noted, to such variances as gradual development of free fall in bedded tuff, and abrupt impact phase onset at some near-surface stations in alluvium.

D. Spall From Near-Surface Detonations

Little, if any, analysis for spall has been accomplished on the relatively small amount of existing groundshock data from near-surface nuclear detonations. Current knowledge of spall caused by near-surface detonations is therefore based almost entirely on data obtained from HE experiments.

MISERS BLUFF, Phase II, Event I (MB II-1) was a single 120 T half-buried HE detonation in alluvium overlaying sandstone, at Planet Ranch, Arizona, 25 KM east of Parker Dam on the Colorado River separating Arizona and California, on August 2, 1977. Figures 2.7 and 2.8 show consistent

spall features observed in near-surface (0.5 M depth) vertical velocity waveforms at ranges between 12.5 M and 200 M [Phillips, Melzer and Bratton (1979:33, 35)].

MISERS BLUFF, Phase I, Event 4 (MB I-4) and PRE-HYBRID GUST, Phase II, Event 1 (PHG II-1) were both hexagonal array multi-burst, surface tangent spherical HE shots in alluvium. MISERS BLUFF Phase I was conducted at the Queen 15 site on the White Sands Missile Range, New Mexico, while PRE-HYBRID GUST Phase II was conducted at McCormick Ranch on Kirtland AFB, New Mexico. MB I-4 used six 1000 LB TNT charges spaced 21.35 M apart, and was detonated on September 7, 1977. PHG II-1 used six 256 LB TNT charges spaced 10.86 M apart and was detonated on September 12, 1979. Figure 2.9 shows the near-surface vertical velocity waveform at the center of the MB I-4 array. Typical spall features are evident, with the -1g dwell (slope of velocity curve of -0.98 MPS in 100 MS) from approximately 140 to 200 MS. Figures 2.10 through 2.18 show vertical velocity waveforms at various depths near the center of the PHG II-1 array. Spall features are not apparent in any of these waveforms, although it is possible that spall occurred after 200 MSEC. (Figures 2.10 through 2.18 show both vertical velocity and displacement. The velocity curves can be easily distinguished in two ways: the displacement curves are smoother; and the displacement curves have zero slope when the velocity is zero.) Since spall occurred at the center of the MB I-4 array, but apparently not near the center of the PHG II-1 array, it must be that spall depends not only on what explosion effects are present (e.g., directly transmitted groundshock, reflected waves, refracted waves, surface waves, and airblast), but also on the timing and relative magnitudes of these effects.

It may be that the PHG II-1 airblast suppressed spall near the center of the shot array; but under other conditions airblast (particularly the negative phase) appears to be a principal cause of spall [Ullrich (1978); Phillips, Melzer and Bratton (1979:64)]. Figure 2.19 shows a vertical velocity waveform for MB II-1 in which the negative airblast phase apparently was the main cause of near-surface uplift, followed by free fall from approximately 275 to 480 MSEC, and rejoin at 480 MSEC. Pore air model calculations appear to have predicted the general vertical velocity waveform shape quite well, but the timing somewhat less well.

## E. Consequences of Spall

[Port and Auld (1980:55)] define groundshock spall as "the physical parting of the originally intact near-surface material, under tensile forces created by stress wave interactions at the ground surface." It is evident, however, even from the relatively small amount of data already presented above, and especially from Perret's observations, that spall can occur well beneath the ground surface, and without the necessity of stress wave/surface interaction. Nevertheless, the above definition probably describes the most common type of explosion-induced groundshock spall, particularly for a near surface explosion.

Spall has several important consequences for the intelligence, the nuclear weapon effects and the earthquake engineering communities, all stemming basically from the fact that spall is a nonlinear phenomenon. For the intelligence community this means that linear methods of source characterization will be in error by some indeterminate amount, creating difficulties in estimating the energy released in an underground or surface explosion, and in discriminating between an explosion and an earthquake [Bolt (1976)]. For the nuclear weapon effects and protective construction community the nonlinear nature of spall creates serious obstacles to the use of superposition (a linear technique) for multiple burst groundshock predictions [Ullrich (1978); Phillips, Melzer and Bratton (1979: 1, 7, 8, 156, 214); Bratton (1979)]. Spall also creates obstacles to the extrapolation of HE groundshock data to nuclear yields, and generates waveforms which may require special missile shock isolation provisions [Lipner (1979)]. Finally, for the earthquake engineering community, spall creates difficulties in simulating earthquakes with HE detonations [Higgins et. al. (1979)], and in using the ground motion generated by a nuclear weapon test as an earthquake simulation [Blouin, Bratton and Bultmann (1980)].

## F. Spall Mechanisms

An explanation of groundshock spall requires consideration of two classes of spall mechanisms: one (<u>cause</u> mechanisms) includes the stress history at the point(s) under consideration, and the loading conditions which created this stress history; the other (<u>strength</u> mechanisms) includes

the ways in which rocks and soils respond to dynamic tensile stress. Both mechanisms are discussed in Chapter IV, following a further discussion of field test data in Chapter III. Chapter V discusses spall prediction, and Chapter VI contains a summary and conclusions.

## III. FIELD TEST DATA ANALYSIS

### A. Spall Identification and Prediction

In the MX groundshock environments summary, [Port and Auld (1980)] summarized recent observations on groundshock spall, following the September 1979 Defense Nuclear Agency Spall Workshop. Figures 3.1 through 3.6 show typical vertical and horizontal velocity waveforms from the PRE MINE THROW IV series of HE tests, conducted in the Yucca Flat playa in Area 6 at the Nevada Test Site [Stubbs, Kochly and Sauer (1976)]. On the basis of these and other similar data [Melzer (1979:3)] concluded that spall had occurred out to ground ranges corresponding to peak airblast overpressures of 20-50 PSI and 8-10 crater radii. Melzer used the following spall identification criteria, relying mainly on the first two:

approximately 1 g fall
rejoin (impact)
vertically distended material
    vertical separations
    vertical bulking
    vertical negative [tensile] stresses
trapped waves [propagating within a spalled slab]

Identifying spall is one thing, predicting it another; and Melzer maintained that a reliable method for predicting the depth and range of spall, for given explosive loading and site conditions, is still beyond the current state of the art. There are numerous reasons for this, but two of them are:

1. In many tests, ground motion gages have not been placed deep enough to record the depth of spall penetration. When the deepest gage records spall, there is no direct indication of how much deeper spall penetrated.
2. Airblast can cause or inhibit near-surface spall, and the influence of the negative airblast phase/pore air gradient effect depends on soil permeability.

One of Melzer's conclusions which has troubling implications for both the intelligence and the weapon effects communities is that, in addition to being caused by stress waves, spall also causes stress waves, which can propagate to distant ranges.

## B. Spall Indicators and Initiation Criteria

Figure 3.7 shows the vertical acceleration at 100 FT range and 5 FT depth from the SIMQUAKE IB HE event at McCormick Ranch, Kirtland AFB, New Mexico. From this and other similar acceleration records [Higgins (1979)] concluded that spall, as evidenced by downward accelerations at or near 1g, with a significant dwell time, had obviously occurred. However, he also noted some downward accelerations near 1g in the same event, e.g., the record shown in Figure 3.8, which may not have been spall, and commented:

> Although the first downward acceleration [at 200 ft range] is near 1g, it is not clear from this record alone whether spall has actually occurred. The fact that a downward acceleration of almost -1.7g is encountered, as well as the relatively short dwell time compared to the behavior at 100 ft suggests that tensile failure has not occurred. The second downward acceleration is only 0.6g. No spall is evident here. Note that the waveform is similar to that at 100 ft. This suggests that relatively high, "spikey" accelerations following downward accelerations near 1g are not, by themselves, evidence that spall has occurred at that point. They may, however, be a reflection of spall rejoin at ranges near to the source. This possibility has not been evaluated yet for these data.

Higgins' contention that downward accelerations at 1g do not necessarily indicate spall was based on Figure 3.9, which shows the peak magnitude of the first ($a_v^{1-}$) and second ($a_v^{2-}$) negative vertical acceleration pulses for Event SQ II(F), plotted as a function of range, for a depth of 1.52 M. This figure shows vertical accelerations at -1g in a region where spall was not thought to have occurred, as well as a vertical acceleration of only -0.8g at a point where spall was thought to have occurred. Of course, such an analysis hinges on the definition of, or identification criteria for spall. Figure 3.10 shows dwell times for the first ($t_1$) and second ($t_2$) negative acceleration pulses, for Events SQ II(B) and SQ II(F), plotted as a function of distance from the shot array, also for a depth of 1.52 M.

From this data Higgins suggested that dwell time may be a spall indicator. More specifically, he suggested that relatively long dwell times, decreasing with range at a relatively high rate, seem to indicate spall. He defined the point (range) at which the rate of decrease of dwell time with range suddenly decreases to be the extent of spall for the front array event [SQ II(F)], and used that same definition to denote the spall regime in Figure 3.9. He also noted that constant or increased inward horizontal acceleration often accompanies the second downward acceleration phase, in the near-surface region where spall occurs. Using dwell time and downward acceleration as spall indicators, he then plotted spall region boundaries for events SQ II(F) and SQ IB. These boundaries, shown in Figures 3.11 and 3.12, define the region(s) within which spall occurred following the first and second upward motions, respectively. Higgins examined several ground motion conditions preceding obvious spall at 1.52 M depth, and found two consistent pre-spall conditions. The first, which was certain in all data, was an upward vertical particle velocity in excess of 0.5 M/S. No other ground motion condition (horizontal acceleration, horizontal velocity, vertical acceleration, etc.) was always satisfied before spall occurred. The second consistent condition was vertical extensional strain of more than 0.5% at 1.52 M depth. In Figures 3.13 and 3.14, which show how Higgins obtained the above spall initiation criteria, $V_v^1$ is the peak upward vertical particle velocity just before the first downward vertical acceleration pulse ($a_v^{1-}$), and $V_v^2$ is the peak upward vertical particle velocity just before the second downward vertical acceleration pulse ($a_v^{2-}$). These figures show that both peak upward vertical particle velocity and peak average vertical extensional strain at 1.52 M depth were not only steadily decreasing functions of range, as were the dwell times used to define spall in Figure 3.10, but also each reached about the same value in both events, at the range at which the dwell time slope discontinuity occurred. It was their consistent behavior with respect to both slope, and value at the defined spall limit, that led Higgins to propose peak upward vertical particle velocity and peak vertical extensional strain as spall initiation criteria. His data supported the following conclusions:

Spall, in the context of tensile failure, is characterized by downward accelerations near 1g with relatively long dwell times (compared with characteristic times in the region where spall does not occur), and high rejoin accelerations.

Spall, in the context of tensile failure, occurs in the alluvium at McCormick Ranch when upward vertical particle velocities exceed 0.5 M/S and/or when vertical strains exceed about 0.5%. (Tensile strength of 35-70 PSI implied).

The above criteria appear to be valid without regard to the specific wavefield structure causing the upward particle motion, i.e., spall will occur in above-ground and buried explosions, as well as earthquakes, if some threshold upward velocity is exceeded.

C. Spall Radius

Although there remain difficulties in formulating a dimensionless relationship which will predict the extent of spall under general conditions, some estimates of spall extent have been made for past nuclear and high explosive events, which can help in formulating such a relationship. Figure 3.15 shows two proposed relationships between spall radius and weapon yield, for twenty-two contained nuclear events [Viecelli (1973); Sobel (1978); Port and Auld (1980: 57-58)]. The difference between the two plots is due mainly to different definitions of spall radius. Viecelli used the definition formulated earlier by [Eisler and Chilton (1964)], in which spall radius is the range corresponding to the minimum spall rejoin wave arrival time. Sobel, on the other hand, defined spall radius as the smallest range beyond which the time difference between first arrival and spall rejoin signal arrival is constant. [Port and Auld (1980)] observed that both definitions are subjective, and neither is very accurate for building a predictive model. Despite their differences, the two plots both yield the same general conclusions:

1. Spall radii for megaton-level, contained nuclear shots can exceed a few thousand meters.
2. The factor of uncertainty in spall radius is approximately three.
3. Spall radius scales approximately as the cube root of yield.

[Rinehart (1979)] reviewed HE data from the PRE-MISERS BLUFF Phase II series, in an attempt to relate spall radius to depth of burst, particularly for near- and on-surface bursts. He assumed that spall had occurred if the slope of the vertical velocity curve was -1g or (algebraically) less. Neither negative acceleration dwell time nor upward rejoin was used as a spall criterion. It was not possible to derive an analytical expression for spall radius as a function of depth of burst. However, Rinehart did note that the surface tangent charge produced spalling at much greater range than any other charge. He suggested this was due to complex interaction between spalling induced by upstream airblast-induced effects and the reflected waves from the local airblast. He also suggested that pore air effects may play a strong role in causing [near-surface] spall for surface tangent HE events. Because of the sensitivity of spall radius to depth of burial, data for contained bursts are of limited use in predicting spall radius for near- or on-surface bursts.

## D. Influence of Airblast

Figures 3.16 and 3.17 illustrate the dramatic influence of airblast on spall radius for a surface tangent HE burst [Stump and Reinke (1980)]. Figure 3.16 shows the extent of spall in Event PHG I-6, an 84 LB HE single burst surface tangent shot, detonated in a bermed configuration to suppress local airblast effects [Babcock (1980 I)]. Figure 3.17 shows the extent of spall in Event PHG I-7, a 256 LB HE single burst surface tangent shot (without berm), designed to couple the same amount of energy directly to the ground as that coupled in Event PHG I-6 [Babcock (1980 I)]. The close-in spall region in both events was about the same, indicating that the direct energy coupling equivalence design goal had been achieved. Even more significant, however, is the dramatic increase in spall radius in Event PHG I-7, due to airblast. In fact, Stump and Reinke noted that the airblast-coupled motion at all ranges, particularly near the surface, dominated the ground motion. Of course, the details of Figures 3.16 and 3.17 depend on the criteria used to identify spall. [Stump and Reinke (1980:35)] used the following spall identification criteria:

PRIMARY CRITERIA

1. -1g (-0.5 to -2.0) vertical acceleration dwell (identifiable directly on a vertical acceleration plot, or as the slope of a velocity time plot)
2. impulsive rejoin signal on all (i.e., both vertical and horizontal) components.
3. horizontal acceleration dwell NOT necessary.

SECONDARY CRITERIA

4. dwell time
5. rejoin amplitude

Numerical values for criteria 2, 4 and 5 were not specified. No matter what spall criteria are used, it seems likely that spall radius will scale with $(\text{yield})^{1/3}$ as does airblast pressure, and so will close-in spall depth; but because the pore air effect involves both diffusion and wave propagation effects, spall depth at large range may not scale with $(\text{yield})^{1/3}$.

E. Spall From Multiple Bursts

Spall in a multiburst situation is even more complex than in a single burst situation, as has already been noted. Whether spall occurs at all depends not only on whether airblast is present, but on the timing of the airblast and the various other directly induced groundshock effects. In a bermed, multiburst situation, where local airblast is absent, spall appears to be greatly enhanced, as compared to a bermed, single burst situation [Stump and Reinke (1980:37)].

F. Spall Without Prior Upward Velocity

A particularly interesting feature of the vertical waveforms at and near array center for shots PHG II-2 and II-3, shown in Figures 3.18 and 3.19, was an apparent spall condition at depth with little or no prior upward acceleration [Babcock (1980 II); Ake (1980); Stump and Reinke (1980:39)]. Both events used six 256 LB surface tangent, spherical, bermed

HE charges in a hexagonal configuration. PHG II-3 was essentially a repeat of PHG II-2, but without sand charge bedding, and using alternate sand and grout gage columns instead of all sand gage columns, at a site about 200 YDS from the PHG II-2 site. Both shots yielded essentially the same results at locations where both shots had gages. Figure 3.20 shows the extent of spall in Event PHG II-2, insofar as definable by available gages, and Figure 3.21 shows similar but sparser data (due to lack of gages) for Event PHG II-3. Figure 3.20 contains data along both charge lines and bisectors, out to a radius of 5 M from array center; beyond 5 M the data is for charge lines. Although identically placed gages did not all give identical results, Stump and Reinke found no obviously significant difference between spall/no spall results, for radii less than 5 M, between charge lines and bisectors. Figure 3.21 contains data for bisectors only.

## G. Summary

The above overview of field test data shows that groundshock spall is a common occurrence, particularly for HE detonations. However, a single definition of spall has yet to be adopted by all or even most investigators. Although spall is most likely to occur near a free surface, it can and frequently does occur at depth. The occurrence of spall is strongly influenced by site geology, and by both the presence and timing of airblast. Because it involves tensile failure, spall is, by its very nature, a highly nonlinear phenomenon, and therefore superposition approaches to spall prediction have had only very limited success.

[Lipner (1979)] has suggested that spall and other tensile-failure related effects that are significant in high explosive tests are much less important for nuclear conditions, but this has yet to be proven. Even if it were true, spall still must be understood, because the principal experimental means of nuclear explosion groundshock study, at least for the United States, is high explosive simulation.

## IV. SPALL MECHANISMS

### A. Basic Phenomenology

Groundshock spall is caused by tensile failure of rock or soil under intense stress wave propagation conditions. Spall commonly results in a rock mass or soil particles becoming separated from supporting material beneath, undergoing ballistic motion under the influence of gravity, and finally impacting the material beneath to reestablish vertical support.

In principle, spall can be described by a system of partial differential equations which express three conditions:

1. Newton's second law of motion
2. Stress-strain behavior (including tensile separation or fracture)
3. Strain-displacement relations

In practice, when a theoretical analysis of spall is attempted, a simple (often linearly elastic) stress-strain relation is assumed in order to calculate the stress history at points of interest. Then a tensile strength criterion is employed to determine whether spall will occur. What this approach sacrifices is the ability to predict spall-induced motions. However, one frequently wants simply to define the extent of spall, so as not to locate a structure inside the spall region, or so as to define an explosive "source region", beyond which material response can be considered elastic. This approach is similar to that still used in the ultimate strength design of reinforced concrete framed structures.

### B. Material Tensile Stress-Strain Behavior

One conclusion reached at the 1979 DNA Spall Workshop was that the state of the art for modeling the tensile behavior of material is not the limiting factor in predicting spall motions. The main difficulty in calculating spall from near-surface detonations was held to be the difficulty in accurately predicting the stress waves causing spall. Geometrically simple spall experiments were called for, to evaluate and develop adequate spall prediction techniques.

Although the above argument regarding the state of the art for modeling the tensile behavior of material appears reasonable at first glance, it needs closer examination, in light of the three basic sets of equations which describe stress wave propagation and spall. If lack of knowledge of material tensile behavior is not the limiting factor in predicting spall motions, then the limiting factor must be either lack of knowledge of Newton's second law or lack of knowledge of the geometry of strain, both of which are material independent. But if any aspects of dynamic material behavior are well understood, they are Newton's second law and the geometry of strain. Therefore it must be that lack of knowledge of material tensile behavior is the limiting factor in predicting spall motions. The problem here lies in not being specific about what is meant by tensile behavior. Tensile strength behavior may be relatively well understood, thus permitting one to predict whether spall will occur under given stress conditions. But what is not well enough understood is the tensile stress-strain behavior of soil. This inadequate understanding severely limits one's ability to predict the stresses which cause spall, and the ground motions accompanying spall. Significant progress in understanding and predicting spall in soil therefore depends on advancing the state of the art for modeling the tensile stress-strain behavior of soil.

The principal question regarding the theoretical, calculational approach to spall in soil is whether a continuum material model of some sort can provide spall predictions of acceptable accuracy. The alternative, a particulate computational model, would require an extensive amount of effort to develop, and hopefully will not be necessary.

## C. Classes of Spall Mechanisms

[Rinehart (1975:207)] assesses the factors which influence spall as follows:

> Whether spalling occurs at all, and where the fracture or fractures are located depend upon three factors: the resistance of the material to fracture; the magnitudes of stress in the stress wave; and even more important, the shape of the stress wave.

The first of the above factors is herein referred to as strength mechanisms, and the latter two are called cause mechanisms. Separating spall mechanisms into strength mechanisms and cause mechanisms is fundamentally artificial. Nevertheless, it is convenient, provided the pivotal role of material stress-strain behavior is kept in mind.

## D. Tensile Strength Mechanisms

Time-dependent fracture models have been developed for complicated materials used for reentry vehicles, as well as for some geologic materials [Curran (1979); Grady (1979); Port and Auld (1979)]. However, determination of tensile strength parameters for these models requires extensive laboratory testing. [Zelasko (1979)] noted that no significant amount of tensile failure testing has been conducted for any near-surface soils at the various test sites, or at sites of strategic interest for current or future ICBM systems. He indicated that a standard tensile test for soils does not exist, and that most tensile test procedures require the theory of elasticity or plasticity to deduce the tensile stress state in soil at the time the specimen fails. He advocated a program to develop suitable laboratory or insitu test techniques to obtain data for developing tensile failure models of near-surface materials.

First of all, the conceptual framework for describing soil strength and/or stress-strain behavior under any stress system, including tension, should be that of effective stress [Merkle (1971)]. Zelasko's data appear to have been reported using total stress. The several tensile test schemes described by Zelasko give results which, when viewed in terms of effective stress, appear to be fairly consistent with results of other compressive, shear, or true triaxial tests. It is therefore not clear that special (and generally more difficult) tensile tests are worth the effort, although [Thorne, Tovey and Bryant (1980)] have recently described a new recording unconfined tension tester for soil. Second, what is needed is soil test data obtained specifically to assess the accuracy of a proposed general triaxial stress-strain model, not restricted to any particular stress state. Third, such a stress-strain model must be of such a form that it can be incorporated in a finite difference or finite element computer program. The computer program can be used to predict the static and dynamic behavior

of soil masses larger than the test specimens used to obtain the stress-strain model parameters, and the predicted behavior can then be checked by independent measurements.

Although metal rods have been used to illustrate the static behavior of a loaded soil mass [e.g., Lambe and Whitman (1969:190, 197)], similar models have not yet been developed for studying spall in granular material. However, a very simple demonstration of spall in a granular material can be performed by striking the bottom of a half-full peanut jar with the palm of the hand. Approximately the top half of the peanuts fly upward, each losing contact with its original neighbors, and finally falling back to rest in approximately its original position. Spall in soil probably occurs in somewhat the same manner. Individual soil particles become separated from each other and undergo rigid body motion under the action of gravity. During this period the soil is said to be in a distended state. It behaves like a fluid, because although the particles are separated from one another, their separation distance (mean free path) is of the same order of magnitude as the particle dimensions. The distended medium is capable of transmitting a dilatation wave by successive particle collisions, but cannot transmit a rotational wave.

In summary, the two basic strength mechanisms of spall are fracture in a competent rock or cemented soil, and distension in a granular material. A knowledge of generalized dynamic stress-strain behavior in soil, including the distension phase, is needed to be able to accurately predict the occurence of and motions associated with spall in soil.

## E. Cause Mechanisms in General

Spall cause mechanisms, i.e., the dynamic stress states which lead to spall, are numerous and often complex. The most common are those associated with reflection of a compressive wave from a stress-free boundary in a brittle, elastic material. The remarks of [Kolsky (1953:183)] are still applicable:

> The fractures produced by stress pulses differ from those produced 'statically' for several different reasons. First, since the velocity of crack propagation is generally considerably lower than the velocity of propagation of the pulse, ... for pulses of short duration any cracks that are formed do not have time to grow before

> the pulse has passed on and the stress has been removed. Secondly, with a short pulse only a small part of the specimen is stressed at any one time and fractures may form in one region of a specimen quite independently of what may be occurring elsewhere. Thirdly, ... when a compression pulse is incident on a free boundary it gives rise to a reflected tension pulse, whilst when it is reflected obliquely both a dilatational and a distortional pulse are produced. The interference of such reflected pulses may ... give rise to very complicated stress distributions, and the superposition of several reflected pulses may produce stresses which are sufficiently large to cause fracture when the amplitude of the incident pulse was too small to do so. Lastly, ... the dynamic elastic behaviour of many solids may differ considerably from that observed statically, and at the very high rates of loading associated with intense stress pulses, materials which are normally regarded as ductile may behave in a brittle manner.

Obviously Kolsky's remarks cover both cause and strength mechanisms, emphasizing that the two are in reality inseparable.

F. Surface Waves

Surface (Rayleigh) waves play a key role in causing near-surface spall in granular material, and are associated with both the direct- and the airblast-induced phases of NE and HE explosive loadings. [Bleich (1964)] analyzed the dynamic response of a simple mechanical model of a granular material, and concluded that surface disintegration (= distension) is possible, and will occur if a problem has no mathematical solution for which the pressure acting on the surface vanishes. The outward acceleration of surface particles produces (or requires) a reactive pressure, which in turn produces in the interior a state of stress satisfying the Coulomb shear strength condition. See also [Bleich and Heer/AFSWC (1963); and Bleich and Heer/ASCE (1968)]. For discussions of surface waves on an elastic half space, and their role in explosive groundshock, see [Kolsky (1953:16); Baron and Lecht (1961); Baron and Check (1963); Baron, Bleich and Wright (1967); Coates (1967:8-54); Richart, Hall and Woods (1970:80); Rinehart (1975:Ch 8); and Auld and Murphy (1979)]. It should be noted that although the Rayleigh wave is often treated as a separate kind of wave, it is basically a combination of dilatational and rotational waves, as the derivation of the apparent Rayleigh wave velocity clearly shows. The

most important feature of the Rayleigh wave, in a spall context, is the large near-surface vertical tensile stresses which it causes.

## G. Crater Related (Direct Induced) Motion

Even under surface or near-surface burst conditions, spall is not necessarily confined to the near-surface region, as extent of spall plots clearly show. One possible explanation for spall in the zone surrounding the crater of a near-surface burst is that the soil particles in the near-crater zone tend initially to undergo the same kind of motion as do those particles which are actually thrown out to form the crater. By definition, the particles initially occupying the crater volume are thrown up and out; while those in the near-crater zone first move in the same general direction as those thrown out, but eventually fall back to approximately their original location. The falling back process is likely to produce spall-type accelerations, since gravity is the principal agent.

Crater related (or direct induced, so-called "DI") motions are characterized by a vertical velocity waveform having a single upward phase, followed by a single downward phase, as shown in Figure 4.1 [Hurdle and Port (1977)]. For some reason the formulae commonly quoted for this crater related waveform do not actually yield the desired waveform. A complete analysis of the crater related waveform is given in Appendix A.

## H. Spall Without Prior Upward Velocity

It is fairly easy to visualize how spall can occur in granular material near a free-surface, when the particles are given initial upward momentum, then fall back to a residual position under the influence of gravity. However, when particles near the center of a multiburst, bermed array undergo spall (i.e. negative 1 g acceleration dwell, followed by an apparent impact rejoin) with little or no prior upward acceleration, as shown in Figures 3.18 and 3.19, the cause mechanism is not nearly so obvious. For a soil particle to undergo vertical free fall from rest, *without first* having acquired upward momentum, the soil beneath the particle in question must first have been pulled down, to give the particle in question space below into which it can fall. Figure 4.2 [Baron, Bleich and Weidlinger

(1960, 45)] suggests that such motion is possible. Shown is the vertical displacement, w, of points in an elastic halfspace subsequent to application of a unit step concentrated vertical load, H(t), on the halfspace surface. The load is applied at the origin of polar coordinates (r, z) as shown in the figure, and c is the dilatational wave velocity. Points near the surface undergo initial upward motion prior to being shoved downward, but points at greater depth, $z \geq z_1$, undergo only downward motion. Since for any given radius, r, there is a finite depth, $z_2$, for which the instantaneous vertical displacement, w, is a maximum, (because $w = 0$ @ $z = \infty$), there must be a column of material above that depth for which $\frac{\partial w}{\partial z} > 0$, and which is therefore in tension. It follows that soil elements for which $z_1 < z < z_2$ are in vertical tension, and therefore tending to spall, and yet have not experienced any prior upward displacement, which is the type of motion shown in Figures 3.18 and 3.19. If soil were linearly elastic, the motions shown in Figure 4.2 would be enhanced by stress wave convergence and superposition near the center of a multiburst array. This probably happens in real soil to some extent, even though it is far from being linearly elastic.

I. Pore Air Expansion

A related mechanism which most nearly addresses the multiphase nature of soil is called pore air expansion [Ullrich (1978)]. The equations describing the pore air expansion effect, in their original form, were the result of an attempt to explain slow propagation velocities and high accelerations at late times, observed in the MISER'S BLUFF Phase I series of HE tests. The original equations treated soil as a heavy gas composed of compressible massless air, and disconnected, incompressible solid particles which comprise the entire soil mass. The assumption (although not stated in the above reference) was that the particulate soil skeleton had already spalled, hence the soil particles were not in contact and offered no resistance to volume change (except for inertia). While the original model yielded reasonably slow values for the dilatational wave velocity in distended soil, it also yielded similar velocities for unstrained soil. A derivation of the original pore air expansion equations, using standard soil mechanics terminology, is given in Appendix B. Pore air expansion

appeared to be the principal mechanism invalidating ground motion predictions using superposition, for near-surface measurements interior to the shot array in event MB I-4 [Ullrich (1978:5)]. Figure 4.3 shows the vertical velocity measured in MB I-4 at a depth of 1.5 FT near array center, compared with the band of superimposed waveforms from event MB I-2 (a single burst event), which had been used to predict the MB I-4 waveform. Superposition failed to predict four important features of the MB I-4 waveform in Figure 4.3, viz.:

1. the magnitude of the peak negative velocity at 25 MS (underpredicted),
2. the magnitude of the peak positive velocity at 50 MS (overpredicted),
3. the magnitude of the downward acceleration following the first positive velocity peak (grossly overpredicted), and
4. occurrence of a major upward velocity pulse from 50 to 140 MS, followed by a major downward velocity pulse from 140 to 260 MS.

Ullrich ascribed the first superposition prediction failure to airblast overpressure enhancement, the second to soil inelasticity (reduced rebound), the third to spall (without identifying a specific cause mechanism), and the fourth to pore air expansion. Essentially, Ullrich's argument regarding the fourth case was that the soil, being in a quick condition due to spall, responded to the negative and second positive airblast phases as a heavy gas. It would appear that the fourth superposition failure was "set up" by the third. Had the near-surface material not been in a distended condition at the time the airblast negative phase arrived, the major upward and subsequent downward velocity pulses between 50 and 260 MS would not have been nearly so large. Figure 4.4 was used to connect the observed major upward velocity pulse with the airblast negative phase, and together with Figure 4.5 was used to estimate the rate at which the uplifting effect of the airblast negative phase propagated into the distended ground (about 60-75 FPS for MB I-4 and 50 FPS for MB I-8). Figure 4.5 also indicated the rate at which the initial effect of the airblast second positive phase propagated into the further distended ground in

MB I-8 (about 39 FPS). These velocities compare favorably with those calculated in Appendix B. The greatly increased compressibility of soil in its distended state is believed to account for the fact that the airblast second positive phase (which had a peak overpressure an order of magnitude less than the first positive phase) caused large accelerations, and a downward velocity change comparable to that caused by the first positive phase.

Despite the success of the pore air expansion equations in predicting the dilatational wave propagation velocity and associated motions in distended soil, it is questionable whether pore air expansion is a separate mechanism from that of spall. This is because the disturbance which initially causes the soil skeleton to become distended propagates much faster in the undistended soil skeleton than in the initially entrained pore air. Thus it is not expansion of the initially entrained pore air that distends the soil skeleton, but a stress wave traveling in the soil skeleton itself. Unlike pore water in a saturated soil, the initially entrained pore air offers little resistance to soil skeleton expansion, and undergoes a relatively small pressure change when the soil skeleton does expand. If the above analysis is correct, preliminary ideas concerning the degree of time dependence of pore air expansion as a mechanism, plus its depth limitation due to overburden weight and underpressure magnitude, and effects of pore air flow and soil tensile strength will need to be reexamined. It is not at all clear that spall will be less important for producing ground motion at dimensions and yields of strategic interest than in small scale HE tests. Since the issue was raised over 40 years ago by Fillunger, and responded to by Terzaghi, Frohlich and Heinrich, very little attention has been paid to the coupling of inertia and flow effects when soil changes volume [Terzaghi and Frohlich (1937); Heinrich (1938); Terzaghi (1943;272)]. The issue now needs to be looked at thoroughly.

## V. SPALL PREDICTION

At present there is no generally accepted method for predicting explosion-induced spall in soil, either from a contained or a surface explosion. Spall indicators, such as peak extensional strain and peak upward velocity, suggested by Higgins, appear to hold promise as spall predictors. However, being able to correlate a particular value of peak measured extensional strain with the occurrence of spall, as defined by measured acceleration and/or velocity waveform features, is one thing; being able to predict the occurrence of extensional strain exceeding that particular value (or the satisfaction of some other strain failure criterion) is quite another. The latter constitutes predictive capability.

Although a spall prediction technique is not yet at hand, the general shape of the spalled region for a near-surface burst, both with and without air blast, is fairly well understood. For both, there will be a bowl-shaped region surrounding the burst, within which spall will occur as a result of direct-induced motion. When airblast is also present, there will be a saucer-shaped region at the surface, surrounding the bowl, within which spall will occur as a result of the airblast. The pore air effect is important in this region. The radius and depth of the bowl, and the radius of the saucer will probably scale as $(\text{yield})^{1/3}$. Whether the depth of the saucer, or wing, will scale as $(\text{yield})^{1/3}$ is not yet clear because the physics of airblast-induced spall is not yet well understood.

When available, spall prediction techniques will probably follow a sequence similar to the following:

1. Define a strain failure (spall) criterion.
2. Using test results and/or a wave propagation computer code, predict when and where the strain failure (spall) criterion will be satisfied.
3. Use a modified constitutive equation for spalled material to predict motions and pressures while the material is in a spalled condition.

4. Present spall predictions in the form of extent of spall plots with peak motion contours, plus representative time domain motion waveforms and shock response spectra.

## VI. SUMMARY AND CONCLUSIONS

Previous chapters have examined the present state of the art on explosion-induced spall in geologic materials, especially spall in soil due to near-surface explosions. Specific aspects of spall examined have been its occurrence in nuclear and high explosive tests; spall mechanisms; and current spall prediction capability.

At present there is neither a generally accepted, precise, technical definition of, nor a generally accepted technique for predicting spall in soil. However, it is generally agreed that spall in soil is associated with tensile failure, i.e., a distended condition, in which soil particles become separated from each other and behave as separate particles in air, rather than as a particulate skeleton with air as the pore fluid.

No single mechanism causes spall in soil under all explosive loading conditions. Under any particular explosive loading condition, spall in soil can be caused by interaction of stress waves with a free surface, stress wave convergence within a soil mass, or simply the shape of a single propagating stress wave (often the unloading portion of a compressive wave). Spall is strongly influenced by local geologic structure.

Being a highly nonlinear phenomenon, and causing a sudden, drastic change in stress-strain behavior, spall generally invalidates multiburst superposition techniques for ground motion prediction. In addition, the impact rejoin phase, which generally terminates a spalled condition, often generates high frequency waveform components which can propagate to far ranges, but which are not representative of the original explosive pressure disturbance which caused the spall. In this sense, spall converts explosive energy from a low frequency signal to a higher frequency signal.

More detailed conclusions follow:

1. The most consistent symptom of spall is a -1 g vertical acceleration dwell, observable directly on an acceleration record, or indirectly as the slope of the corresponding integrated velocity record.

2. Generally the -1 g dwell is terminated by a sharp upward acceleration spike, called impact rejoin. This is caused by individual soil particles suddenly impacting other particles beneath, which are no longer in a distended condition.

3. Because gravity acts only vertically, the horizontal motion response of spalled soil is less consistent than its vertical response. However, being in a distended condition, spalled soil should exhibit the same relatively large horizontal accelerations and velocity changes under small horizontal stress gradients as it does vertically under small vertical stress gradients, and the same relatively slow apparent horizontal propagation velocity. Ullrich's heavy gas constitutive equation for spalled soil should be as applicable in the horizontal as in the vertical direction.

4. The direction in which spall features (especially impact rejoin) appear to propagate reflects not only the direction of propagation of the stresses causing spall, but also the magnitude of peak interparticle separations while the material is in a spalled condition, and thus the time for recovery (rejoin).

5. Soil spall data for contained explosions comes mainly from nuclear tests, while that for near-surface explosions comes almost entirely from high explosive tests. There is thus very little geometrically consistent spall data on which to base an HE/NE spall scaling relation.

6. The occurrence and extent of spall depend not only on what mechanisms are present, e.g., directly transmitted waves, reflected waves, refracted waves, surface waves, and airblast, but also on both their timing and relative magnitudes.

7. Although stress wave interaction with a free surface is perhaps the most common cause of spall, spall in soil can occur at depth, and without prior upward movement.

8. Spall radii for megaton-level contained nuclear shots can exceed a few thousand meters, with an uncertainty factor of approximately three.

9. Because of airblast, spall radius is extremely sensitive to depth of burial. Therefore, data from contained bursts are of limited use in predicting spall radius for near- or on-surface bursts.

10. For a particular NE or HE burst geometry, spall radius and direct-induced spall depth probably scale approximately as $(\text{yield})^{1/3}$, but the probable scaling relation for airblast-induced spall depth is not yet known.

11. It is not yet clear whether spall is as important for nuclear yields as for high explosive yields, because of the lack of geometrically consistent data for both kinds of tests, and because the energy release rate

and mass of explosion products vary between the two, for a given yield. However, even if spall were less significant for nuclear yields, it would still be essential to thoroughly understand HE-induced spall, because HE is currently the only feasible method of simulating NE-induced groundshock.

12. The major barrier to an improved understanding of explosion-induced spall in soil is an inadequate understanding of soil tensile stress-strain behavior.

## APPENDIX A

### Formulae for Crater Related (Direct Induced) Vertical Velocity Waveform

Figure 4.1 shows a typical crater related (direct induced) vertical velocity waveform (Hurdle and Port (1977:14). It has a single upward phase, followed by a single downward phase, with the two phases being of approximately equal duration, $t_p$. The formulae usually quoted for this crater related waveform are the following:

$$t_1 \leq t \leq t_2 \qquad v = v_2 \sin \frac{\pi}{2} \left( \frac{t}{t_2 - t_1} \right) \tag{A-1}$$

$$t_2 \leq t \leq t_3 \qquad v = v_2 \cos \frac{\pi}{2} \left( \frac{t - t_2 + t_1}{t_3 - t_2} \right) \tag{A-2}$$

$$t_3 \leq t \leq t_4 \qquad v = - v_2' \sin \frac{\pi}{2} \left( \frac{t - t_3 + t_1}{t_4 - t_3} \right) \tag{A-3}$$

$$t_4 \leq t \leq t_5 \qquad v = - v_2' \left[ \left( 1 - \frac{2}{\pi} \right) \cos \frac{\pi}{2} \left( \frac{t - t_4 + t_1}{t_5 - t_4} \right) + \frac{2}{\pi} \right] \tag{A-4}$$

$$t_5 \leq t \leq t_6 \qquad v = - \frac{2}{\pi} \left[ 1 - \sin \frac{\pi}{2} \left( \frac{t - t_5 - t_1}{t_6 - t_5} \right) \right] \tag{A-5}$$

where

$$t_1 = \text{time of arrival of direct wave} \tag{A-6}$$

$$t_2 = t_1 + 0.1\ t_p \tag{A-7}$$

$$t_3 = t_1 + t_p \tag{A-8}$$

$$t_4 = t_1 + 1.1\ t_p \tag{A-9}$$

$$t_5 = t_1 + t_4 + \frac{2}{\pi}\ (t_6 - t_4) \tag{A-10}$$

$$t_6 = 2t_p \tag{A-11}$$

The intent of Equations (A-1) through (A-11) is clear: to fit portions of sine or cosine waves to the waveform of Figure 4.1. However, the above formulae do not actually yield the desired waveform, and if they were to be incorporated into a computer code the results would be in error.

The above formulae should read as follows:

$$t_1 \leq t \leq t_2 \qquad v_{12} = v_2 \sin \frac{\pi}{2} \left( \frac{t-t_1}{t_2-t_1} \right) \tag{A-1'}$$

$$t_2 \leq t \leq t_3 \qquad v_{23} = v_2 \cos \frac{\pi}{2} \left( \frac{t-t_2}{t_3-t_2} \right) \tag{A-2'}$$

$$t_3 \leq t \leq t_4 \qquad v_{34} = - v_2' \sin \frac{\pi}{2} \left( \frac{t-t_3}{t_4-t_3} \right) \tag{A-3'}$$

$$t_4 \leq t \leq t_5 \qquad v_{45} = - \alpha v_2' - (1-\alpha)\ v_2' \cos \frac{\pi}{2} \left( \frac{t-t_4}{t_5-t_4} \right) \tag{A-4'}$$

$$t_5 \leq t \leq t_6 \qquad v_{56} = - \beta v_2' \sin \frac{\pi}{2} \left( \frac{t_6-t}{t_6-t_4} \right) \tag{A-5'}$$

where

$$t_1 = \text{time of arrival of direct wave} \tag{A-6}$$

$$t_2 = t_1 + 0.1\ t_p \tag{A-7}$$

$$t_3 = t_1 + t_p \tag{A-8}$$

$$t_4 = t_1 + 1.1\ t_p \tag{A-9}$$

$$t_5 = t_4 + \frac{2}{\pi}(t_6 - t_4) \tag{A-10'}$$

$$t_6 = t_1 + 2\ t_p \tag{A-11'}$$

The constants $\alpha$ and $\beta$ in Equations (A-4') and (A-5') are determined by matching the ordinate and slope of the two velocity curves at time $t_5$, as follows:

@ $t = t_5$

$$v_{45} = -\alpha v_2' \tag{A-12}$$

$$\dot{v}_{45} = \frac{\pi(1-\alpha)v_2'}{2(t_5 - t_4)} \tag{A-13}$$

$$v_{56} = -\beta v_2' \sin \frac{\pi}{2}\left(\frac{t_6 - t_5}{t_6 - t_4}\right) \tag{A-14}$$

$$\dot{v}_{56} = \frac{\pi\beta v_2'}{2(t_6 - t_4)} \cos \frac{\pi}{2}\left(\frac{t_6 - t_5}{t_6 - t_4}\right) \tag{A-15}$$

Now let $$t_5 - t_4 = \phi(t_6 - t_4) \tag{A-16}$$

and

$$\frac{\pi}{2}\left(\frac{t_6 - t_5}{t_6 - t_4}\right) = \frac{\pi}{2}(1-\phi) = \theta \tag{A-17}$$

Matching velocities and accelerations at time $t_5$ yields

$v_{45} = v_{56}$: $$- \alpha v_2' = - \beta v_2' \sin \theta \tag{A-18}$$

$\dot{v}_{45} = \dot{v}_{56}$: $$\frac{\pi(1-\alpha)v_2'}{2\phi(t_6-t_4)} = \frac{\pi\beta v_2'}{2(t_6-t_4)} \cos \theta \tag{A-19}$$

Equations (A-18) and (A-19) reduce to

$$\left.\begin{aligned} \alpha - \beta \sin \theta &= 0 \\ \alpha + \beta\phi \cos \theta &= 1 \end{aligned}\right\} \tag{A-20}$$

so that

$$\beta(\phi \cos \theta + \sin \theta) = 1$$

$$\beta = \frac{1}{\phi \cos \theta + \sin \theta} \tag{A-21}$$

$$\alpha = \frac{\sin \theta}{\phi \cos \theta + \sin \theta} \tag{A-22}$$

If $$\phi = \frac{2}{\pi} \tag{A-23}$$

then

$$\theta = \frac{\pi}{2}\left(1 - \frac{2}{\pi}\right) = \frac{\pi}{2} - 1 = 0.5708 \tag{A-24}$$

so that

$$\sin \theta = 0.5403 \tag{A-25}$$

$$\cos \theta = 0.8415 \tag{A-26}$$

$$\beta = 0.9294 \tag{A-27}$$

$$\alpha = 0.5021 \tag{A-28}$$

In some instances it may be desirable to use a single formula to fit the entire crater related vertical velocity waveform. One possible formula is

$$v = - A \left[ e^{- \alpha(t-t_1)} - e^{- \beta(t-t_1)} \right] \cos \frac{\pi(t-t_1)}{2t_p} \qquad \text{(A-29)}$$

The constants A, $\alpha$, $\beta$, t, and $t_p$ in Equation (A-29) can be found from the time of arrival ($t_1$); upward phase duration ($t_p$); time of upward and downward peaks and magnitude of upward peak (A, $\alpha$ and $\beta$).

APPENDIX B

Propagation Velocity in Spalled Soil

It is assumed that the soil skeleton is distended, and therefore occupies volume but carries no load. Thus the material can transmit hydrostatic pressure but not shear, and the total hydrostatic pressure equals the air pressure. The effective stress is zero.

$$\bar{p} = p - p_A = 0 \qquad \text{(B-1)}$$

where

$\bar{p}$ = effective (intergranular) pressure

$p$ = total pressure

The standard soil phase diagram applies.

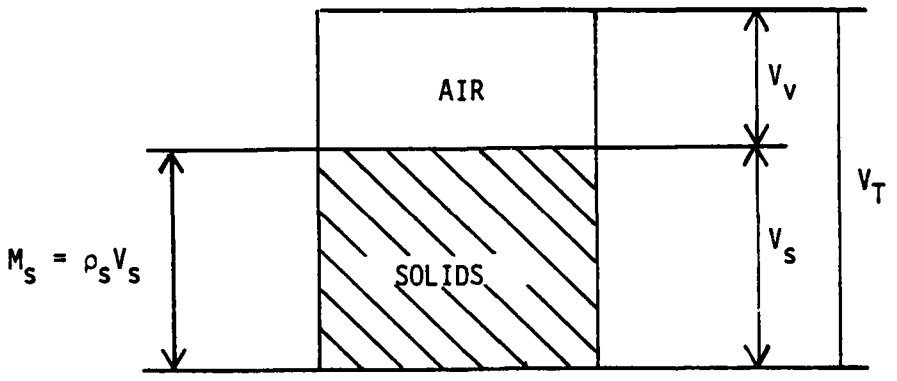

For rapid pressure changes, the relation between pore air pressure and pore air (void) volume is the adiabatic equation

$$pV_v^{\gamma} = p_o V_{vo}^{\gamma} = \text{constant} \tag{B-2}$$

where $\gamma = 1.4$ for air.

By definition, the soil porosity, n, is the ratio of the volume of voids, $V_v$, to the total volume, $V_T$.

$$n = \frac{V_v}{V_T} \tag{B-3}$$

When the soil undergoes expansion, the volumetric strain is

$$\varepsilon = \frac{V_T - V_{To}}{V_{To}} = \frac{(V_s+V_v) - (V_s+V_{vo})}{V_{To}} = \frac{V_v - V_{vo}}{V_{To}}$$

$$= \frac{V_{vo}}{V_{To}} \left( \frac{V_v}{V_{vo}} - 1 \right) = n_o \left( \frac{V_v}{V_{vo}} - 1 \right) \tag{B-4}$$

Therefore, the ratio of current to initial void (air) volume is

$$\frac{V_v}{V_{vo}} = 1 + \frac{\varepsilon}{n_o} \tag{B-5}$$

and therefore Equation (B-2) can be written in the form

$$p = p_o \left( \frac{V_v}{V_{vo}} \right)^{-\gamma} = p_o \left( 1 + \frac{\varepsilon}{n_o} \right)^{-\gamma} \tag{B-6}$$

The bulk modulus for spalled soil is therefore

$$E_c = -\frac{dp}{\frac{dV_T}{V_T}} = -\frac{dp}{\frac{dV_T}{V_{To}}} \cdot \frac{V_T}{V_{To}} = -\frac{dp}{d\varepsilon}(1+\varepsilon)$$

$$= \frac{\gamma p_o}{n_o}(1+\varepsilon)\left(1+\frac{\varepsilon}{n_o}\right)^{-(\gamma+1)} \qquad \text{(B-7)}$$

The soil density is

$$\rho = \frac{M_s}{V_T} = \frac{\rho_s V_s}{V_T} = \frac{\rho_s V_s}{V_{To}(1+\varepsilon)} = \frac{\rho_s(1-n_o)}{1+\varepsilon} \qquad \text{(B-8)}$$

Therefore the dilatational wave velocity is

$$c = \sqrt{\frac{E_c}{\rho}} = \left[\frac{\gamma p_o}{\rho_s n_o(1-n_o)}\right]^{\frac{1}{2}}(1+\varepsilon)\left(1+\frac{\varepsilon}{n_o}\right)^{-\frac{\gamma+1}{2}} \qquad \text{(B-9}$$

Typical values for $\rho_s$, $n_o$ and $p_o$ are

$$\rho_s = 5.23\ \frac{\text{LB SEC}^2}{\text{FT}^4}$$

$$n_o = 0.25$$

$$p_o = 14.5\ \text{psi} = 2088\ \text{PSF}$$

Equations (B-7), (B-8) and (B-9) then yield

$$E_c = \frac{(1.4)(2088)}{0.25}(1+\varepsilon)(1+4\varepsilon)^{-2.4} = 81.2\ (1+\varepsilon)(1+4\varepsilon)^{-2.4}\ \text{PSI}$$

$$\rho = \frac{(5.23)(0.75)}{1+\varepsilon} = \frac{3.9225}{1+\varepsilon} \quad \frac{\text{LB SEC}^2}{\text{FT}^4}$$

$$c = \left[\frac{(1.4)(2088)}{(5.23)(0.25)(0.75)}\right]^{\frac{1}{2}} (1+\varepsilon)(1+4\varepsilon)^{-1.2} = 54.598(1+\varepsilon)(1+4\varepsilon)^{-1.2} \text{ FT/SEC}$$

Values of $E_c$, $\rho$ and c are tabulated below for strains between 0% and 10%.

| $\varepsilon$ | $E_c$ | $\rho$ | c |
|---|---|---|---|
| % | PSI | $\frac{\text{LB SEC}^2}{\text{FT}^4}$ | FT/SEC |
| 0 | 81.2 | 3.92 | 54.6 |
| 0.5 | 77.8 | 3.90 | 53.6 |
| 1.0 | 74.6 | 3.88 | 52.6 |
| 1.5 | 71.7 | 3.86 | 51.7 |
| 2.0 | 68.9 | 3.85 | 50.8 |
| 2.5 | 66.2 | 3.83 | 49.9 |
| 3.0 | 63.7 | 3.81 | 49.1 |
| 4.0 | 59.1 | 3.77 | 47.5 |
| 5.0 | 55.0 | 3.74 | 46.0 |
| 6.0 | 51.4 | 3.70 | 44.7 |
| 7.0 | 48.0 | 3.67 | 43.4 |
| 8.0 | 45.0 | 3.63 | 42.3 |
| 9.0 | 42.3 | 3.60 | 41.1 |
| 10.0 | 39.8 | 3.57 | 40.1 |

## REFERENCES


1. Ake, J. P., "Pre Hybrid Gust Phase II-3 Quick Look Report, With Errata from Pre Hybrid Gust Phase I and II Quick Look Reports", UNM/ERI @ CERF, (August 1980).

2. Auld, H. E. and F. R. Murphy, "Surface Wave Calculations", PROCEEDINGS, DNA Strategic Structures Division Biennial Review Conference, Menlo Park, CA, (20-23 March 1979).

3. Babcock, S., "Pre Hybrid Gust Phase I Quick Look Report", UNM/ERI Report CERF-AG-26, (January, 1980).

4. Babcock, S., "Pre Hybrid Gust Phase II Quick Look Report", UNM/ERI Report CERF-AG-27, (January, 1980).

5. Baron, M. L., H. H. Bleich and P. Weidlinger, "Theoretical Studies on Ground Shock Phenomena", Paper No. SR-19, The MITRE Corporation, (October, 1960).

6. Baron, M. L., H. H. Bleich and Joseph P. Wright, "Ground Shock Due to Rayleigh Waves From Sonic Booms", ASCE PROC., Vol. 93, No. EM5, (Oct., 1967), pp. 137-162; disc. Vol. 94, No. EM2, (April, 1968), pp. 702-706; TRANS, Vol. 134 (1969), pp. 885-887.

7. Baron, M. L. and R. Check, "Elastic Rayleigh Wave Motions Due to Nuclear Blasts", ASCE PROC., Vol. 89, No. EM1, (February, 1963), pp. 57-70.

8. Baron, M. L. and C. Lecht, "Elastic Rayleigh Wave Effects Due to Nuclear Blasts", ASCE PROC., Vol. 87, No. EM5, (October, 1961), pp. 33-53; disc. Vol. 89, No. EM4, (August, 1963), p. 89; TRANS, Vol. 127 (1962), Part I, pp. 802-822.

9. Bleich, H. H., "On the Disintegration of Bodies of (Granular) Materials Governed by the Coulomb Rule", ASME TRANS, JAM, Vol. 31, Series E, No. 1, (March, 1964), pp. 1-4.

10. Bleich, H. H. and E. Heer, "Moving Step Load on Half-Space of Granular Material", ASCE PROC., Vol. 89, No. EM3, (June, 1963), pp. 97-129, Paper No. 3551; see also ASCE TRANS, Vol. 129 (1964), pp. 258-259.

11. Bleich, H. H. and E. Heer, "Step Load Moving With Low Subseismic Velocity on the Surface of a Half-Space of Granular Material", AFSWC-TDR-63-2, (April, 1963).

12. Blouin, S. E, J. L. Bratton, and E. H. Bultmann, "Earthquake Ground Motion Simulation Study", EPRI Report NP-1387, TPS 79-734 (April, 1980).

13. Bolt, B. A., NUCLEAR EXPLOSIONS AND EARTHQUAKES - THE PARTED VEIL, W. H. Freeman & Co., (1976).

14. Bratton, J. L., "Multiburst Spall Phenomenon", paper presented at DNA Spall Workshop held at R&D Associates, Marina del Rey, CA, September, 1979.

15. Coates, D. J., ROCK MECHANICS PRINCIPLES, Mines Branch Monograph 874, Canadian Department of Energy, Mines and Resources, (revised 1967).

16. Curran, D., "Time Dependent Fracture Models for X-Ray Deposition Problems", paper presented at DNA Spall Workshop held at R&D Associates, Marina del Rey, CA, September, 1979.

17. DuPont, BLASTER'S HANDBOOK, E. J. DuPont de Nemours & Co., Inc., 175th Edition, (1977).

18. DuPont, FOUR MAJOR METHODS OF CONTROLLED BLASTING, E. J. DuPont de Nemours & Co., Inc., (November, 1976).

19. Duvall, G. E., "Applications", Chapter 9 in DYNAMIC RESPONSE OF MATERIALS TO INTENSE IMPULSIVE LOADING, edited by P. C. Chou and A. H. Hopkins, Air Force Materials Laboratory, (1972), Para. 9.4.2.

20. Eisler, J. D. and F. Chilton, "Spalling of the Earth's Surface by Underground Nuclear Explosions", J.G.R., Vol. 69, No. 24, (15 December 1964), pp. 5285-5293.

21. Glasstone, S. and P. J. Dolan, THE EFFECTS OF NUCLEAR WEAPONS, Third Edition, U. S. Government Printing Office, (1977).

22. Grady, D., "Tension Fracture Relations to Rock Fragmentation for Oil Shales Rubblization", paper presented at DNA Spall Workshop held at R&D Associates, Marina del Rey, CA, September 1979.

23. Heinrich, G., "Wissenschaftliche Grundlagen der Theorie der Setzung von Tonschichten", WASSERKRAFT u. WASSERWIRTSCH, Vol. 33, (1938), pp. 5-11.

24. Hemphill, G. B., BLASTING OPERATIONS, McGraw-Hill, (1980).

25. Higgins, C. J., "Spall Motions Measured on Earthquake Simulation Experiments", paper presented at DNA Spall Workshop held at R&D Associates, Marina del Rey, CA, September, 1979.

26. Higgins, C. J., et. al, "SIMQUAKE I - An Explosive Test Series Designed to Simulate Earthquake Ground Motion Effects on Model Nuclear Power Plant Structures", Summary Report by UNM to EPRI, (February, 1979).

27. Hurdle, P. M. and R. J. Port, "MX Multiburst Ground Motion Study" (draft), RDA-TR-104806-007, R&D Associates, Marina del Rey, CA, (October, 1977).

28. Jaeger, J. C. and N.G.W. Cook, FUNDAMENTALS OF ROCK MECHANICS, Methuen (Barnes and Noble), (1969).

29. Kinslow, R., HIGH-VELOCITY IMPACT PHENOMENA, Academic Press, (1970).

30. Kolsky, H., STRESS WAVES IN SOLIDS, Oxford University Press (1953); Dover reprint (1963).

31. Lambe, T. William and R. V. Whitman, SOIL MECHANICS, Wiley, (1969).

32. Lipner, N., "System Implications of Spall Effects", paper presented at DNA Spall Workshop held at R&D Associates, Marina del Rey, CA, September, 1979.

33. Melzer, L. S., "Typical Spall from Near-Surface High Explosive Events", paper presented at DNA Spall Workshop, held at R&D Associates, Marina del Rey, CA, September, 1979.

34. Merkle, D. H., "The effective Stress Mechanics of Undrained Shear Strength", AFWL-TR-71-85, (July, 1971).

35. O'Brien, J. L. and R. S. Davis, "On the Fracture of Solids Under Impulsive Loading Conditions", in RESPONSE OF METALS TO HIGH VELOCITY DEFORMATION, edited by P. G. Shewmon and V. F. Zackay, AIME, Wiley-Interscience, (1961).

36. Perret, William R., "Free-Field and Surface Motion from a Nuclear Explosion in Alluvium: MERLIN Event", Sandia Lab Report SC-RR-69-334, (November, 1971).

37. Perret, W. R., "Subsurface Motion From a Contained Underground Detonation", WT-1529, Sandia Corporation, (May, 1961).

38. Perret, W. R., "Surface Motion Near Underground Nuclear Explosions in Desert Alluvium", Operation Nougat I, Area 3, Nevada Test Site, SAND 77-1435, Sandia Laboratories, (May, 1978).

39. Phillips, J. S., L. S. Melzer and J. L. Bratton, "Misers Bluff Phase II: Ground Shock Data Analysis", prepared for DNA by CSI, (31 October 1979).

40. Port, R. J. and H. E. Auld, "Spall Effects", Section 4.15 in MX GROUND SHOCK ENVIRONMENTS, STATUS REPORT ON MX NWE TASK V-4 - GROUND SHOCK, edited by Major R. H. Jolley, AFWL, (March, 1980).

41. Richart, F. E., J. R. Hall and R. D. Woods, VIBRATIONS OF SOILS AND FOUNDATIONS, Prentice-Hall, (1970).

42. Rinehart, J. S., "HE Spall Radius Versus Depth of Burst", paper presented at DNA Spall Workshop held at R&D Associates, Marina del Rey, CA, September, 1979.

43. Rinehart, J. S., "Spalling and Large Blasts", UCRL-5675, Lawrence Radiation Laboratory/AEC/SAN, PROCEEDINGS OF THE SECOND PLOWSHARE SYMPOSIUM, Part I, (May 15, 1959); see also PROCEEDINGS OF THE SECOND PROTECTIVE CONSTRUCTION SYMPOSIUM, (Santa Monica, 1959), Part I, pp. 111-129.

44. Rinehart, J. S., STRESS TRANSIENTS IN SOLIDS, Hyperdynamics, Santa Fe, New Mexico, (1975).

45. Rinehart, J. S. and J. Pearson, BEHAVIOR OF METALS UNDER IMPULSIVE LOADS, American Society of Metals, (Cleveland, Ohio, 1954).

46. Rohde, R. W., et. al., METALLURGICAL EFFECTS AT HIGH STRAIN RATES, Session E, "Fracture Processes", AIME, Plenum Press, (1973).

47. Sobel, P. A., "The Effects of Spall on $m_b$ and $M_s$", SDAC-TR-77-12, Seismic Data Analysis Center, Air Force Technical Applications Center, Alexandria, VA, (4 April 1978).

48. Stagg, K. G. and O. C. Zienkiewicz (eds), ROCK MECHANICS IN ENGINEERING PRACTICE, Wiley, (1968).

49. Stubbs, T. J., Kochly and F. Sauer, "Middle North Series, PRE-MINE THROW IV, Air Blast and Ground Motion Project No. MT-301, Volume I - Technical Report, Volume II - Ground Motion and Static Airblast Overpressure Data", DNA POR 6833-1 and 6833-2, (29 October 1976).

50. Stump, B. W. and R. E. Reinke, "Geophysical Studies at McCormick Ranch, New Mexico and the Importance of Spall Waveforms in High Explosive Testing", AFWL/NTE draft report, (August, 1980).

51. Swift, H. F., "Hypervelocity Impact", Appendix in DYNAMIC RESPONSE OF MATERIALS TO INTENSE IMPULSIVE LOADING, edited by P. C. Chou and A. K. Hopkins, Air Force Materials Laboratory, (1972).

52. Terzaghi, K., THEORETICAL SOIL MECHANICS, Wiley, (1943).

53. Terzaghi, K. and O. K. Frohlich, ERDBAUMECHANIK UND BAUPRAXIS: EINE KLARSTELLUNG, Leipzig und Wien, Franz Deuticke, (1937), 33 pp.

54. Thorne, C. R., N. K. Tovey and R. Bryant, "Recording Unconfined Tension Tester", ASCE PROC., Vol. 106, No. GT 11, (November, 1980), pp. 1269 - 1273.

55. Ullrich, G. W., "Airblast/Ground Motion Effects from Simultaneous Detonations of High Explosive Charges", (draft), AFWL TR-78-110 (1978); also NUCLEAR TECHNOLOGY DIGEST, Vol. 1, AFWL (1978).

56. Viecelli, J. A., "Spallation and the Generation of Surface Waves by an Underground Explosion", JGR, Vol. 78, No. 14, (10 May 1973), pp. 2475-2487.

57. Zelasko, J. S., "Tensile Experiments for Soils", paper presented at DNA Spall Workshop held at R&D Associates, Marina del Rey, CA, September 1979.

FIGURES

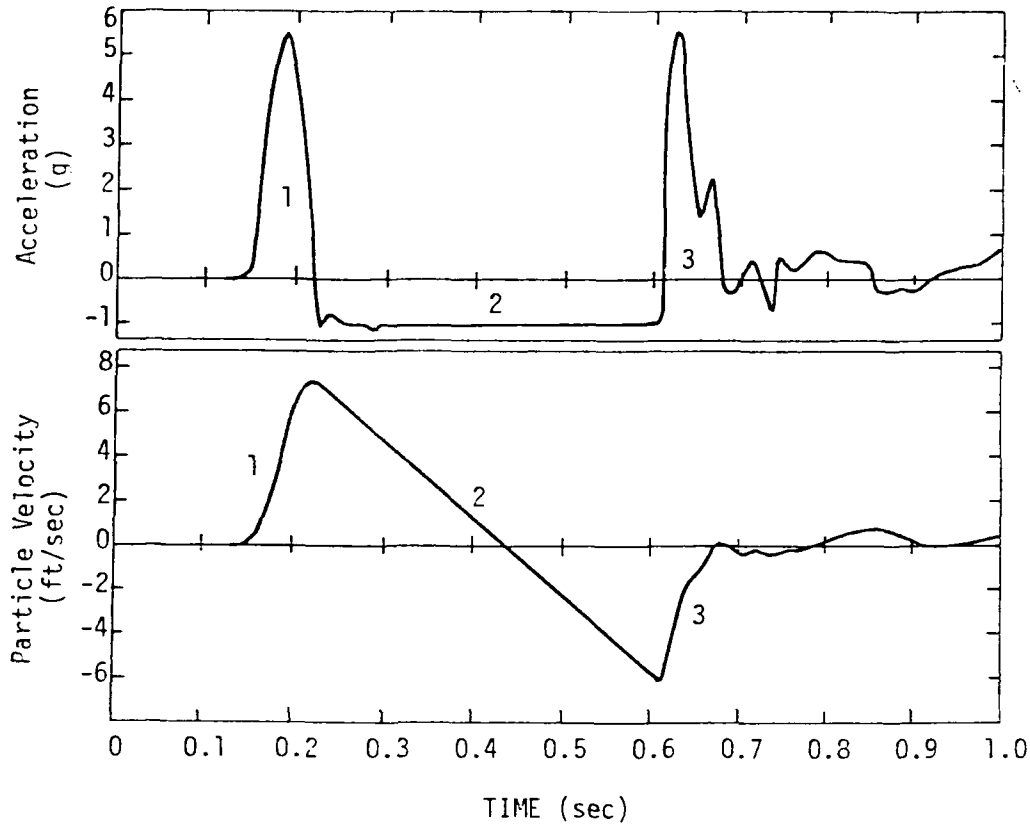


FIGURE 2.1

Surface Vertical Motion Above A Contained Nuclear Detonation In Rock - RANIER Event [From Perret (1971, 114)]

FIGURE 2.2

SULKY Event; Mound Created by the Bulking of Rock Material in a 0.087-Kiloton Nuclear Detonation at a Depth of 90 Feet.

[From Glasstone and Dolan (1977, 233)]

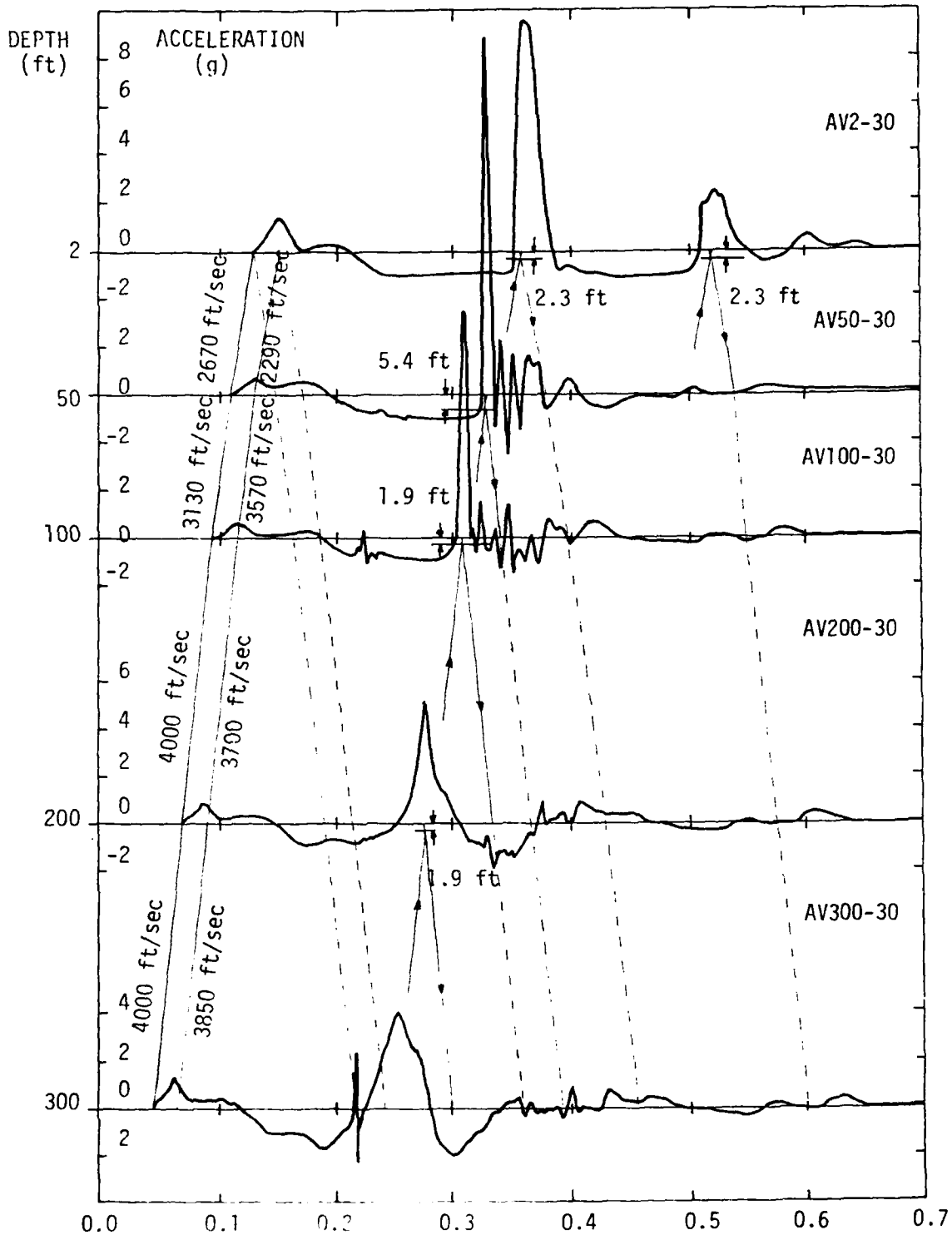


FIGURE 2.3

Vertical Acceleration Records, MINK Event [From Perret (1978,34)]

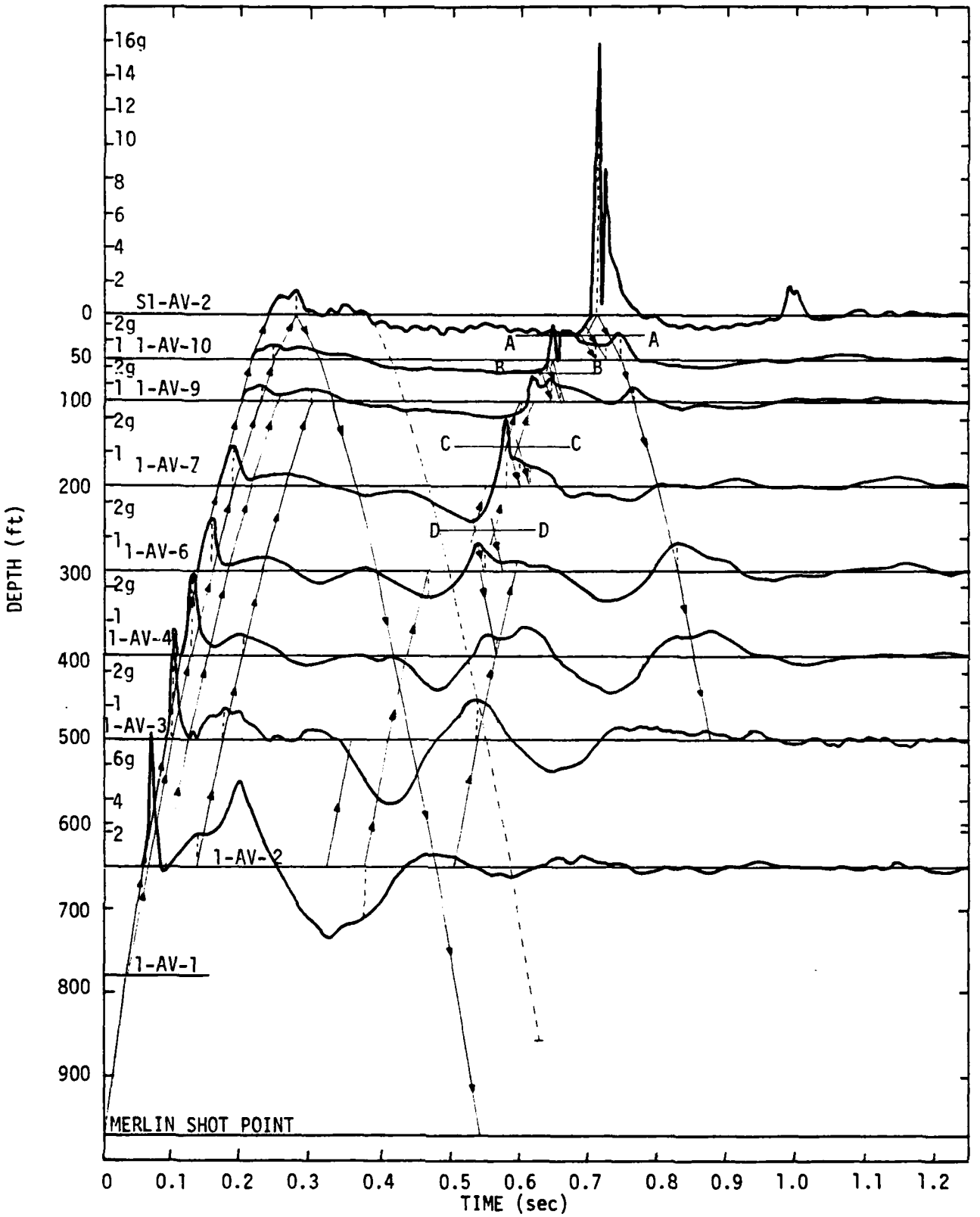


FIGURE 2.4
Vertical Acceleration Records, MERLIN Event (Boring 1, 50 ft Offset)
[From Perret (1971,125)]

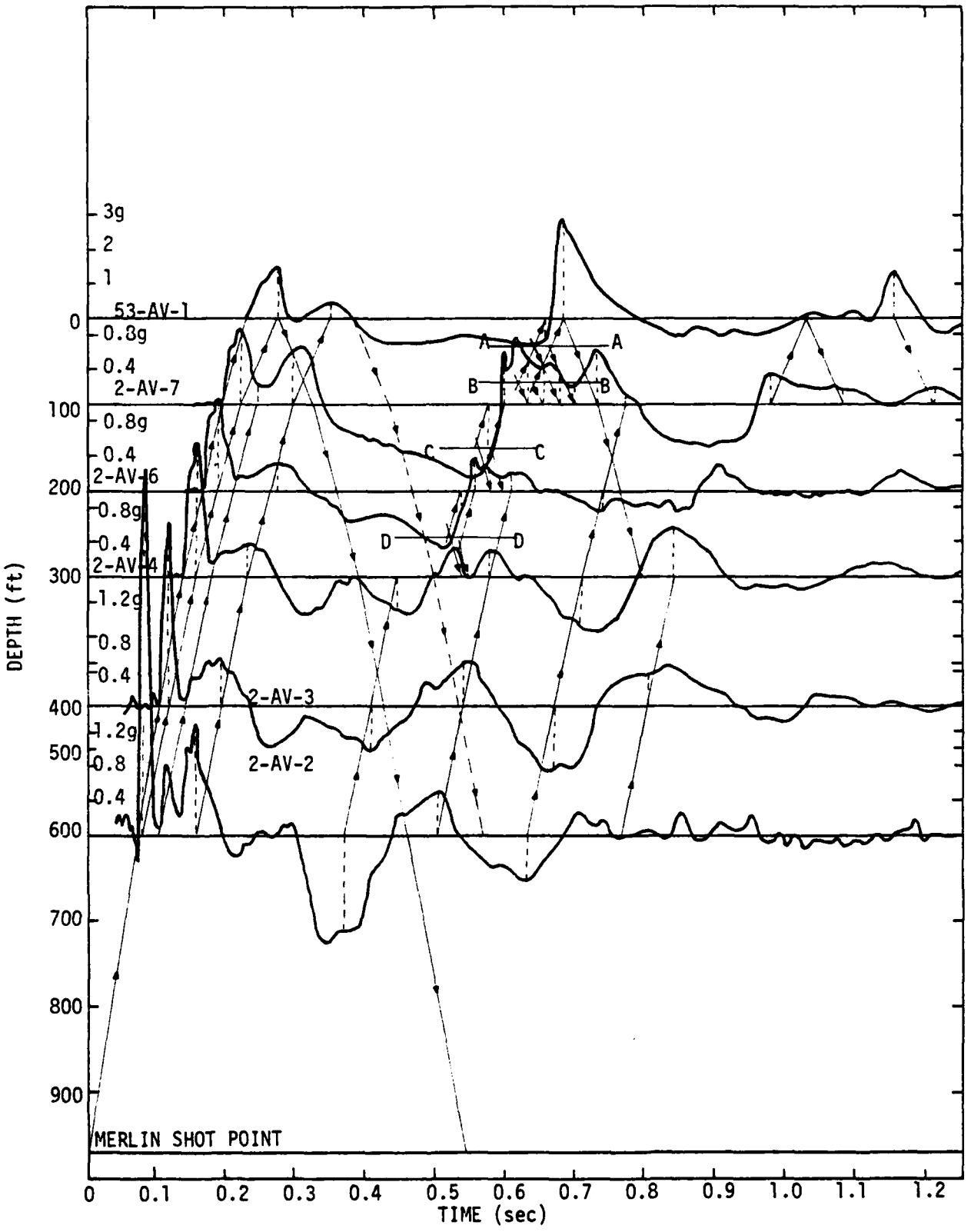


FIGURE 2.5

Vertical Acceleration Records, MERLIN Event (Boring 2, 150 FT offset)

[From Perret (1971,128)]

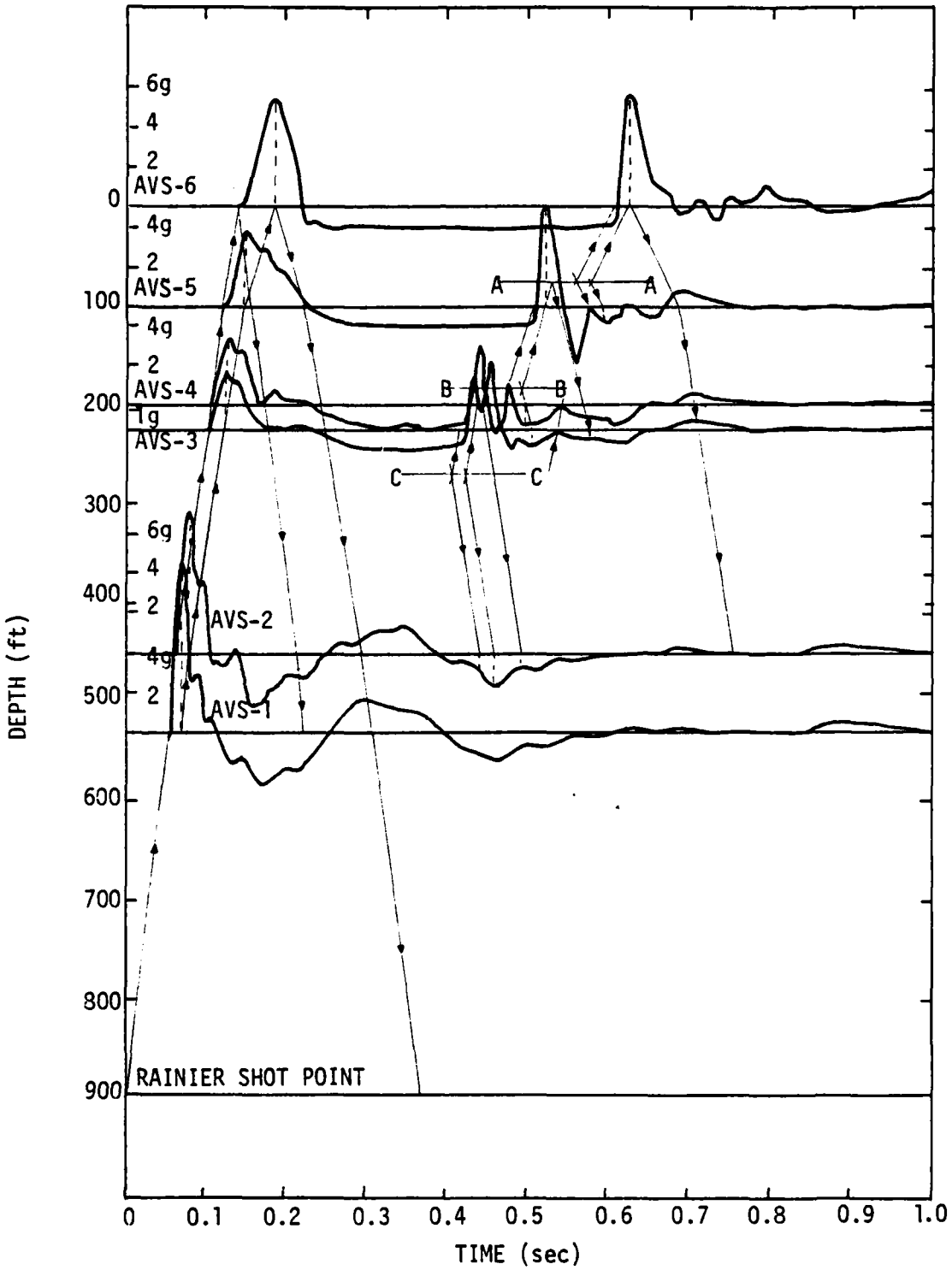


FIGURE 2.6

Vertical Acceleration Records, RANIER Event [From Perret (1971,130)]

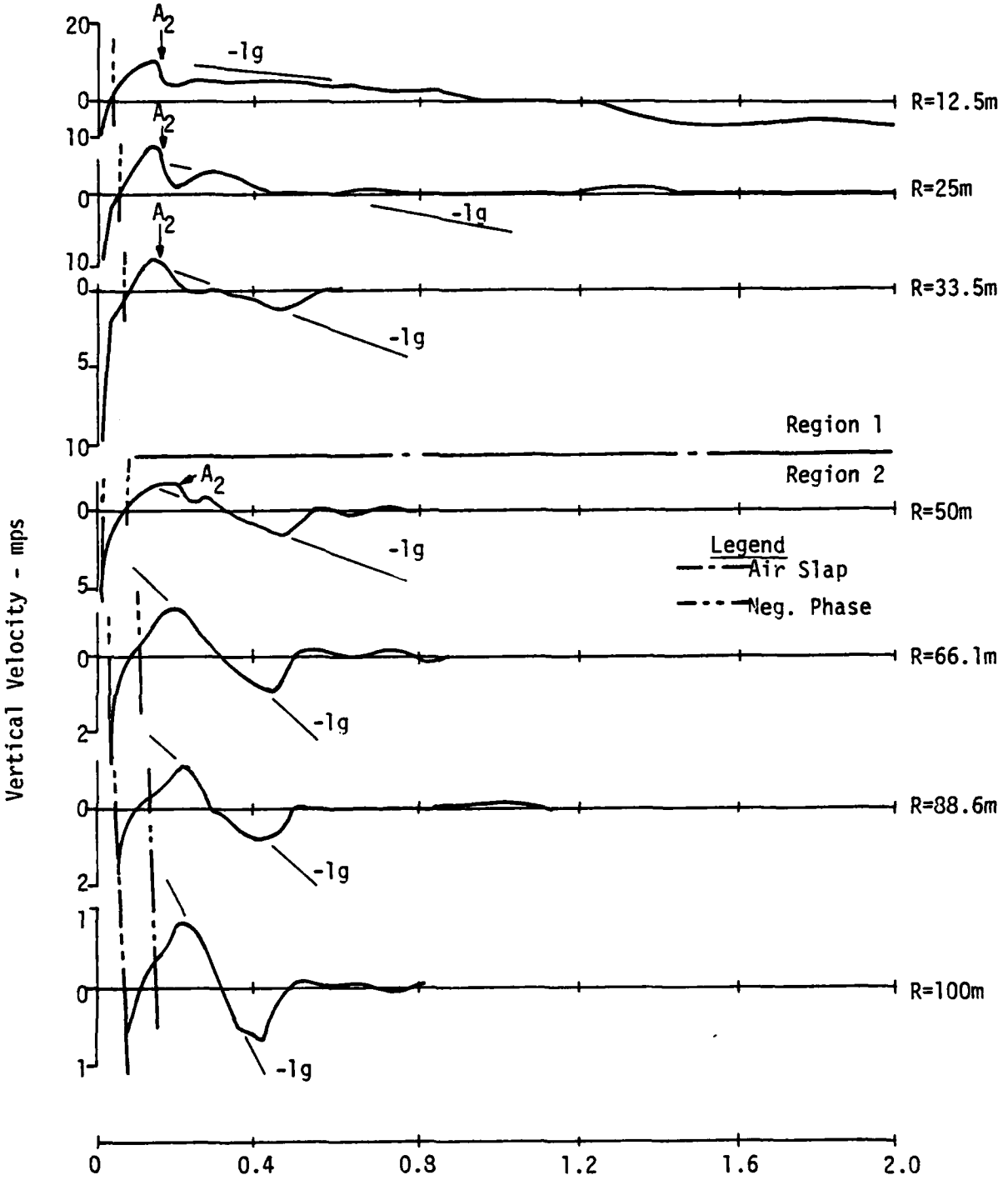


FIGURE 2.7

Vertical Velocity Waveforms at the 0.5 m Depth - MBII-1

[From Phillips, Melzer and Bratton (1979,33)]

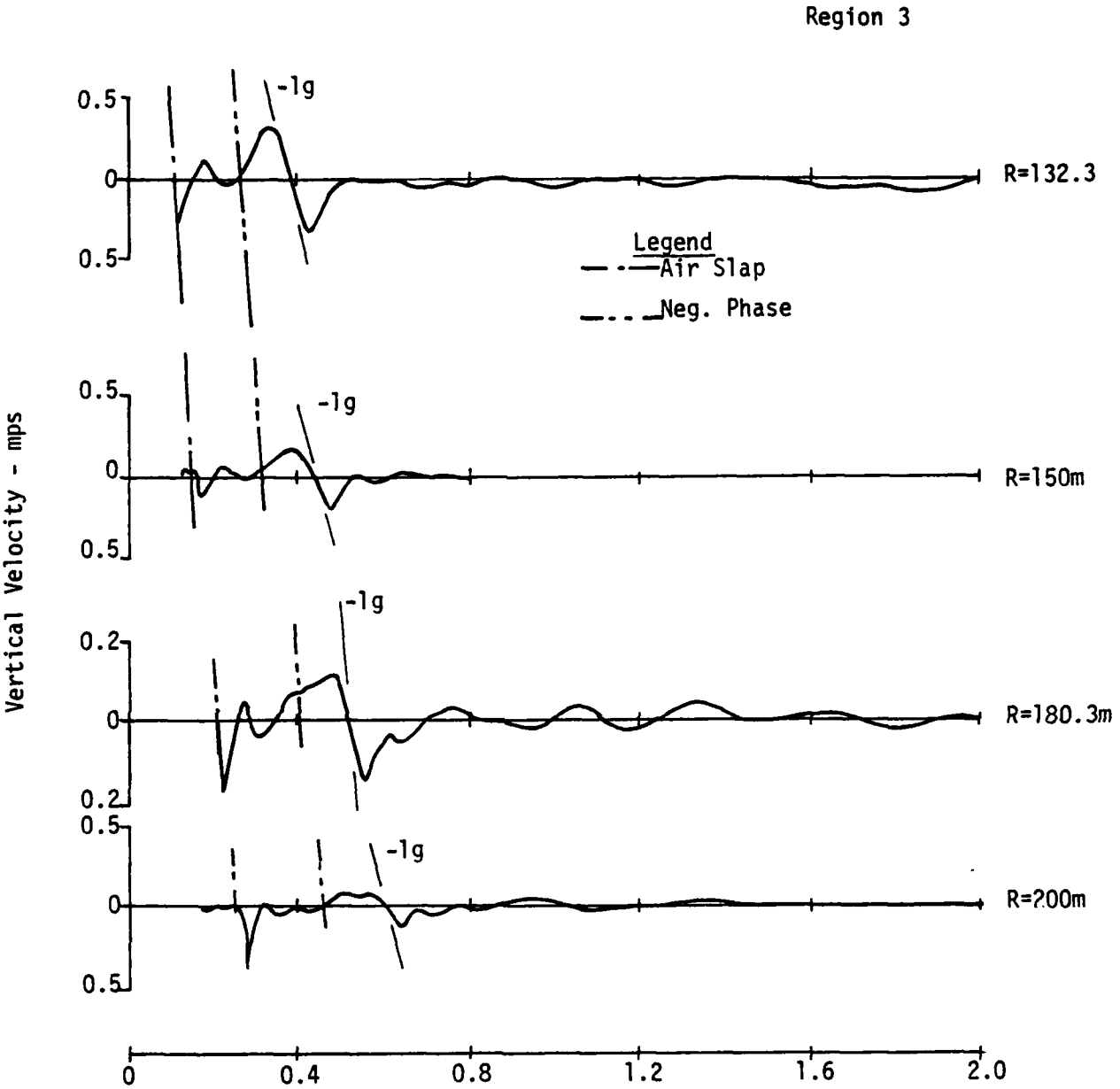


FIGURE 2.8

Vertical Velocity Waveforms at the 0.5 m Depth - MBII-1

[From Phillips, Melzer and Bratton (1979,35)]

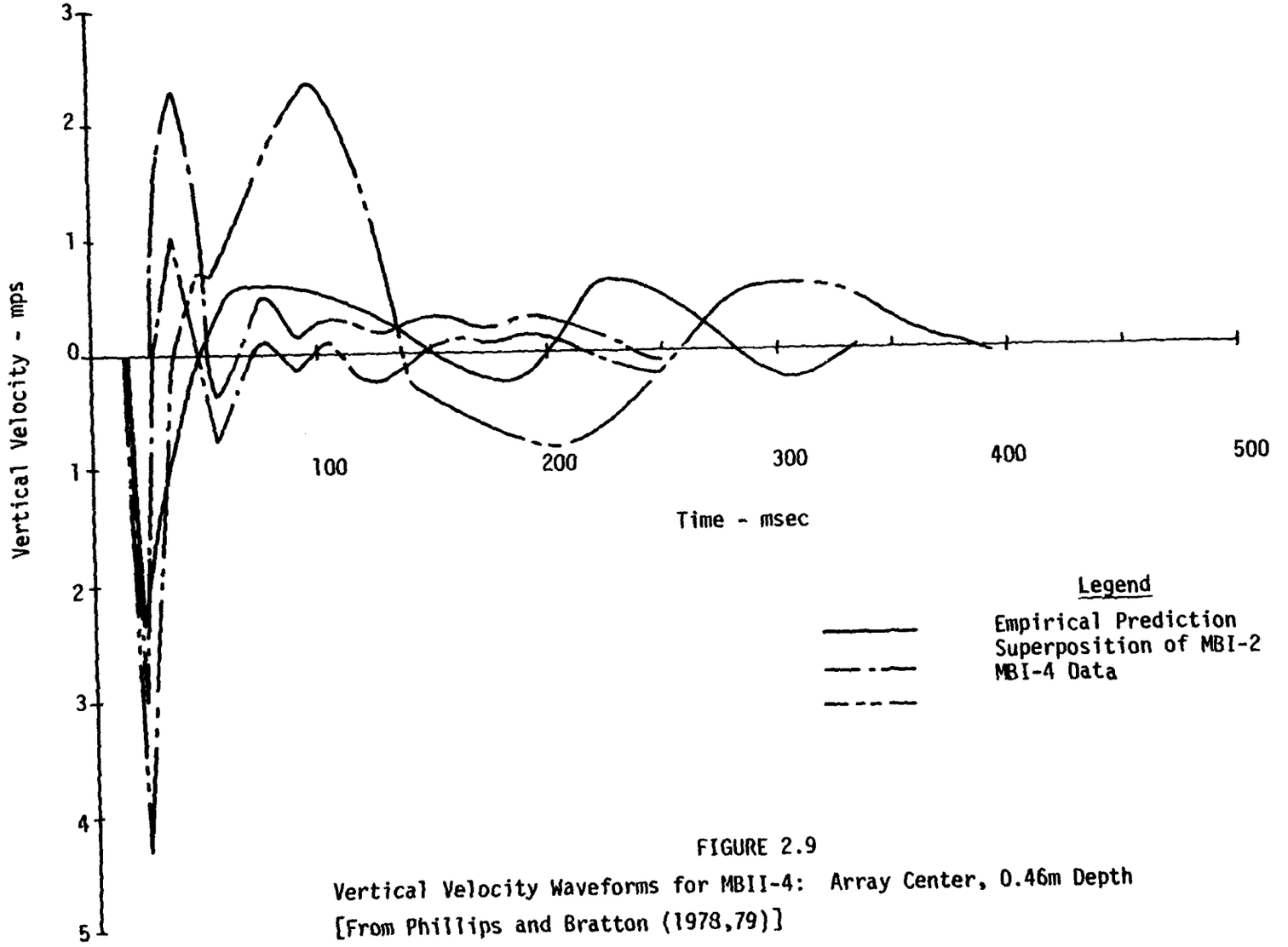


FIGURE 2.9

Vertical Velocity Waveforms for MBII-4: Array Center, 0.46m Depth
[From Phillips and Bratton (1978,79)]

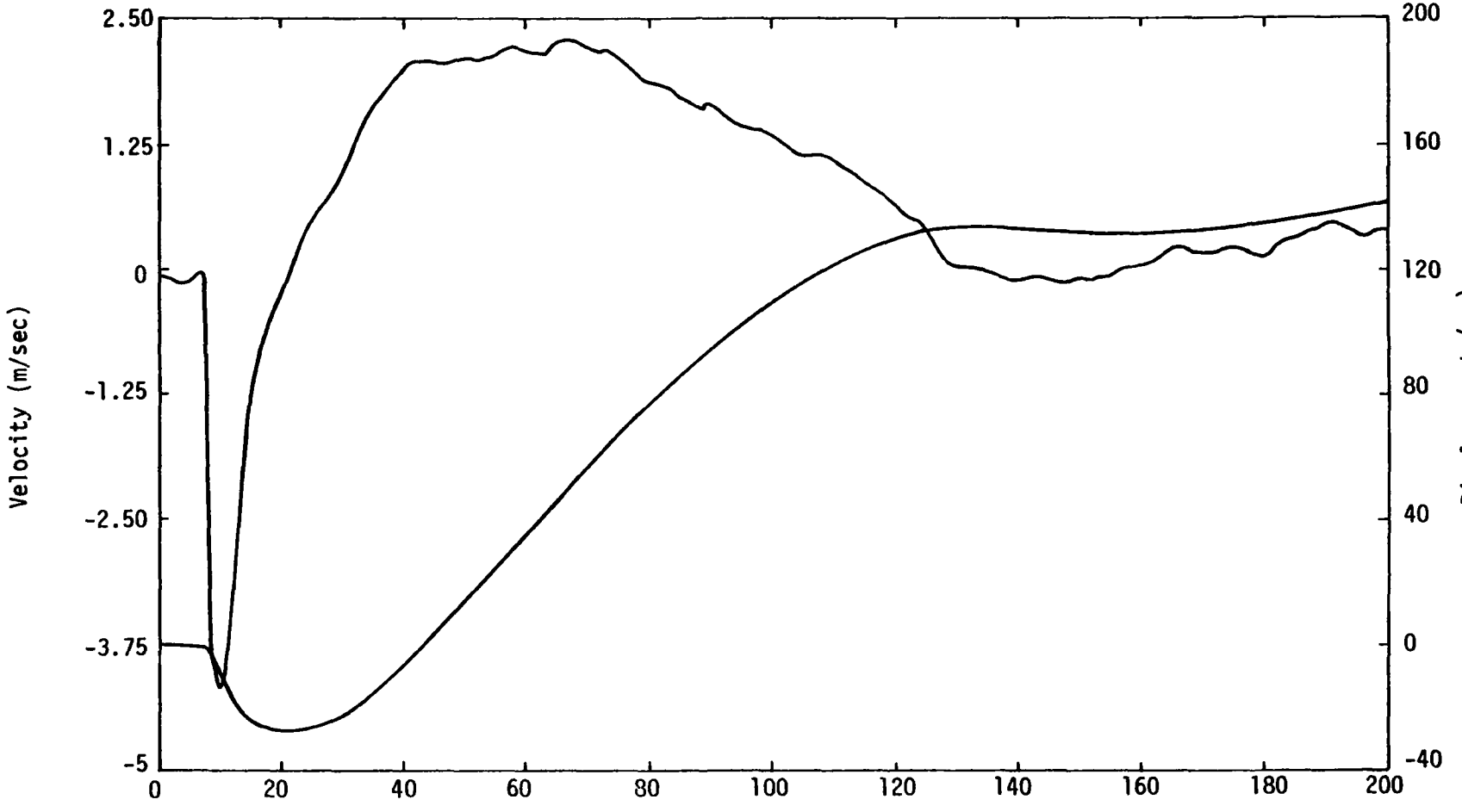


FIGURE 2.10

Vertical Velocity Waveform for PHGII-1 (θ=210°; R=0.6096m; D=0.1524m)

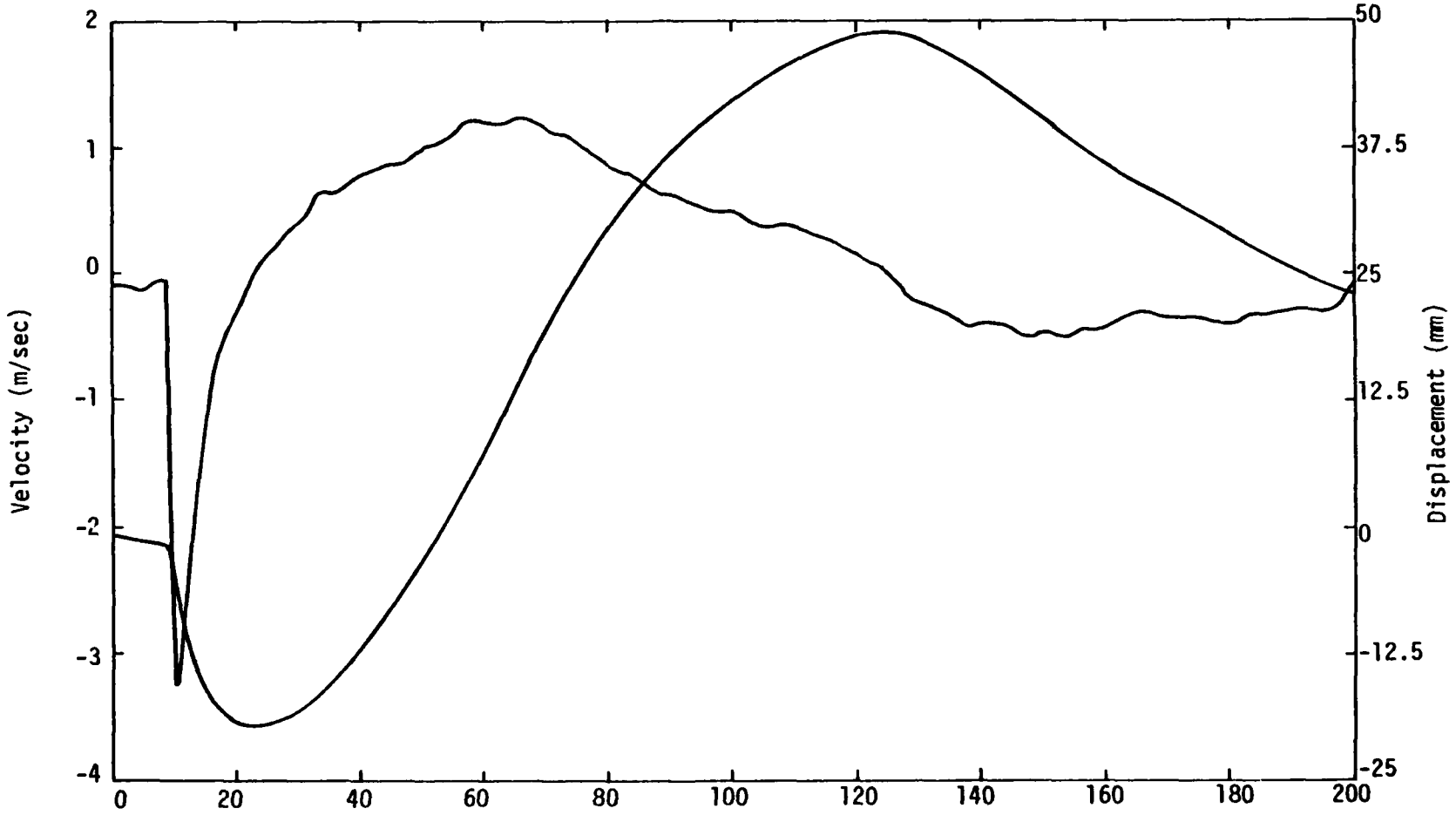


FIGURE 2.11

Vertical Velocity Waveform for PHGII-1 (θ=210°; R=0.6096m; D=0.4572m)

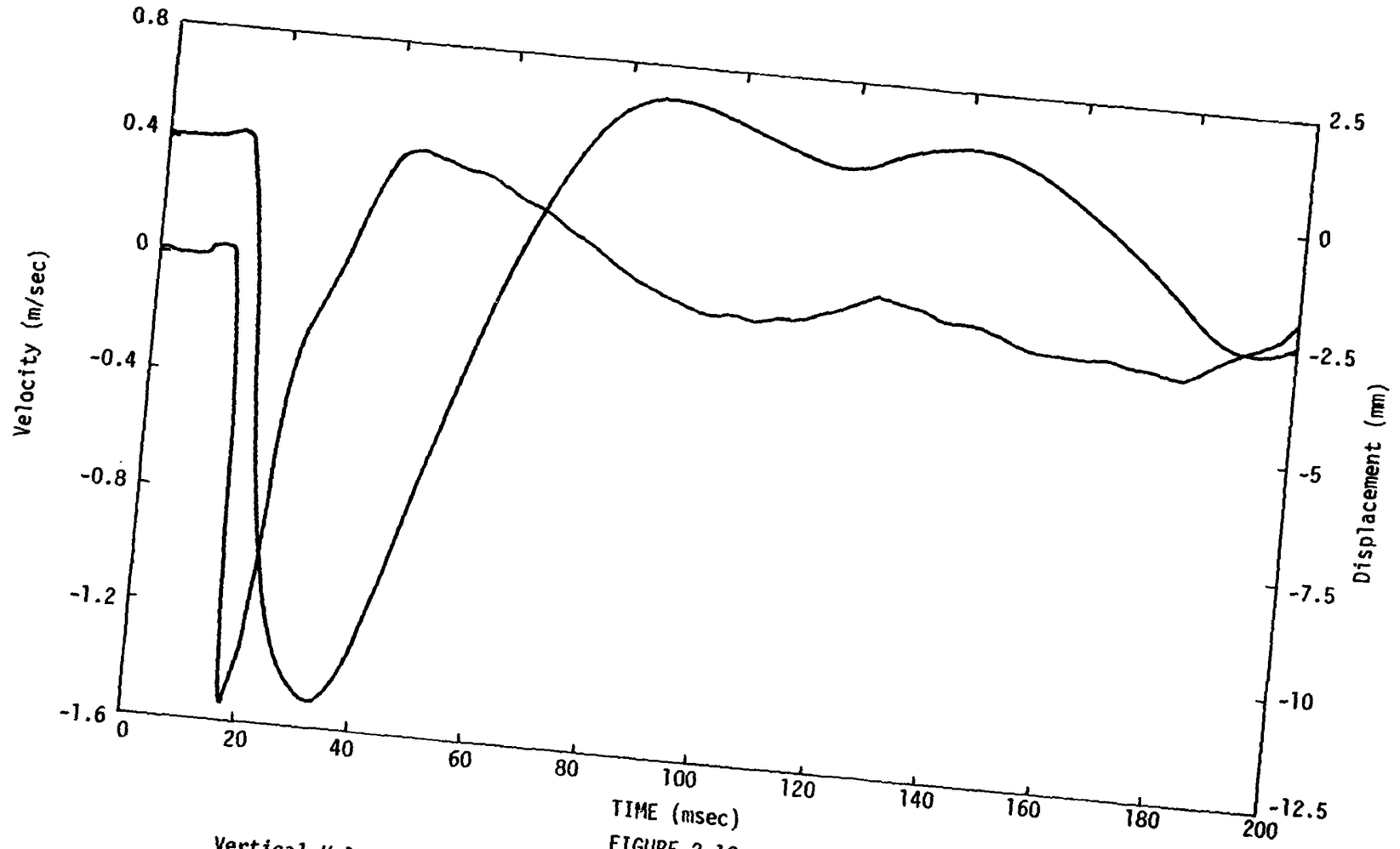


FIGURE 2.12

Vertical Velocity Waveform for PHGII-1 ($\theta$=210°; R=0.6096m; D=1.372m)

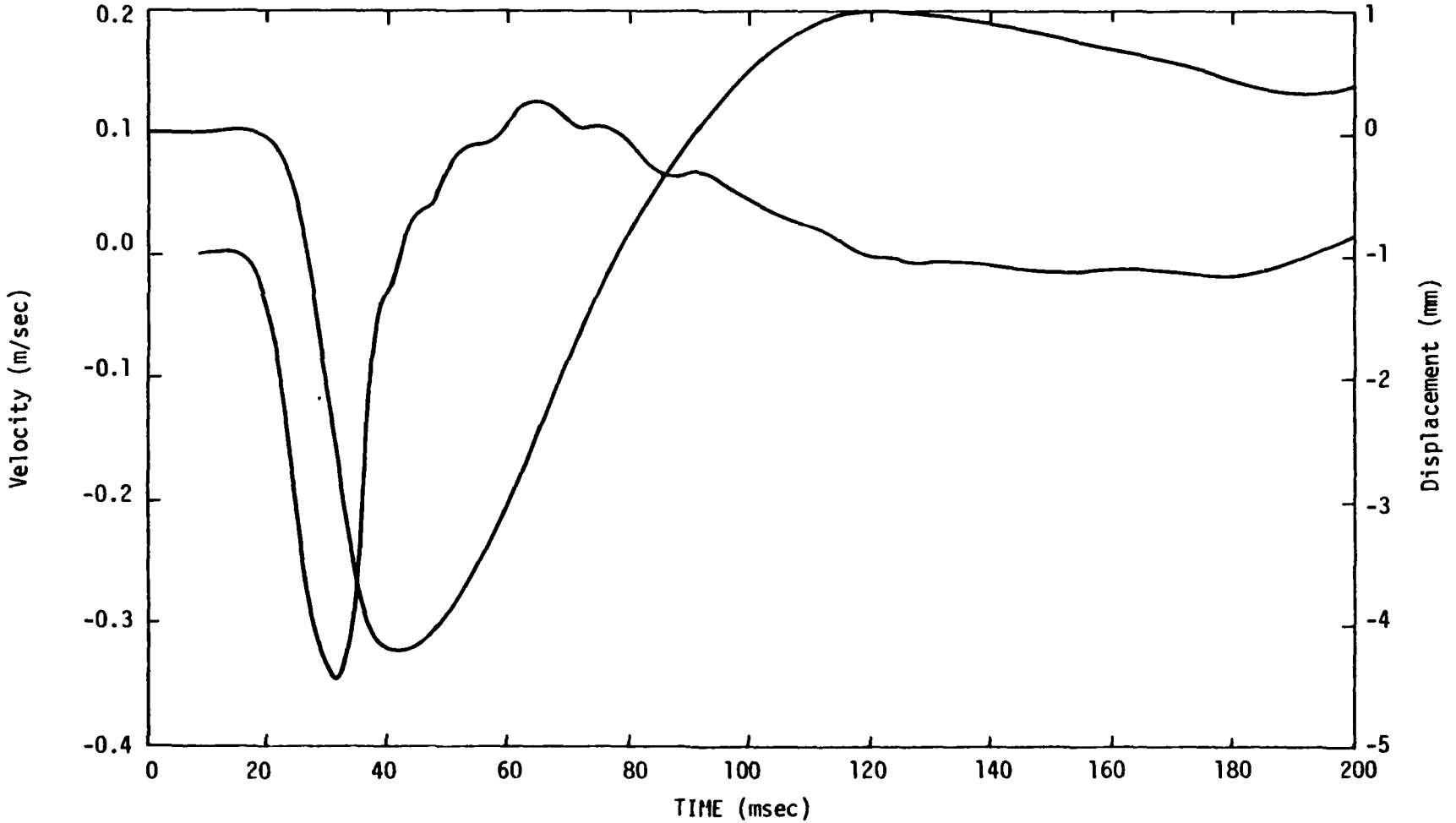


FIGURE 2.13

Vertical Velocity Waveform for PHGII-1 (θ=210°; R=0.6096m; D=4.1148m)

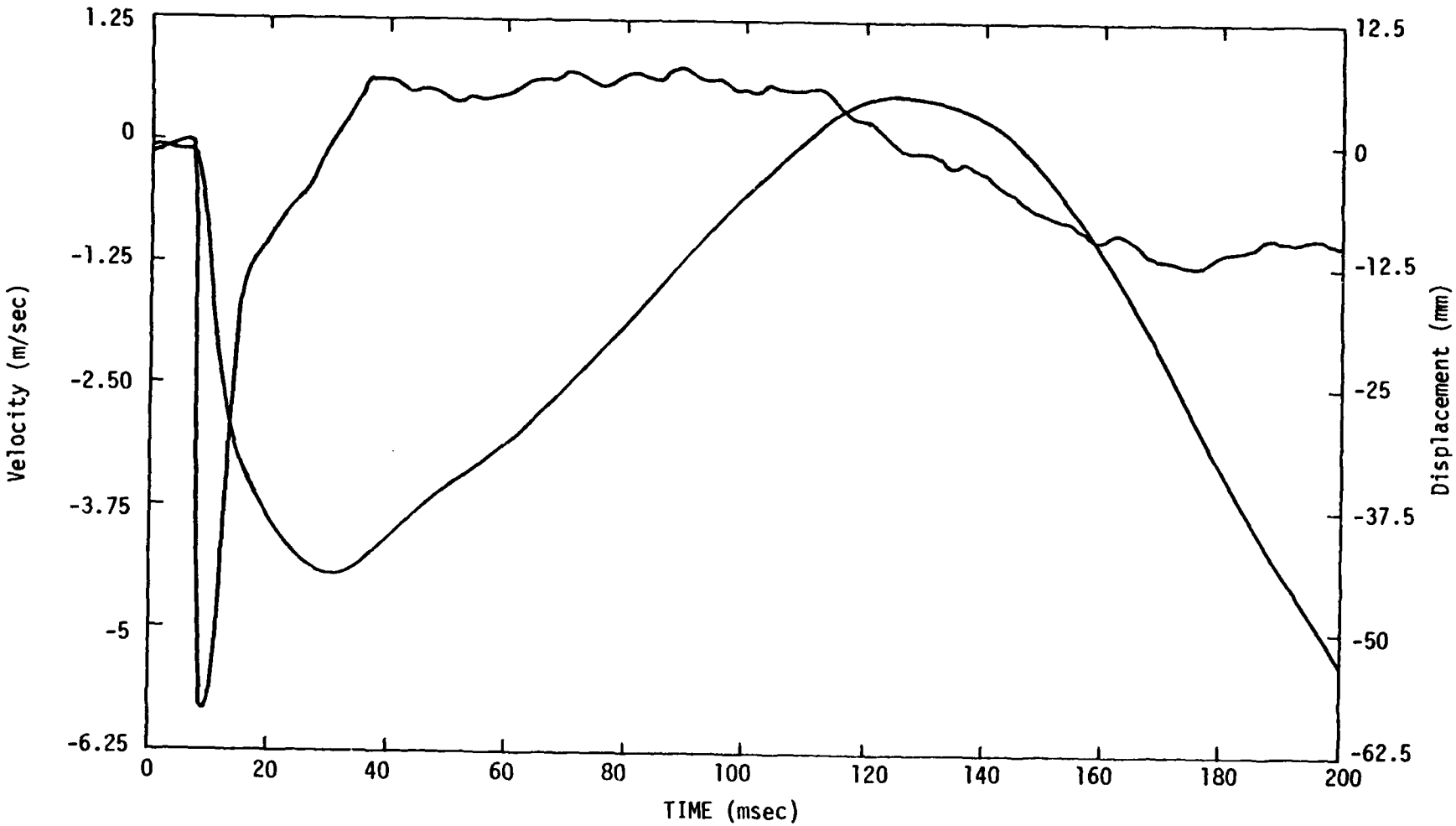


FIGURE 2.14

Vertical Velocity Waveform for PHGII-1 (θ=330°; R=0.6096m; D=0.1524m)

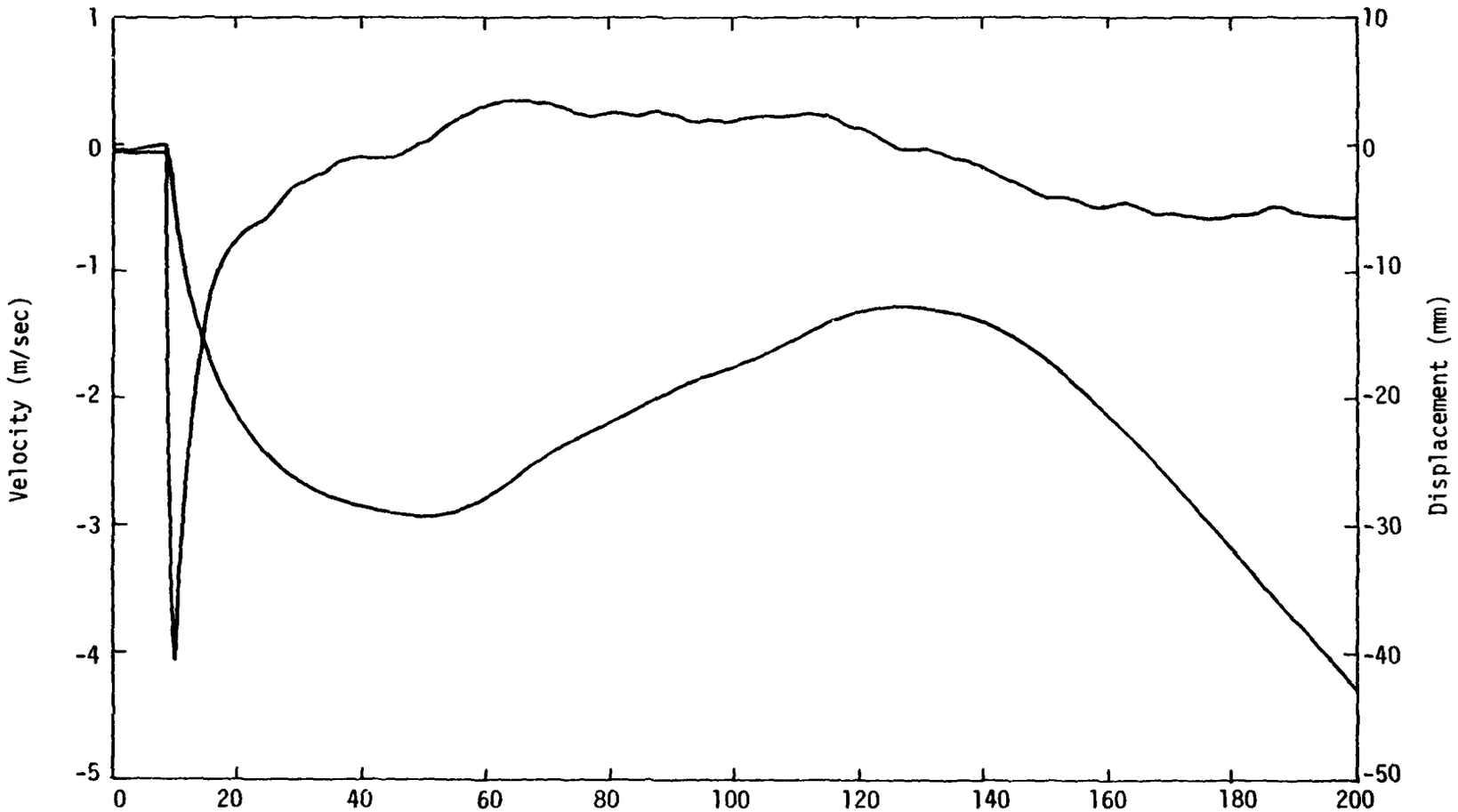


FIGURE 2.15

Vertical Velocity Waveform for PHGII-1 (θ=330°; R=0.6096m; D=0.4572m)

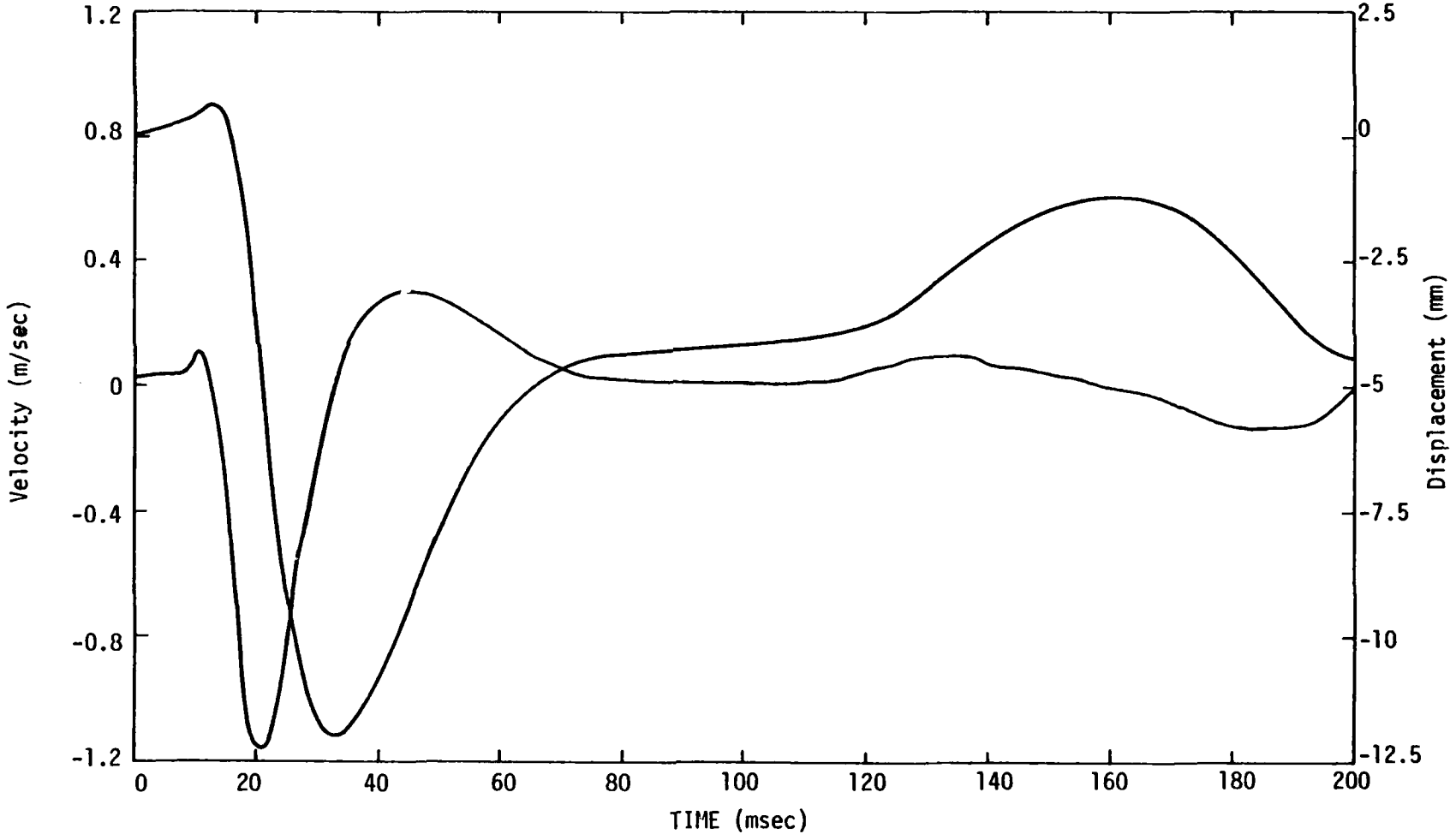


FIGURE 2.16

Vertical Velocity Waveform for PHGII-1 (θ=330°; R=0.6096m; D=1.372m)

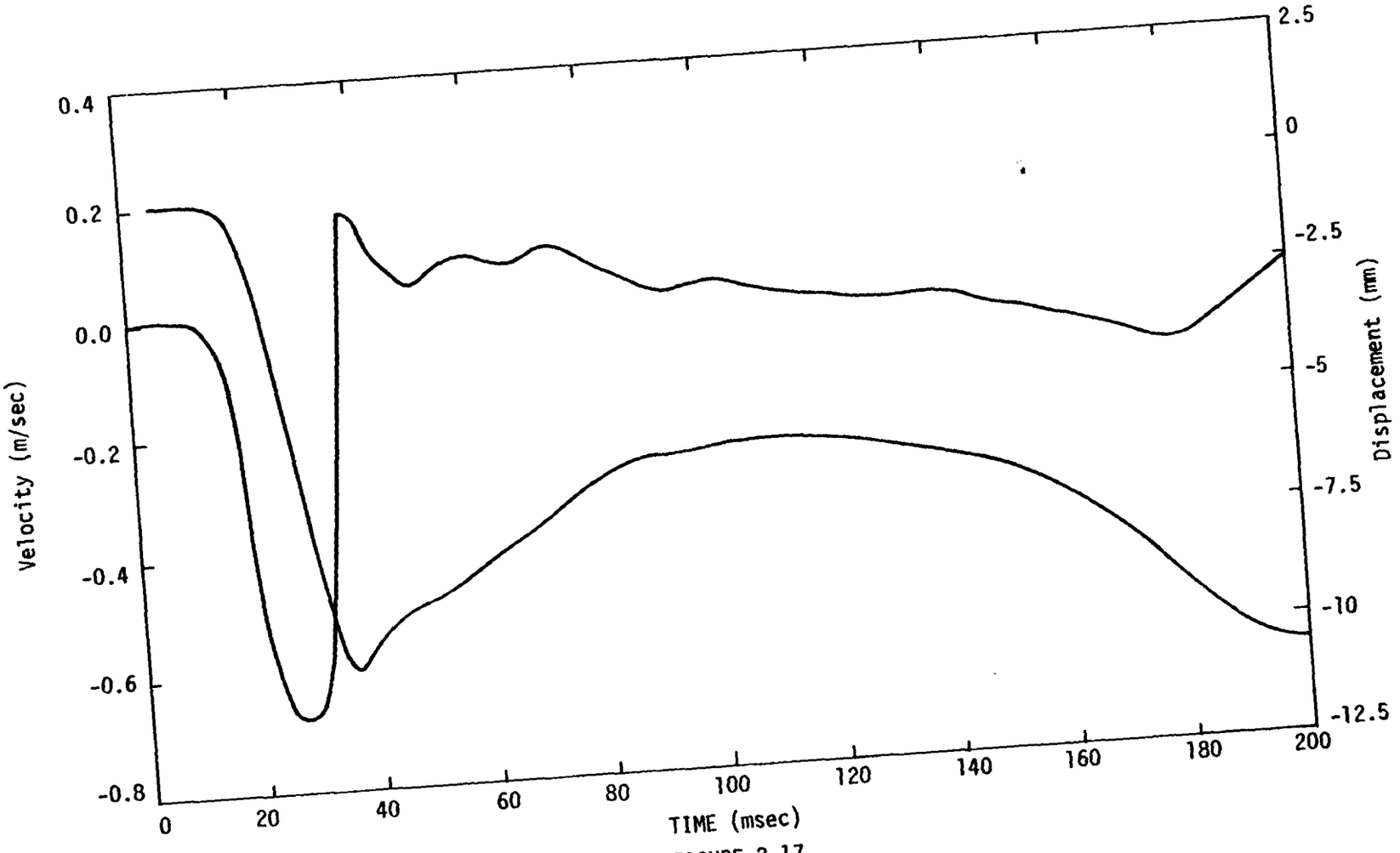


FIGURE 2.17

Vertical Velocity Waveform for PHGII-1 (θ=330°; R=0.6096m; D=2.286m)

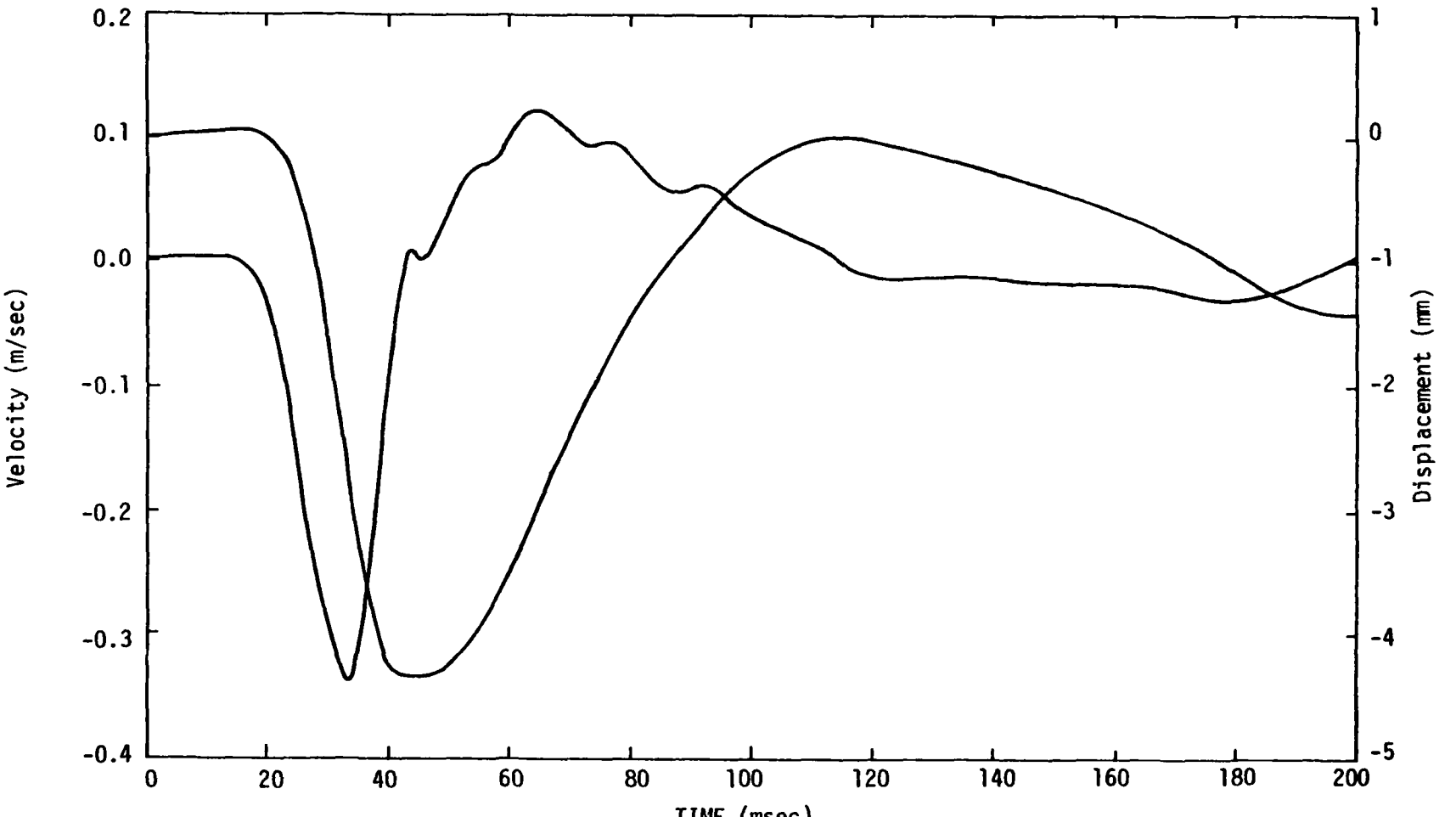


FIGURE 2.18

Vertical Velocity Waveform for PHGII-1 (θ=330°; R=0.6096m; D=4.1148m)

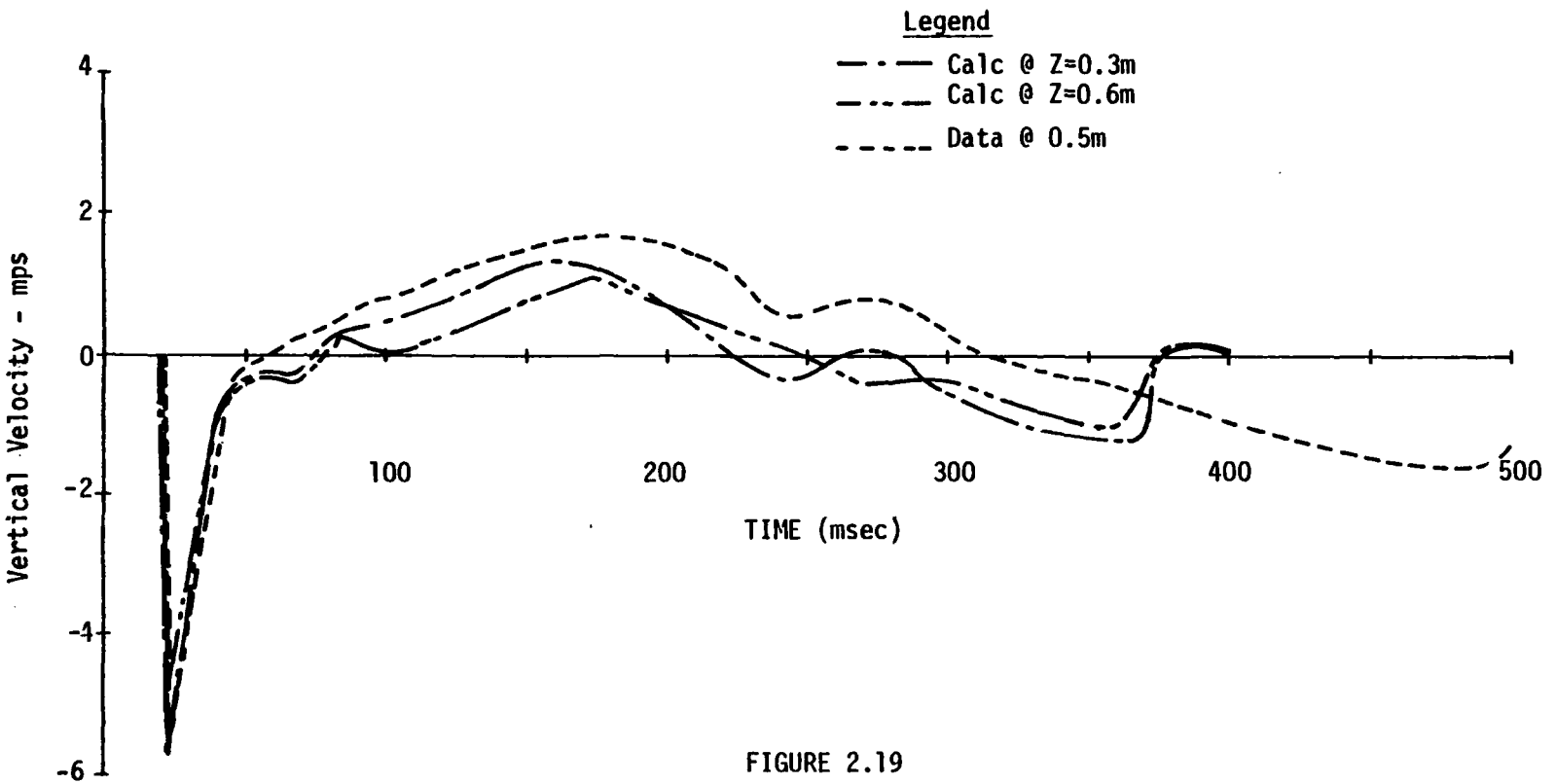


FIGURE 2.19

Comparison of Pore Air Model Calculations and MBII-1 Data @ R=50m; Z=0.5m

[From Phillips, Melzer and Bratton (1979,70)]

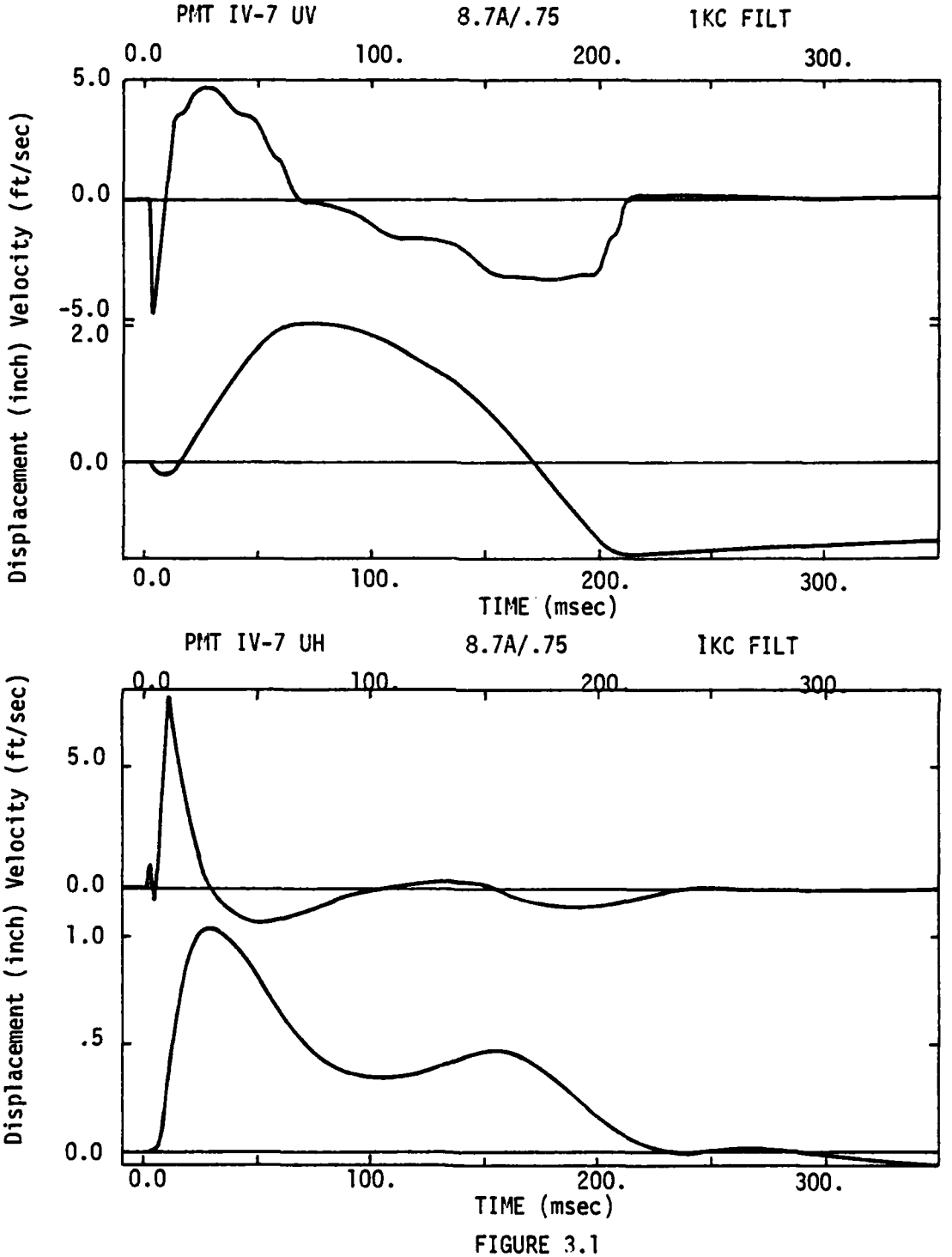


FIGURE 3.1

Ground Motion, 8.5-Foot Epicentral Range, .75 Foot Depth, Line A. [From Stubbs, Kochly and Sauer (1976:32)]

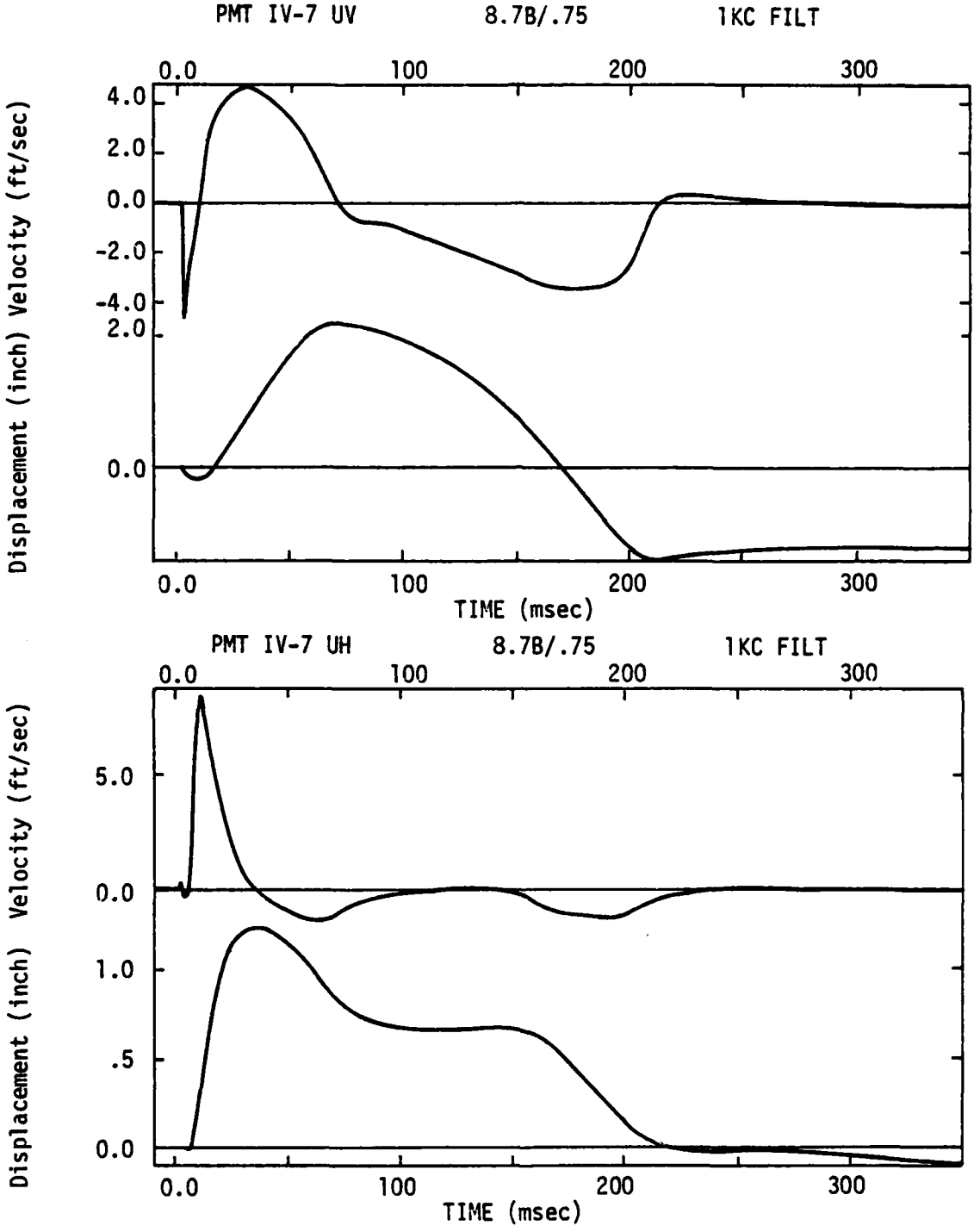


FIGURE 3.2

Ground Motion, 8.5-Foot Epicentral Range, .75 Foot Depth, Line B.
[From Stubbs, Kochly and Sauer (1976:33)]

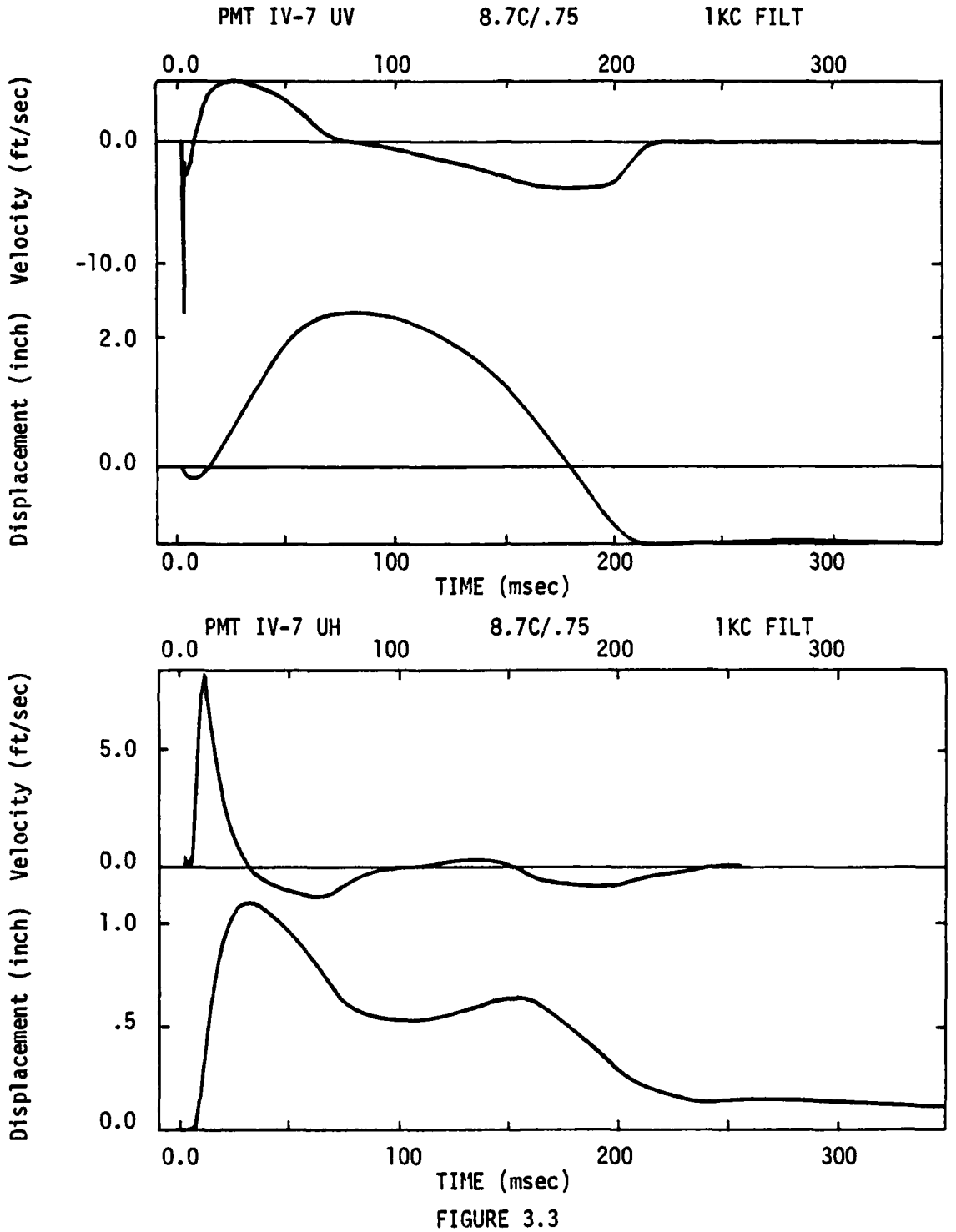


FIGURE 3.3

Ground Motion, 8.5-Foot Epicentral Range, .75 Foot Depth, Line C.
[From Stubbs, Kochly and Sauer (1976:34)]

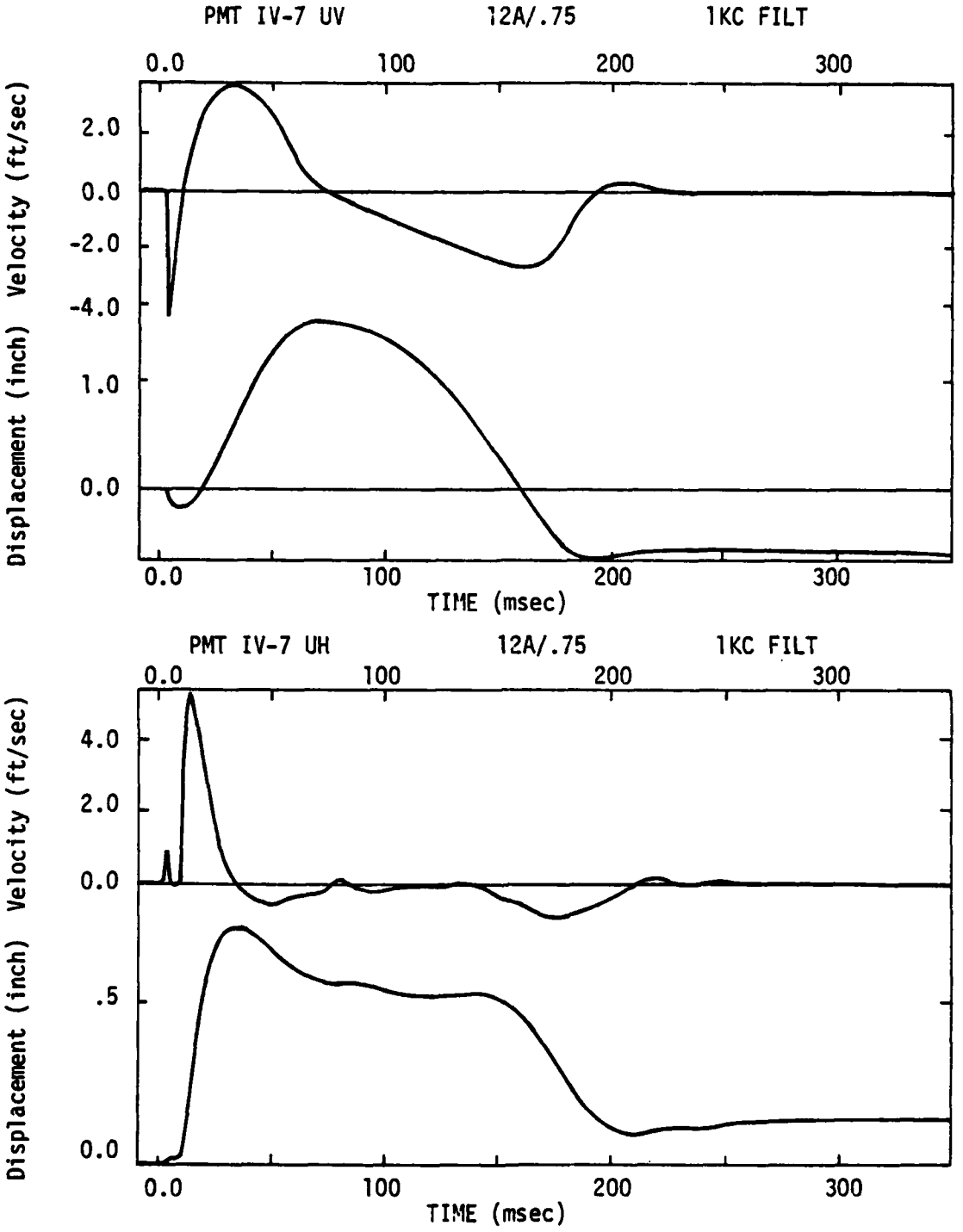


FIGURE 3.4

Ground Motion, 12-Foot Epicentral Range, .75 Foot Depth, Line A.
[From Stubbs, Kochly and Sauer (1976:38)]

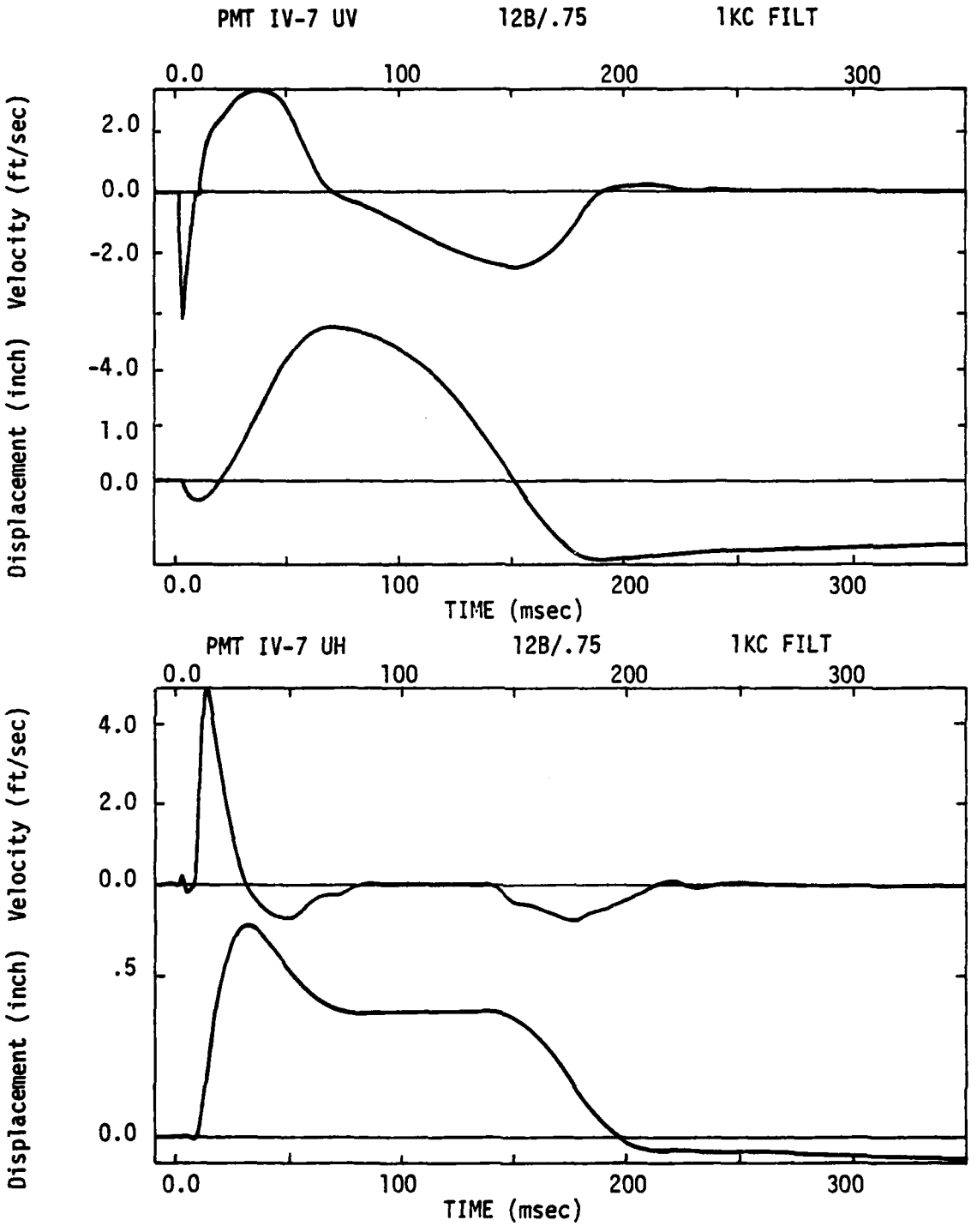


FIGURE 3.5

Ground Motion, 12-Foot Epicentral Range, .75 Foot Depth, Line B.
[From Stubbs, Kochly and Sauer (1976:39)]

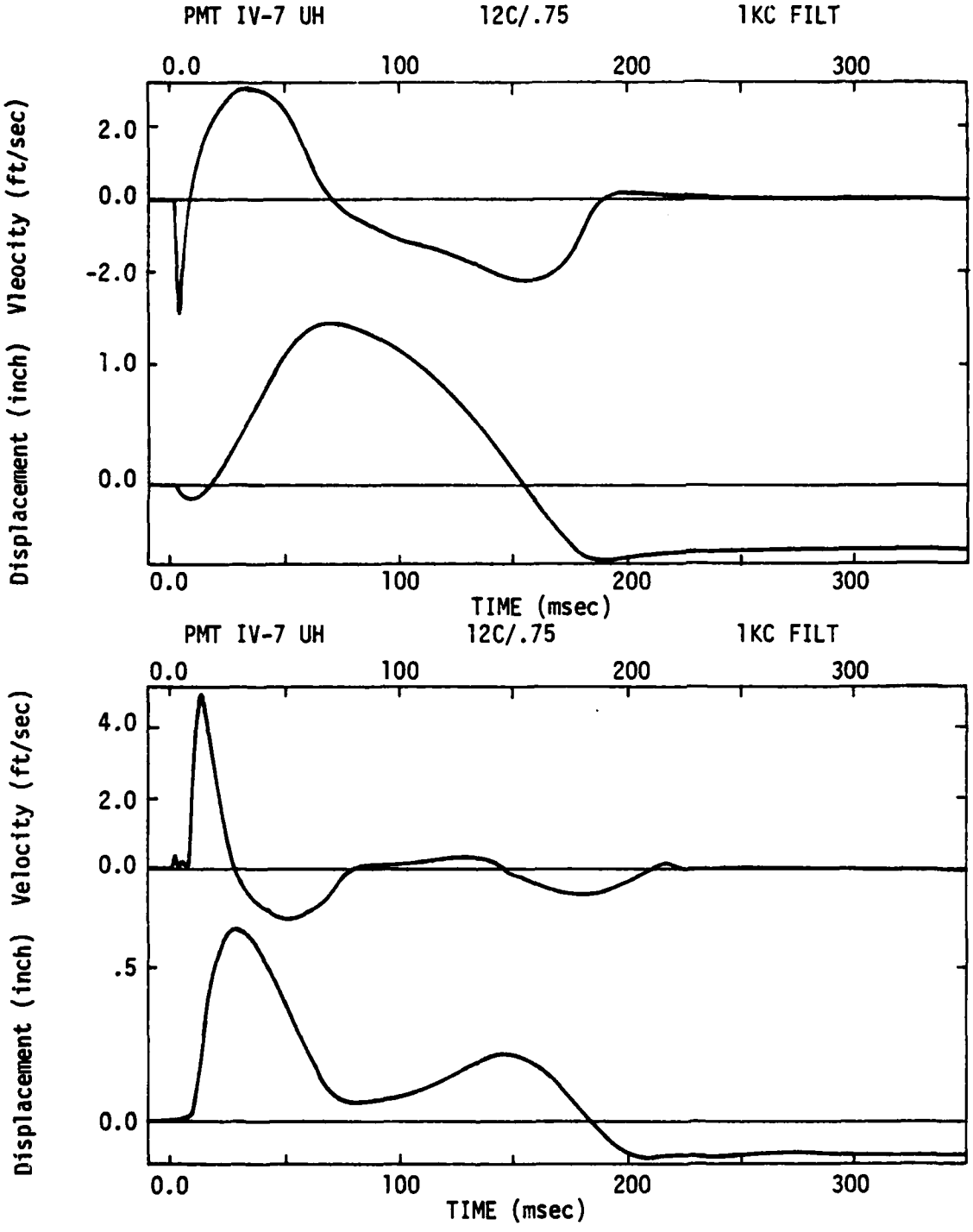


FIGURE 3.6

Ground Motion, 12-Foot Epicentral Range, .75 Foot Depth, Line C. [From Stubbs, Kochly and Sauer (1976:40)]

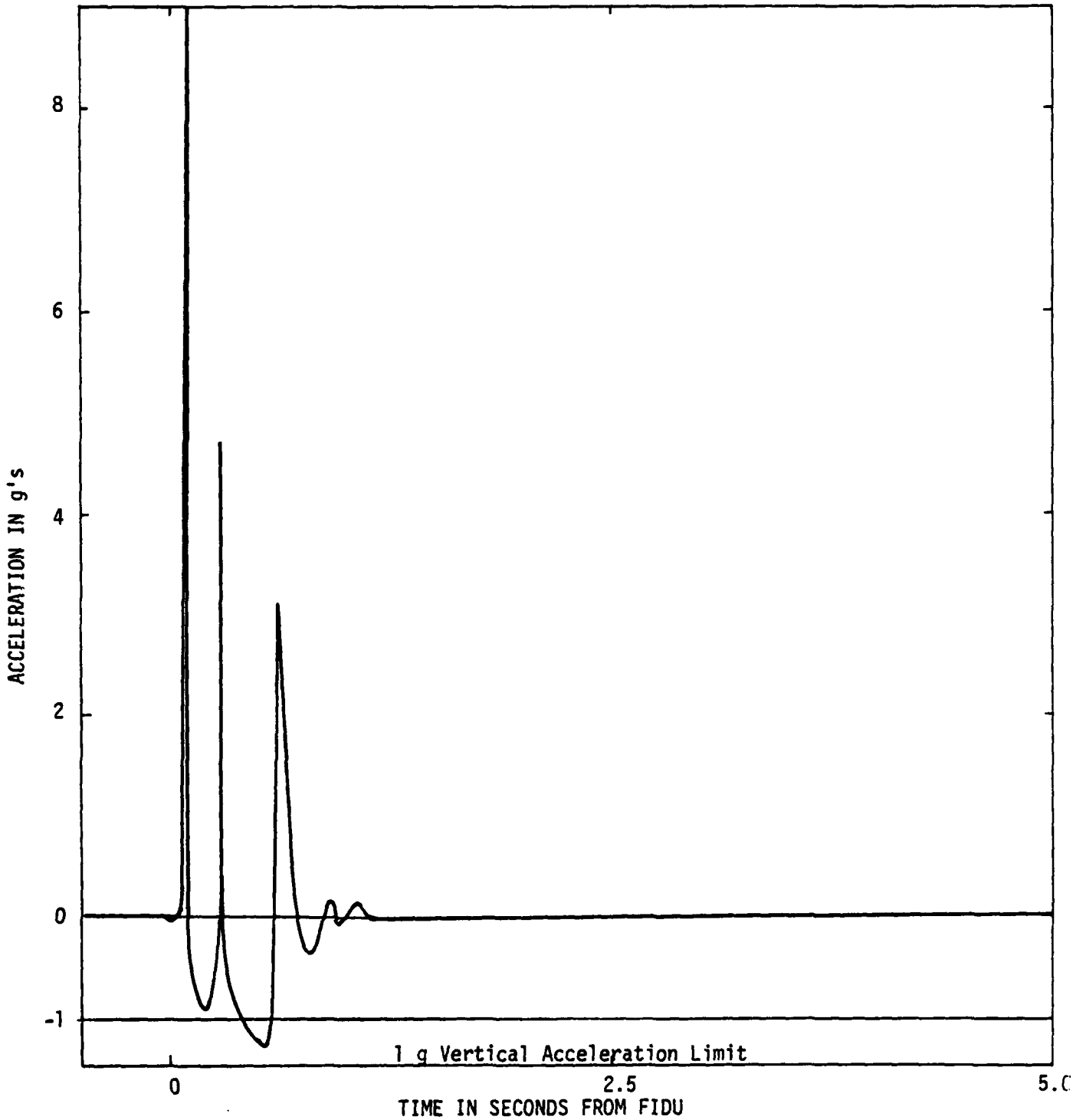


FIGURE 3.7
Vertical Acceleration at the 100-ft Range and 5-ft Depth on SIMQUAKE IB
[From Higgins (1979)]

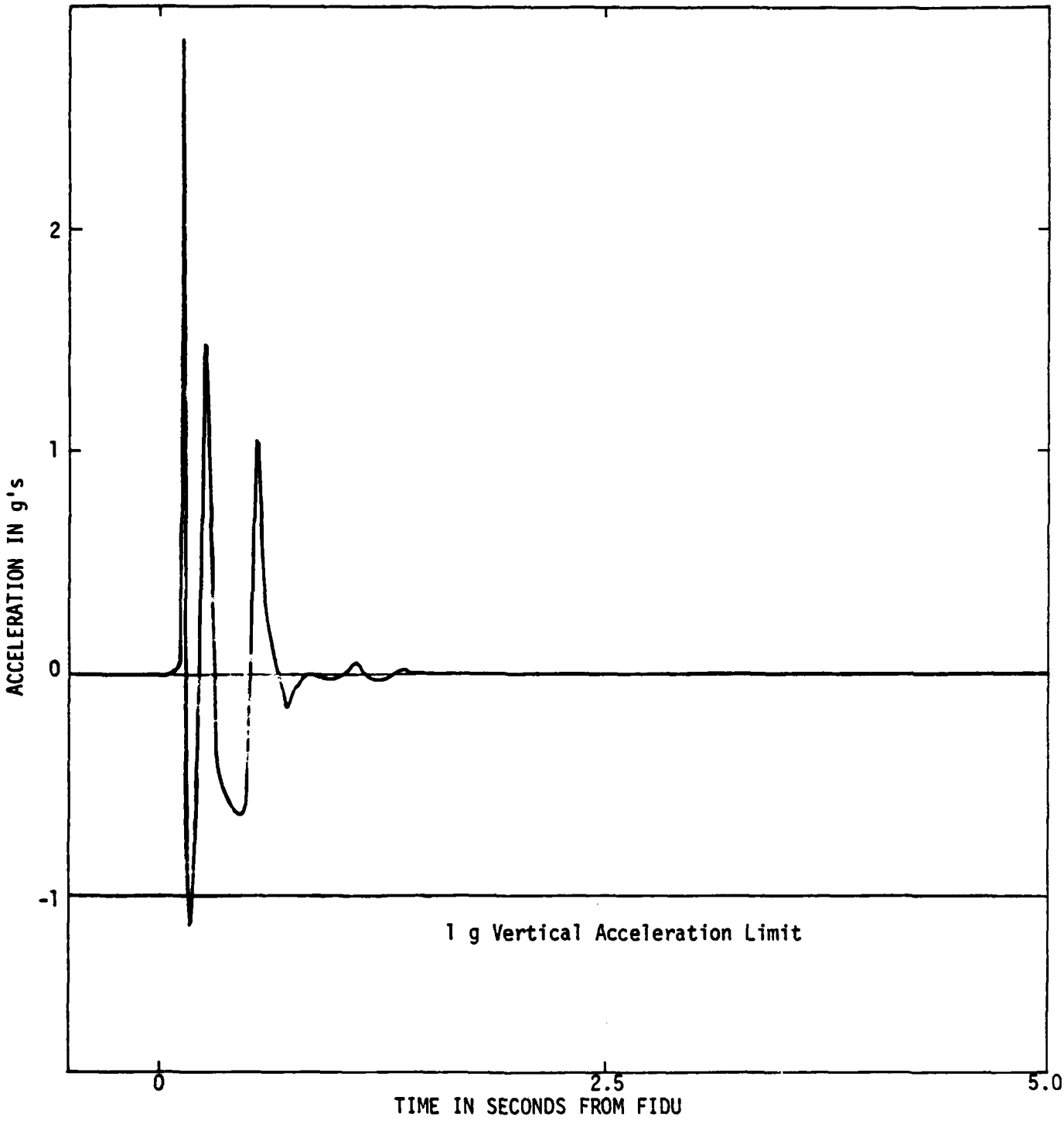


FIGURE 3.8
Vertical Acceleration at the 200-ft Range and 5-ft Depth on SIMQUAKE IB
[From Higgins (1979)]

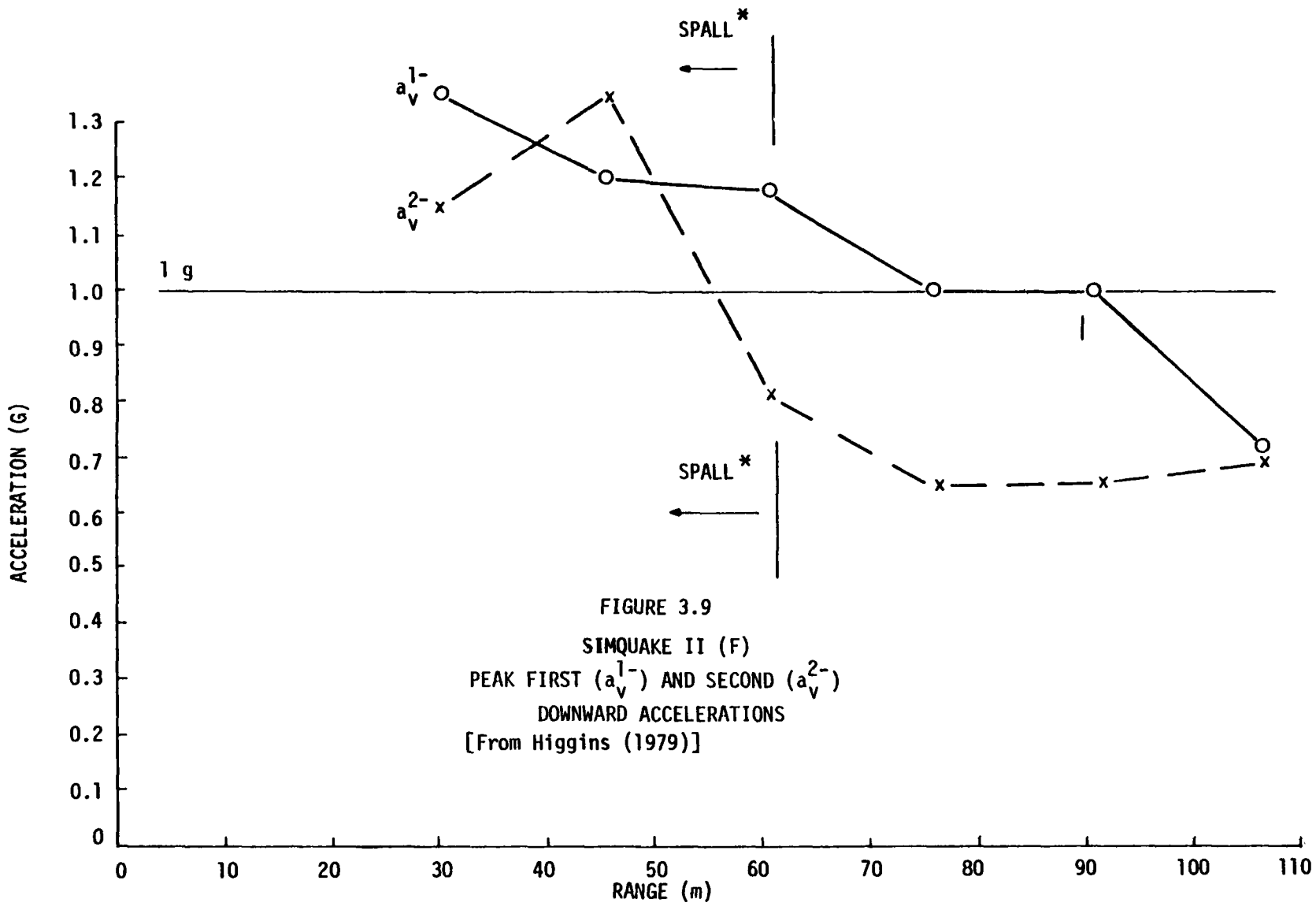


FIGURE 3.9

SIMQUAKE II (F)

PEAK FIRST ($a_v^{1-}$) AND SECOND ($a_v^{2-}$)

DOWNWARD ACCELERATIONS

[From Higgins (1979)]

* See Figure 3.10 for SPALL range definition

FIGURE 3.10

SIMQUAKE II

FIRST ($t_1$) AND SECOND ($t_2$) DOWNWARD ACCELERATION DWELL TIMES AT 1.52m DEPTH
[From Higgins (1979)]

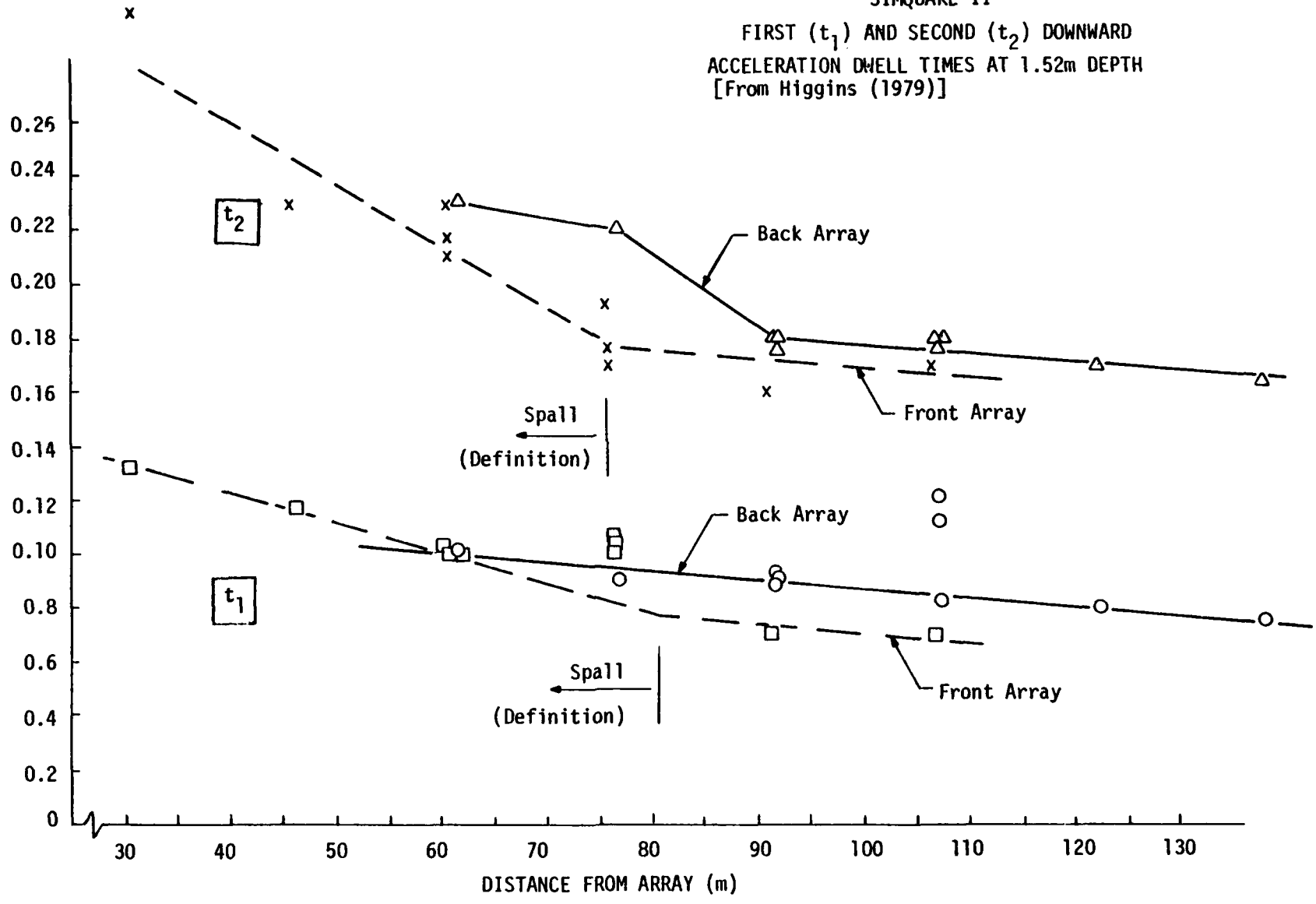

FIGURE 3.11

SPALL REGIONS
SIMQUAKE II FRONT ARRAY

[From Higgins (1979)]

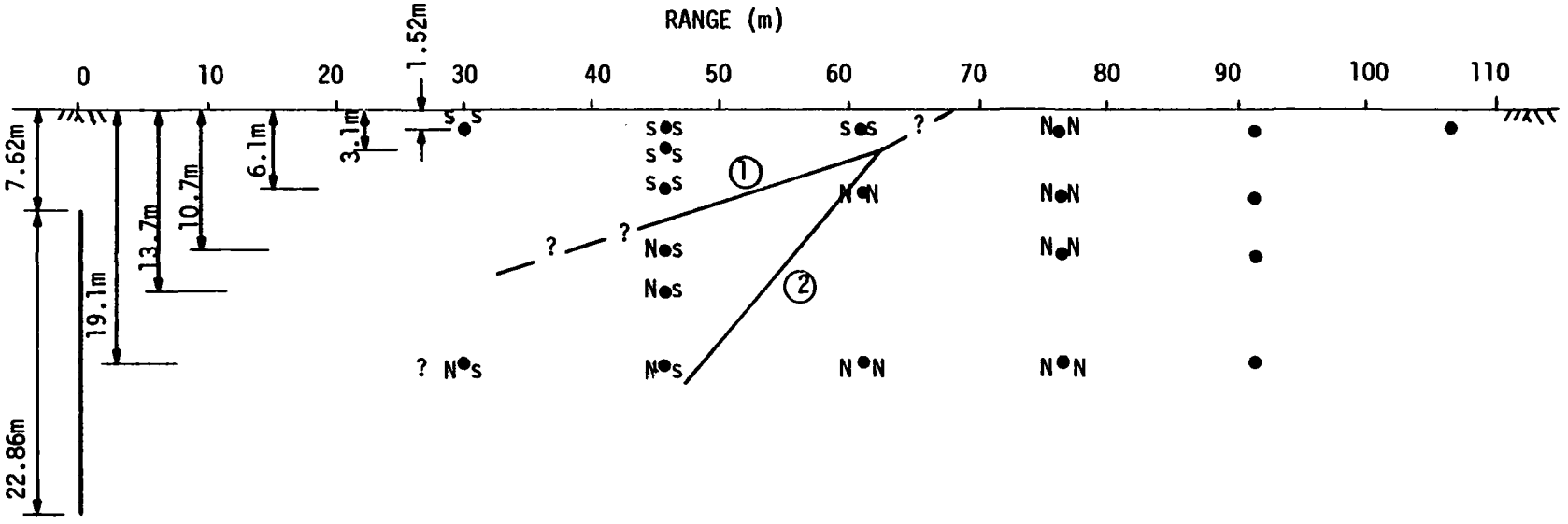


s=SPALL
N=No SPALL

① Following First Upward Motion

② Following Second Upward Motion

FIGURE 3.12

SPALL REGIONS
SIMQUAKE IB (FRONT ARRAY)
[From Higgins (1979)]

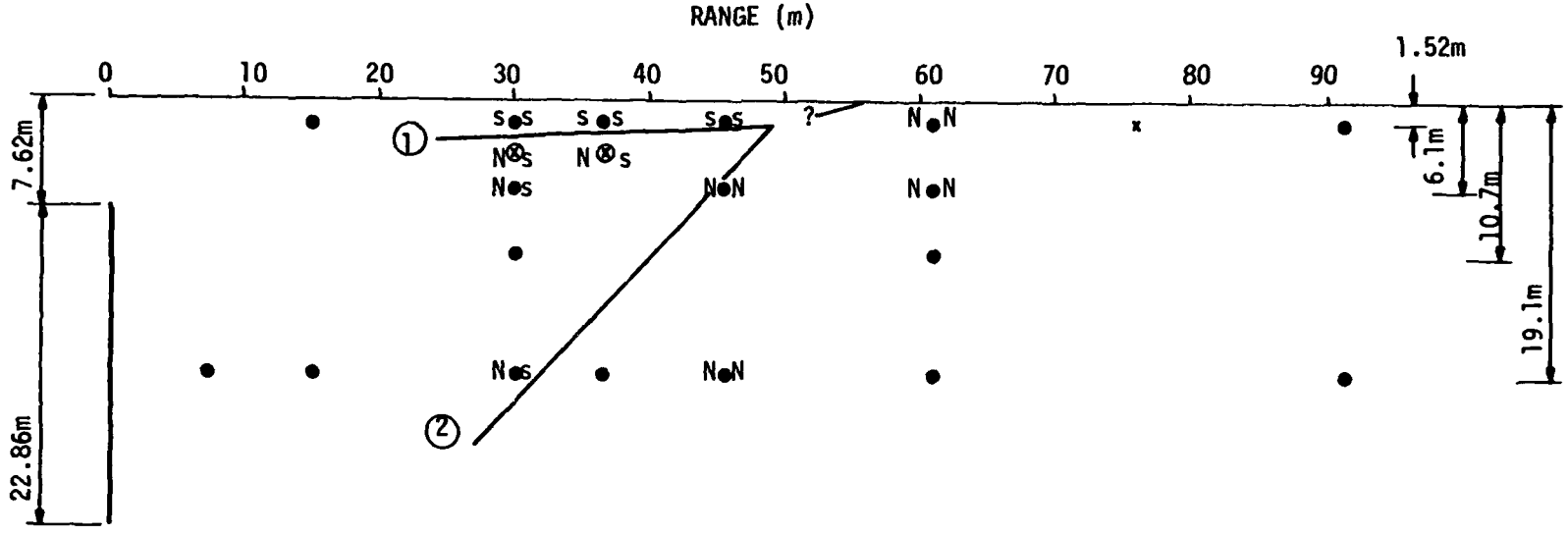


s=SPALL
N= No SPALL

① Following First Upward Motion

② Following Second Upward Motion

FIGURE 3.13

Near-Surface Peak Upward Vertical Velocity
SIMQUAKE II (F)

[From Higgins (1979)]

( ) Approximate Values of Peak Vertical Tensile Strain

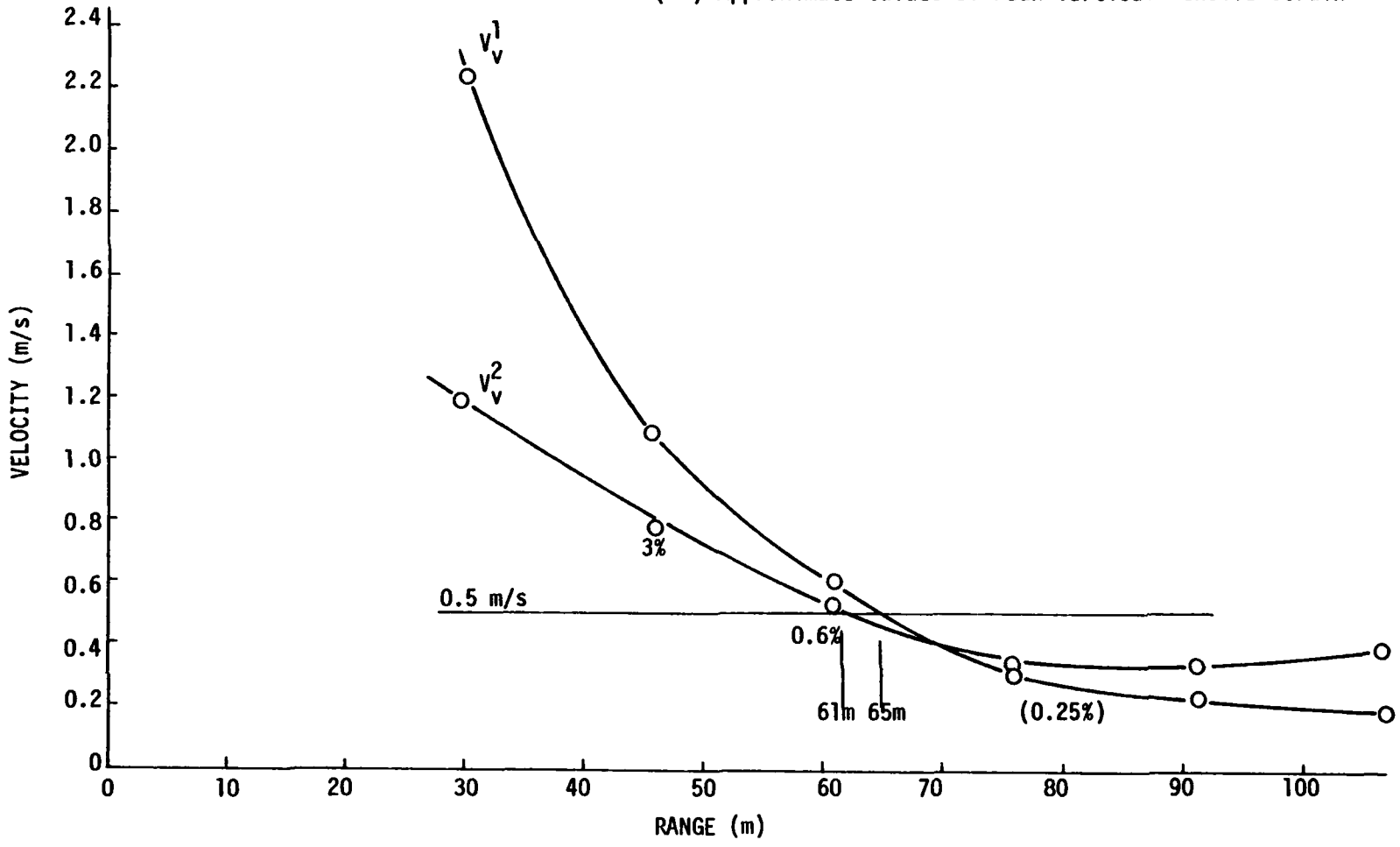

FIGURE 3.14

Near-Surface Peak Upward Vertical Velocities
SIMQUAKE IB

[From Higgins (1979)]

( ) Approximate Values of Peak Vertical Tensile Strain

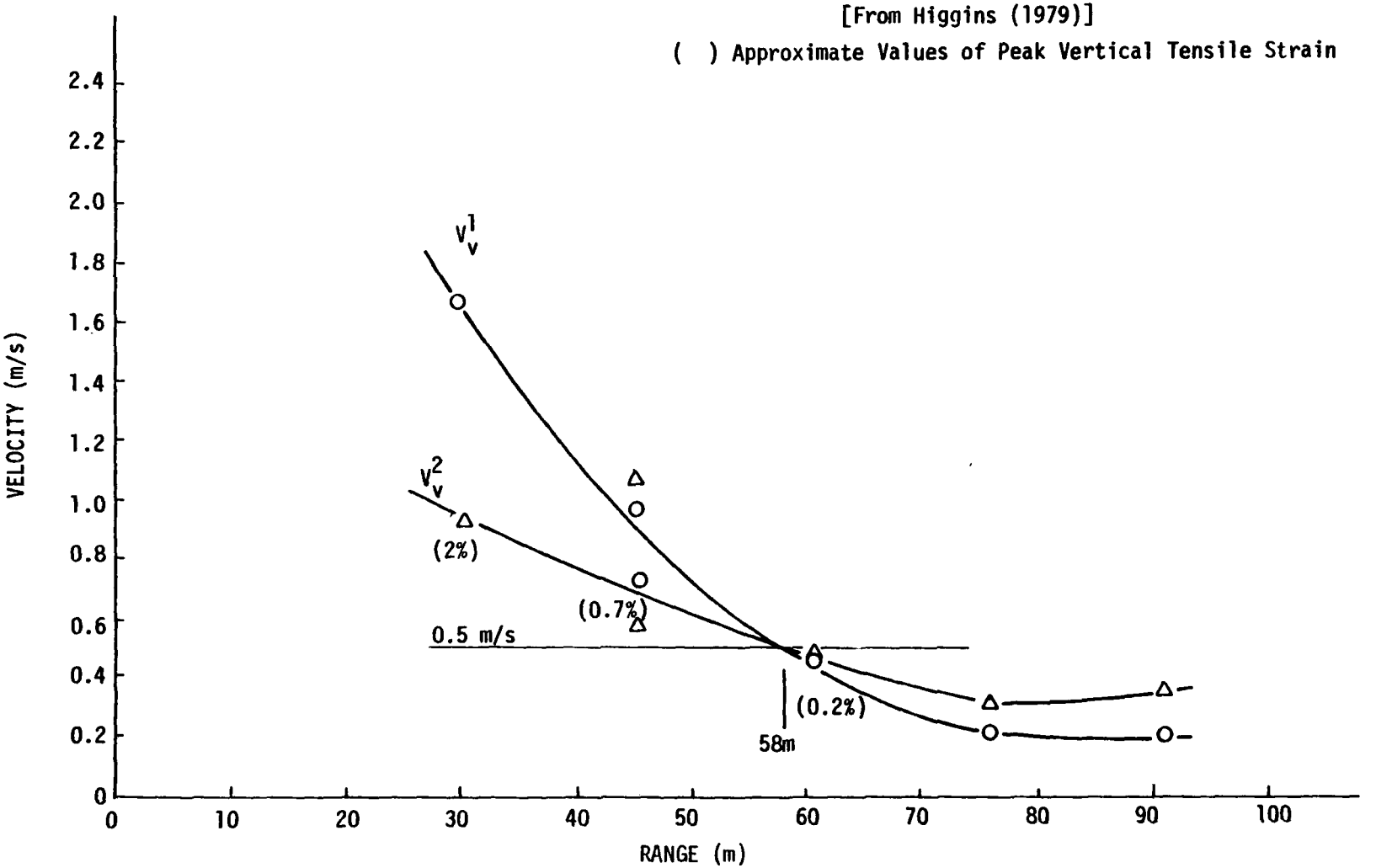

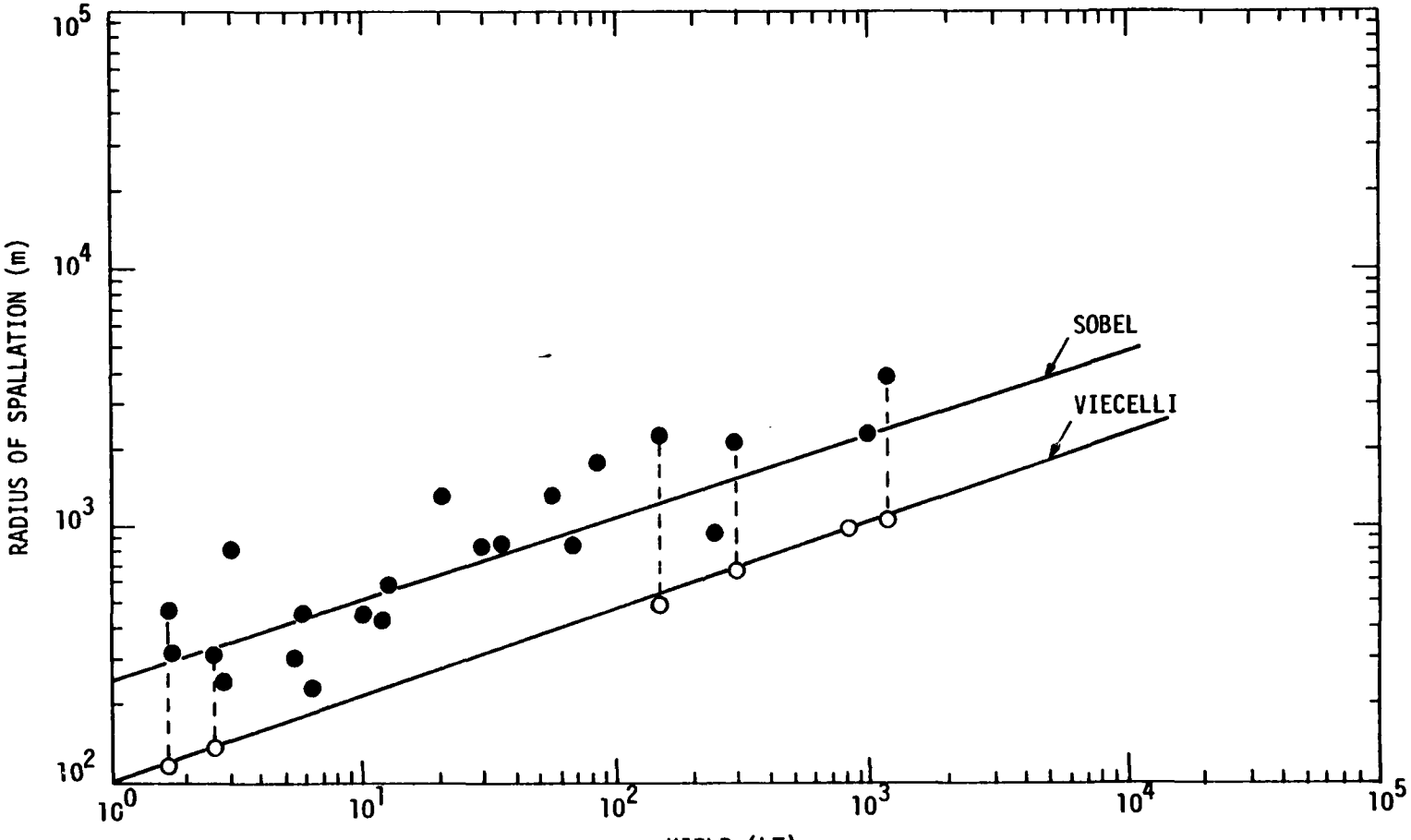


FIGURE 3.15
Comparison of Spall Radius Predictions for Contained Nuclear Events
[From Port and Auld (1980:58)]

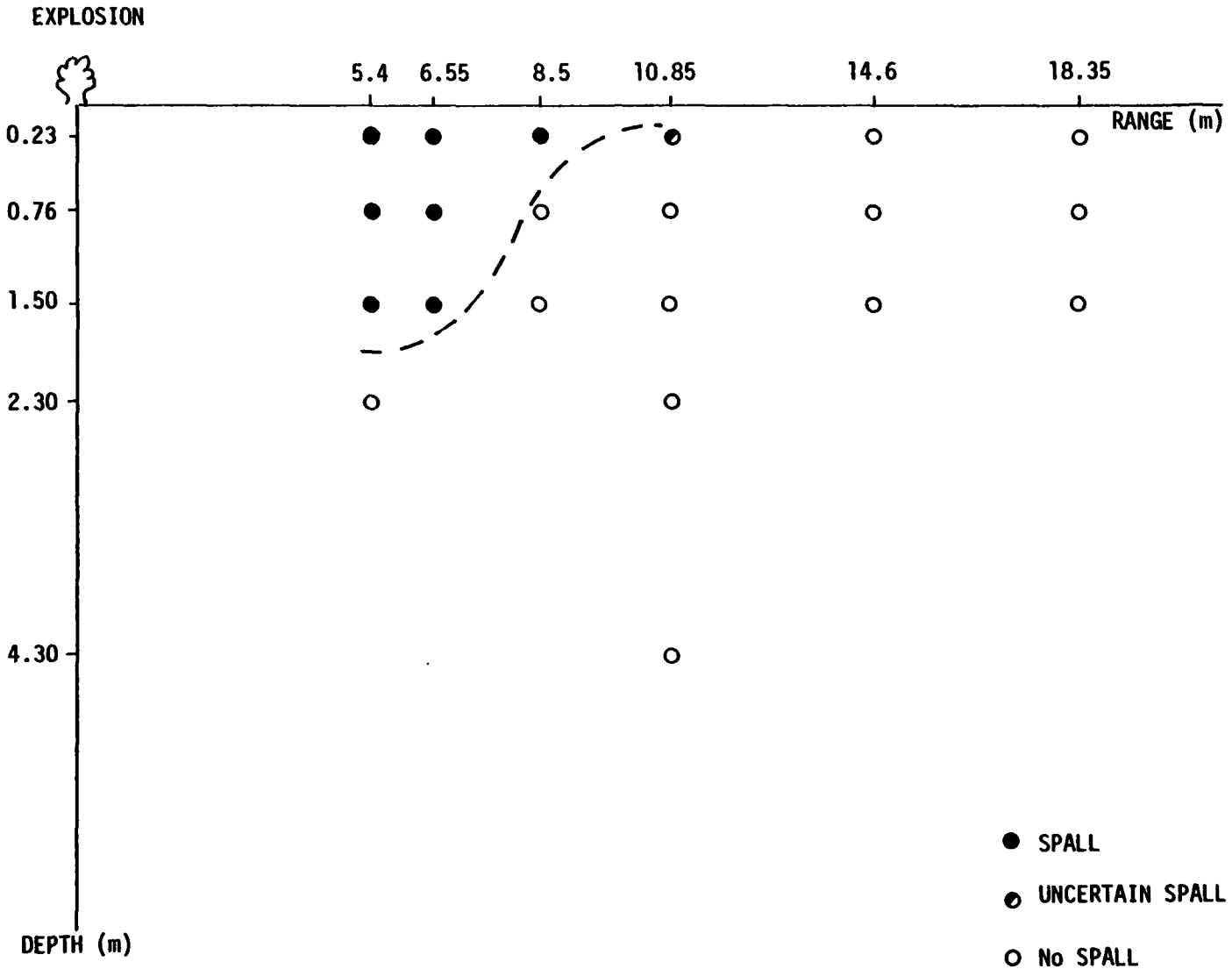


FIGURE 3.16

Extent of Spall in Event PHG-79-06
[From Stump and Reinke (1980:68)]

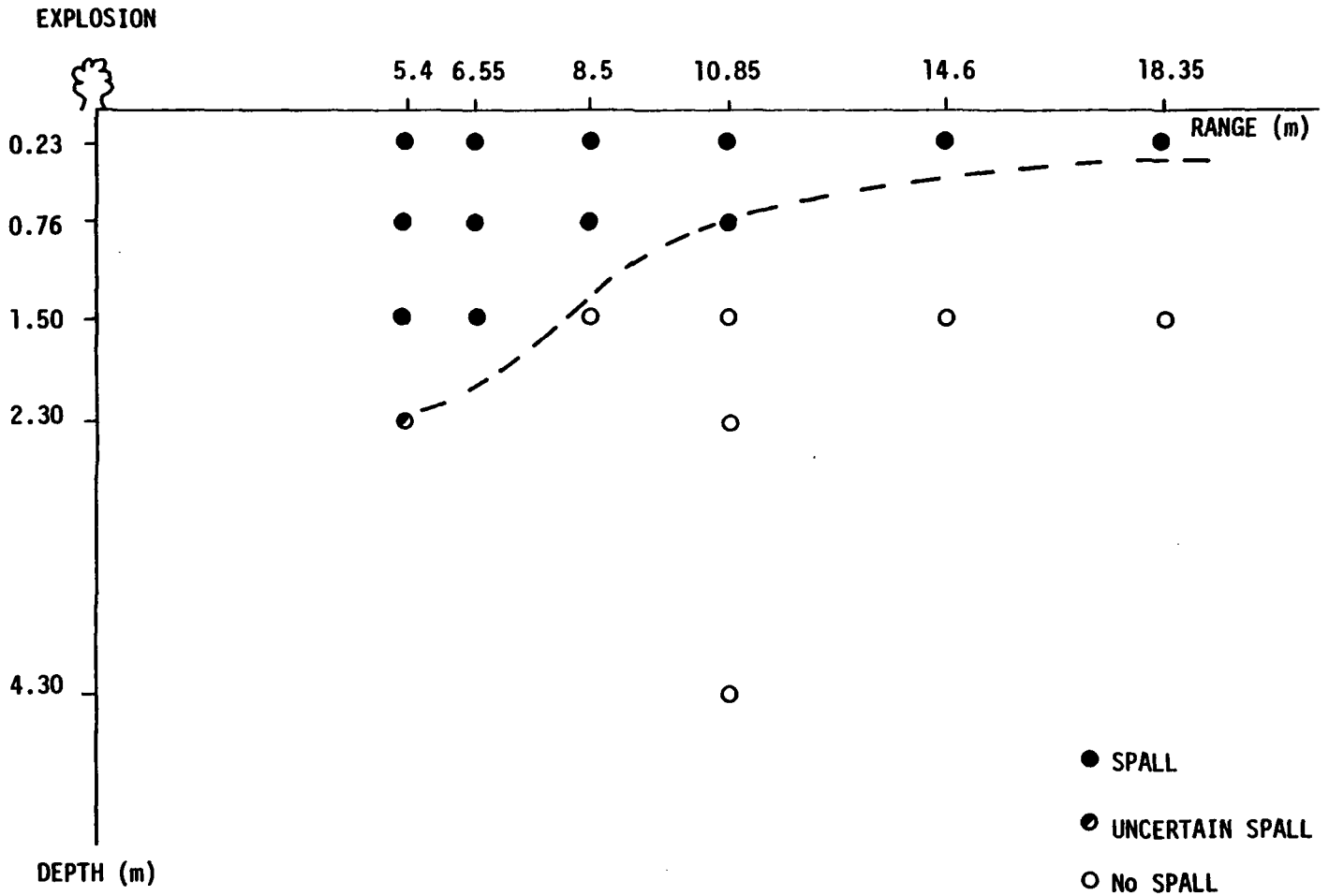


FIGURE 3.17

Extent of Spall in Event PHG-79-07
[From Stump and Reinke (*1980:75*)]

FIGURE 3.18

PHG II - 2
vertical acceleration, R=0.61m, Az=330°

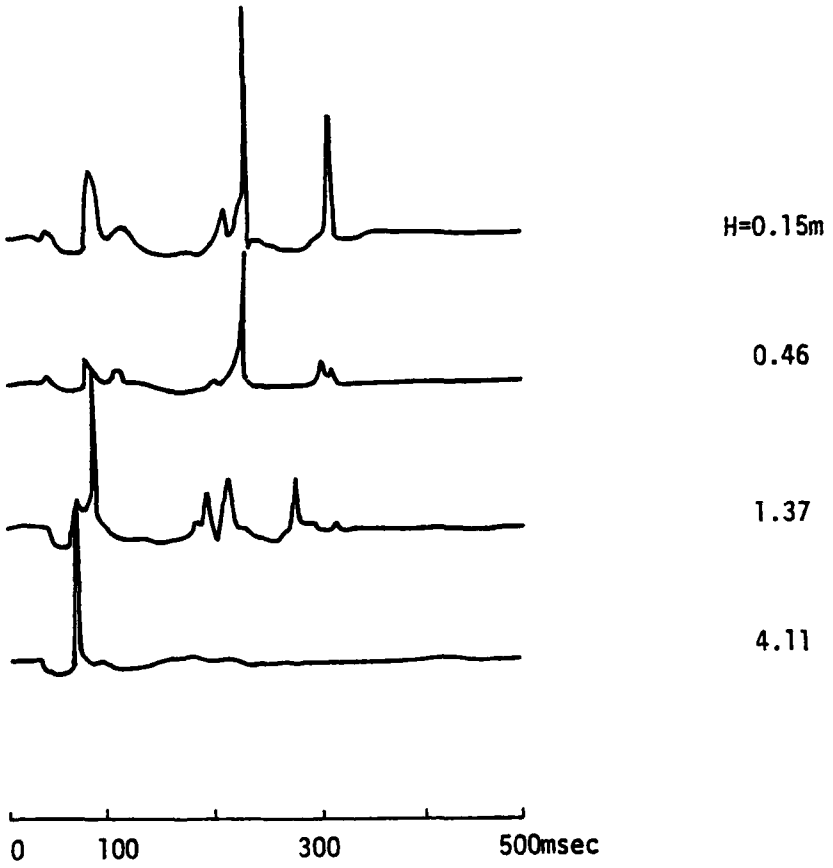


[From Stump and Reinke (1980:83)]

FIGURE 3.19

PHG II - 3
vertical acceleration, R=0.61m, Az=15°

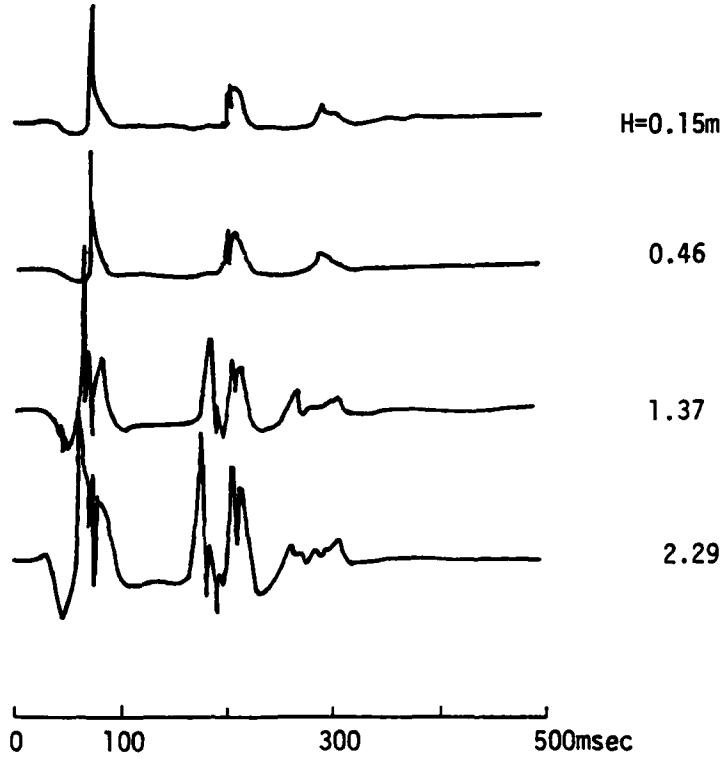


[From Stump and Reinke (1980:84)]

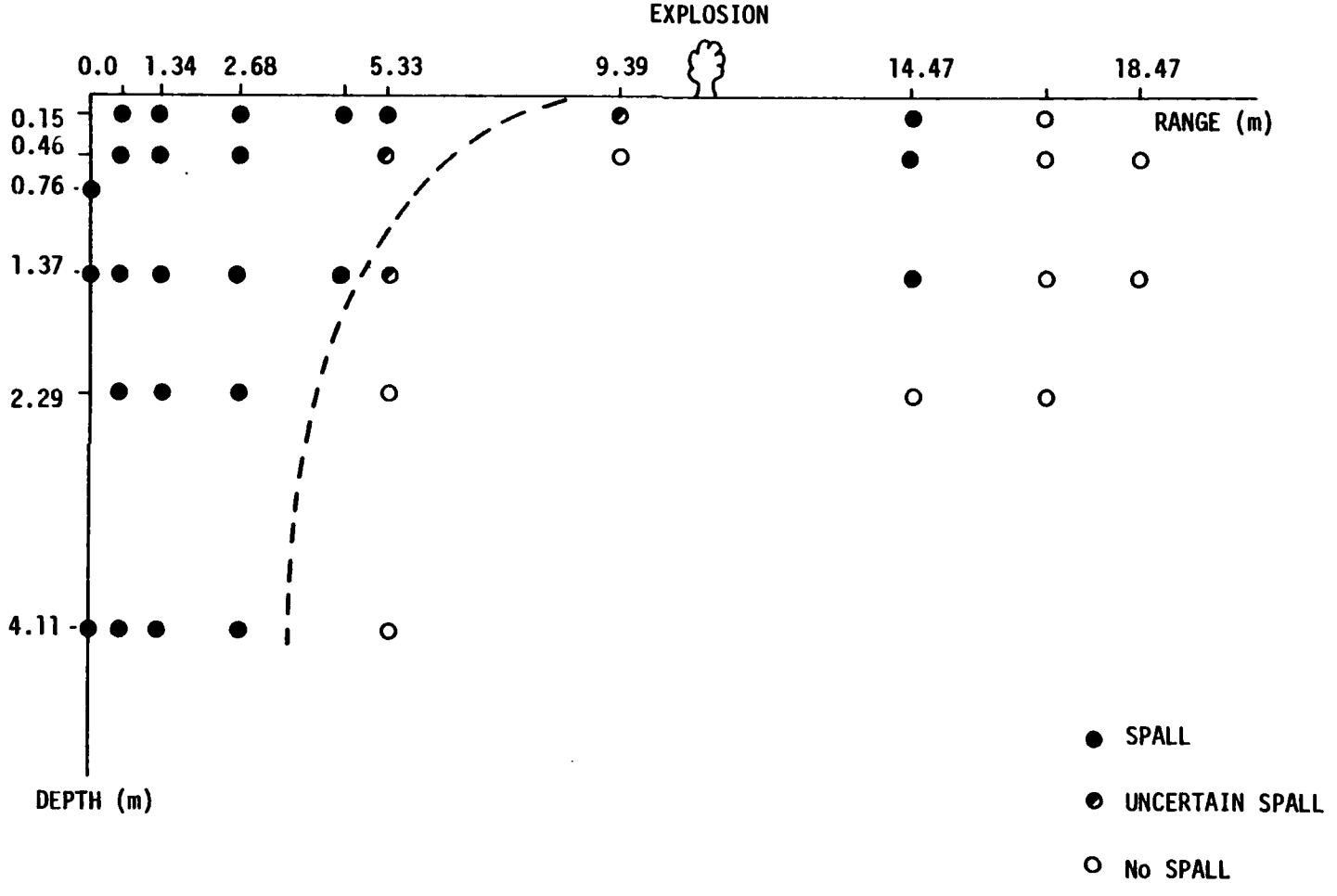


FIGURE 3.20

Extent of Spall in a Radial Plane in Event PHG II-2
[From Stump and Reinke (1980:97)]

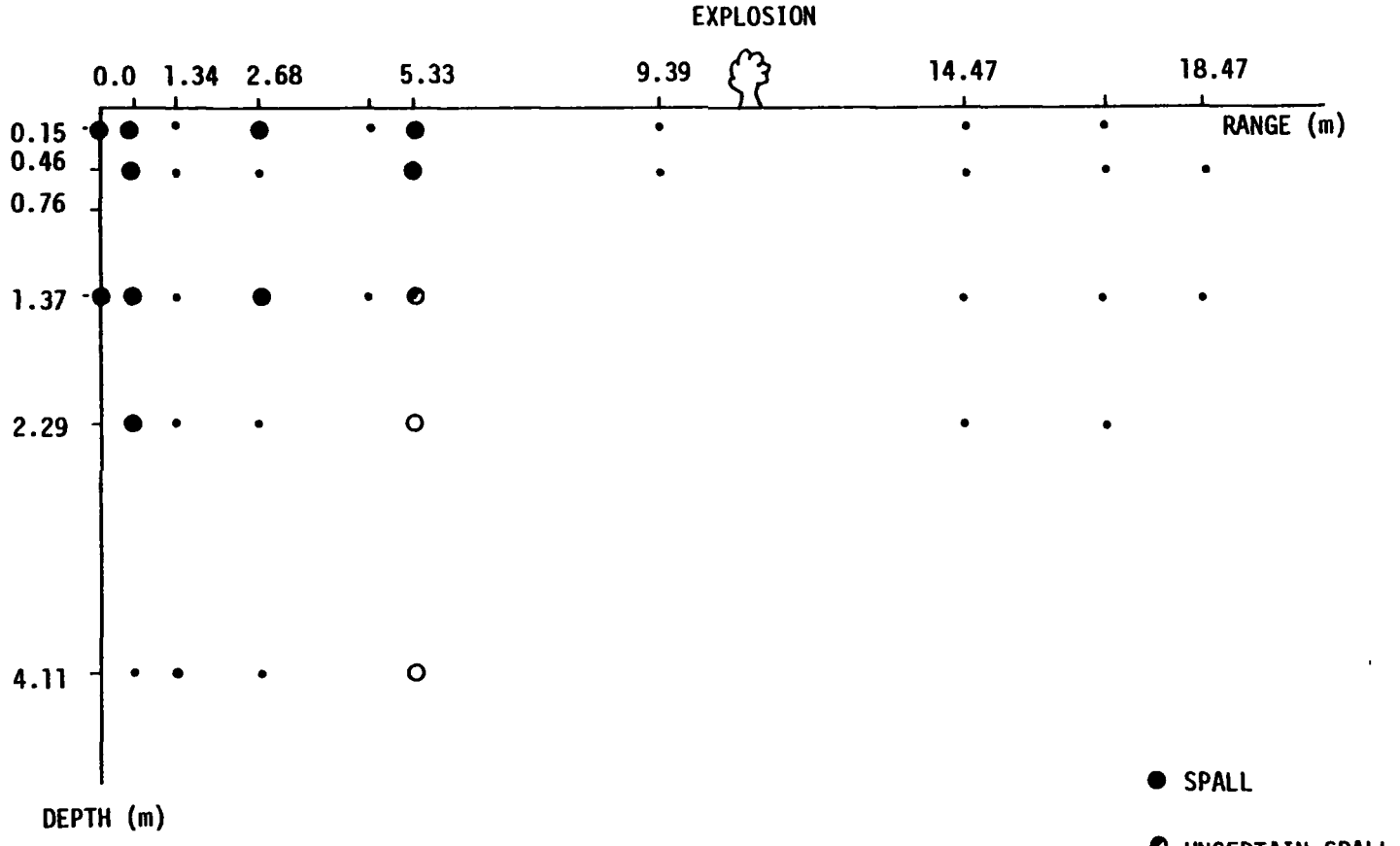


FIGURE 3.21

Extent of Spall in a Radial Plane in Event PHG II-3
[From Stump and Reinke (1980:101)]

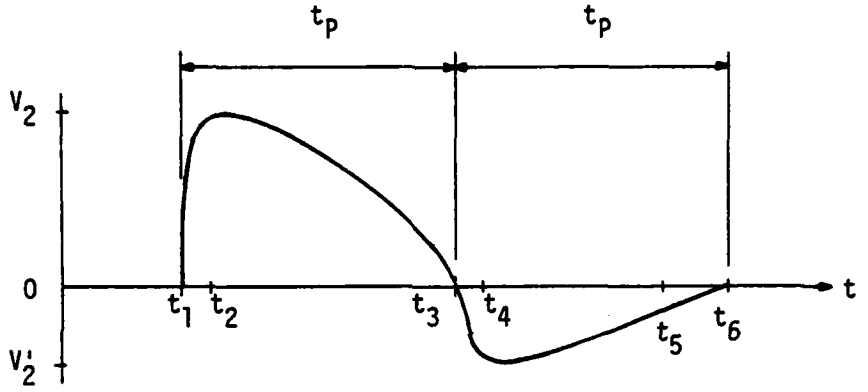


FIGURE 4.1
Crater Related Waveform

DISPLACEMENTS OBTAINED BY PEKERIS AND LIFSON
[From Baron, Bleich and Weidlinger (1960,45)]

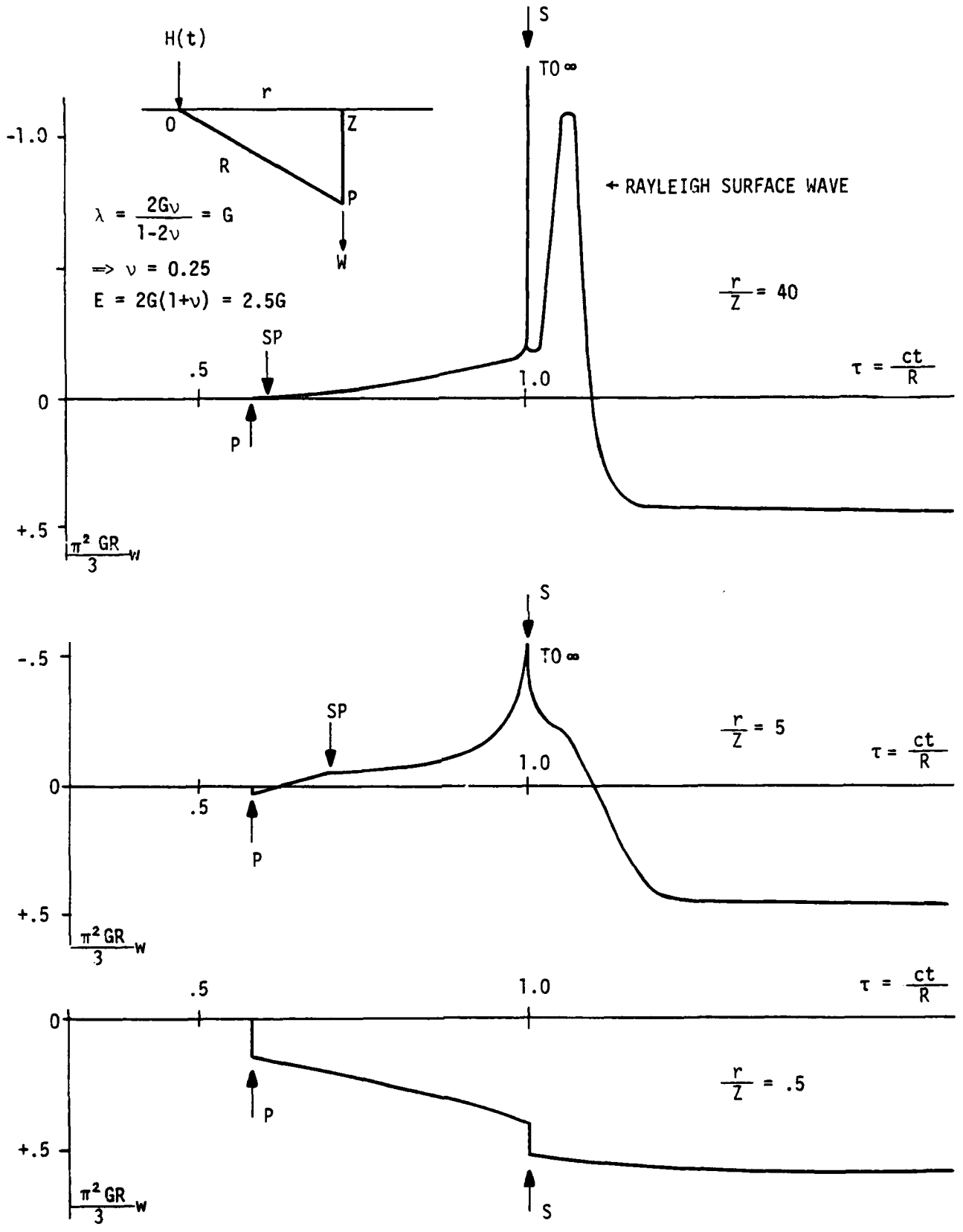


FIGURE 4.2

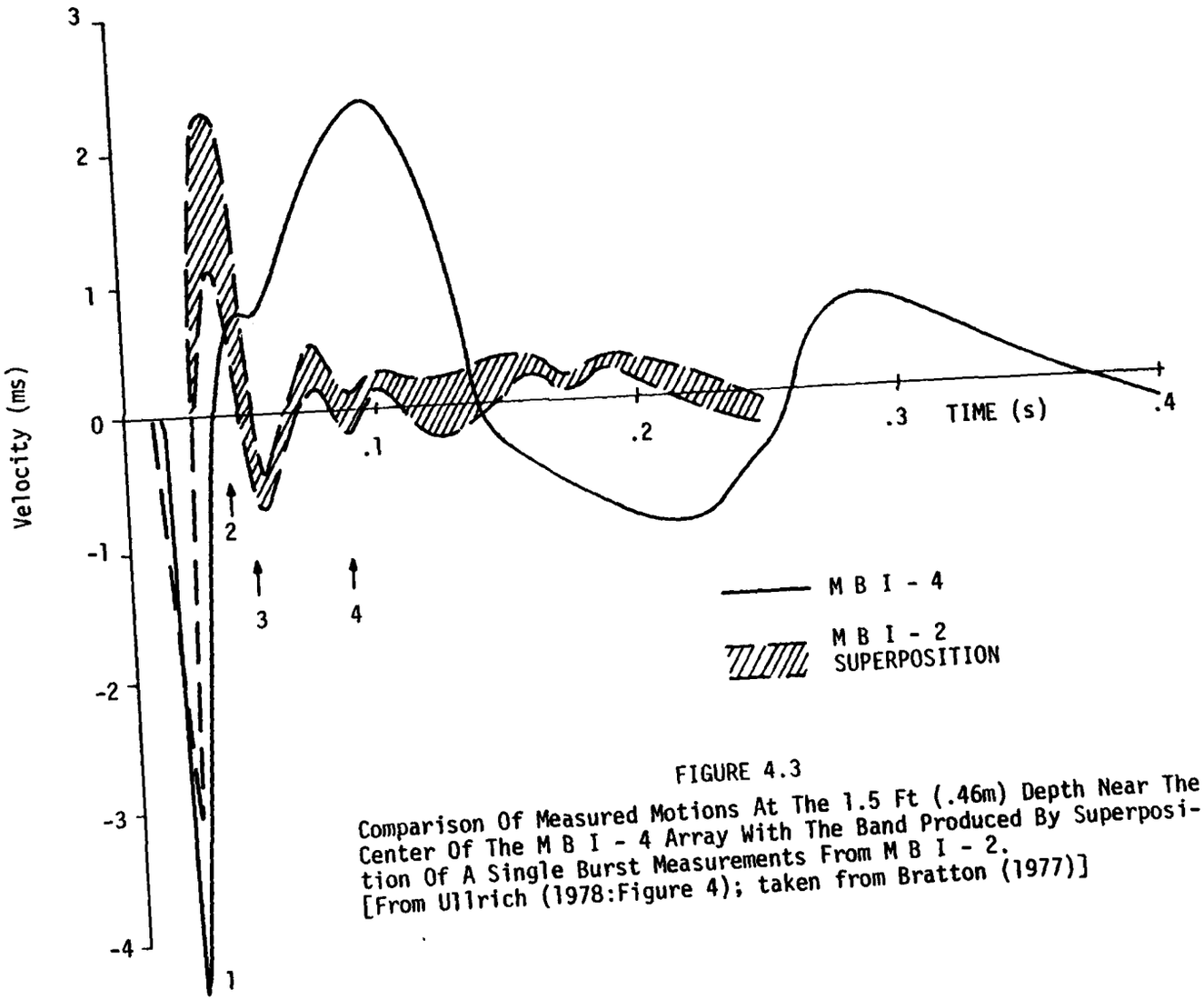


FIGURE 4.3

Comparison Of Measured Motions At The 1.5 Ft (.46m) Depth Near The Center Of The M B I - 4 Array With The Band Produced By Superposition Of A Single Burst Measurements From M B I - 2.
[From Ullrich (1978:Figure 4); taken from Bratton (1977)]

AD-A093 882 APPLIED RESEARCH ASSOCIATES INC ALBUQUERQUE NM F/G 18/3
BASIC MECHANISMS OF SPALL FROM NEAR-SURFACE EXPLOSIONS.(U)
NOV 80 D H MERKLE F49620-80-C-0059
UNCLASSIFIED AFOSR-TR-80-1379 NL

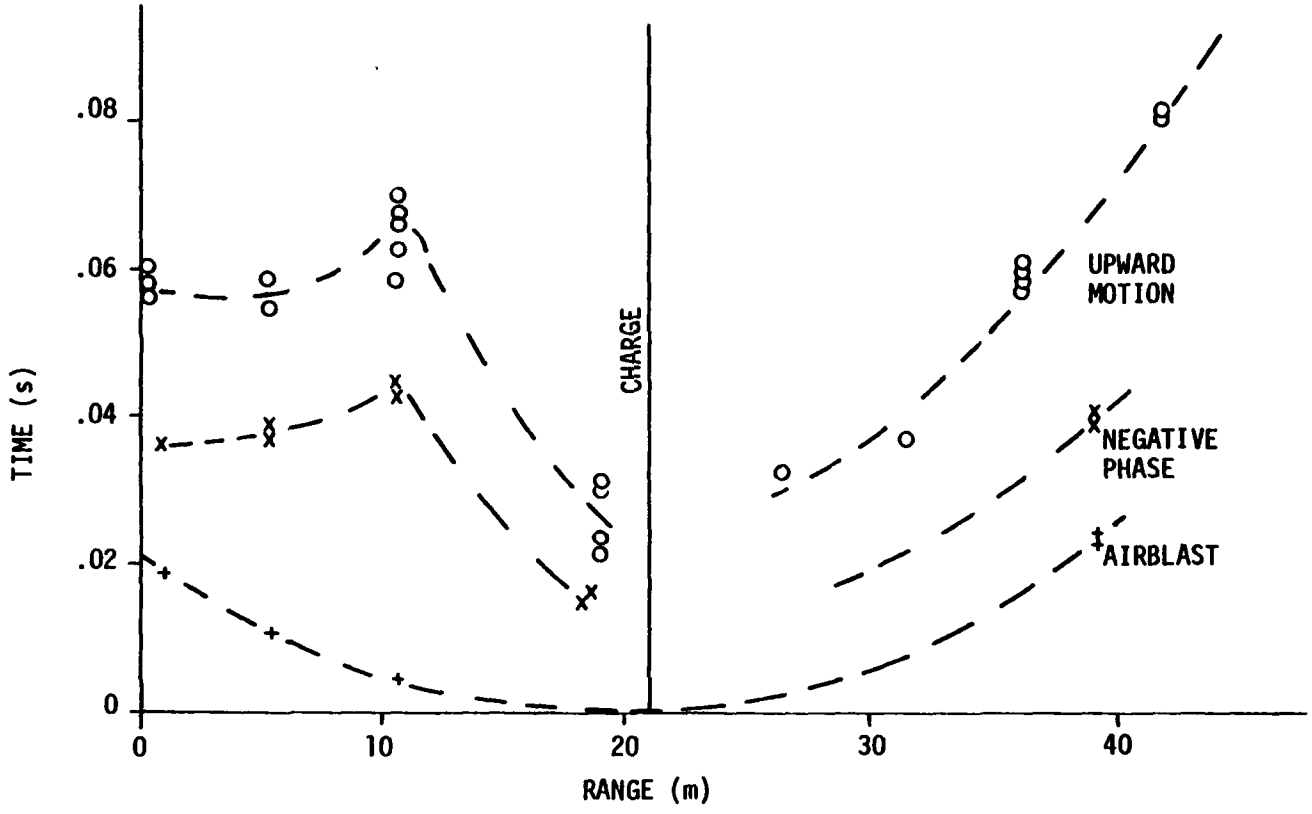


FIGURE 4.4

Time Of Arrivals For The Airblast, A Negative Phase Of Overpressure, And Beginning Of An Upward Motion Phase At 1.5 ft (.46m) Depth Along A Radial Through One Charge Of MB-I-4. The Charge Was Located At The 70 ft (21.3m) Range.
[From Ullrich (1978:Figure 5); courtesy of J. L. Bratton]

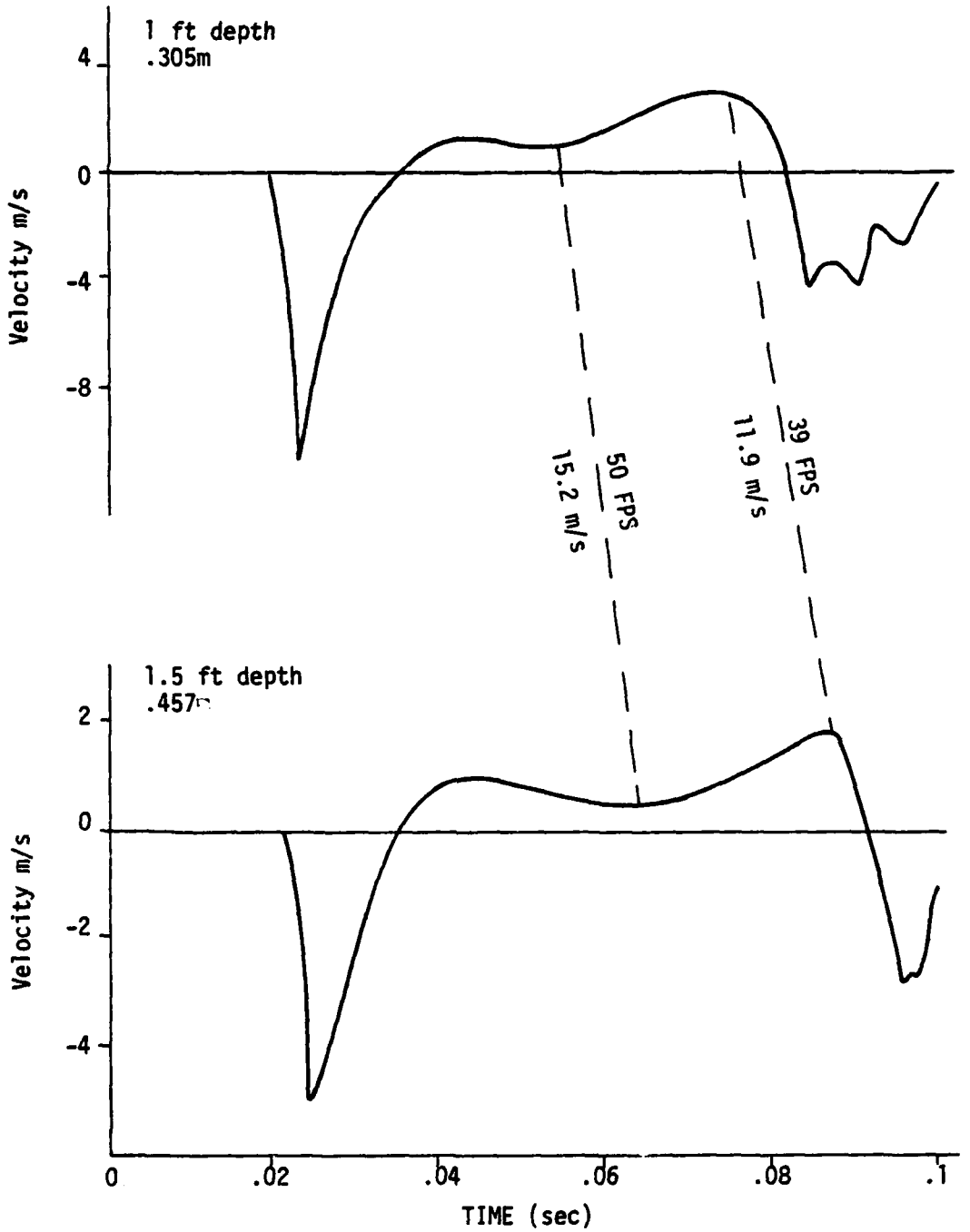


FIGURE 4.5

Vertical Velocities At The 1.0 And 1.5 Ft (.3 and .46m) Depth Near The Center Of Event MB-I-8. The data indicates that the upward acceleration was initiated at the shallower gage 10 msec before being initiated at the deeper gage, and was terminated by a downward propagating wave.
[From Ullrich (1978:Figure 6)]